Band Structure of nuclei in Deformed Hartree-Fock and Angular Momentum Projection theory

C. R. Praharaj
Institute of Physics
Bhubaneswar . India

Outline of talk

- Motivation
- Formalism
  - HF calculation
  - Angular momentum projection
  - Band mixing
- Results and Discussion
  - Configurations and band structure
    - Normal deformed bands
    - Large K bands
    - "Chiral" bands
    - Superdeformed bands
  - B(E2) & B(M1)
  - Q_s, Q_t & μ_N
- Conclusion

Motivation

- After coming of Heavy Ion accelerators and new generation of detector arrays:
  - Extend upto very high spins
  - Many bands are known
- Need theoretical frame work to correlate and understand these starting from a fundamental principle :-
  - Nucleon-nucleon interaction (Strong)
  - Shell model (both closed and away from that)

- Some interesting phenomena in nuclear spectroscopy are
  - Regular and irregular spectra
  - Known upto very high spins
    - Band crossings
    - Inter-band transitions
    - Signature effects
  - Large K bands. K selection violation
  - Identical bands
  - Staggering in B(E2) and B(M1)

Hartree-Fock (HF) method

$$H = \sum_{\alpha\gamma} T_{\alpha\gamma} c^{\dagger}_{\alpha} c_{\gamma} + \frac{1}{4} \sum_{\alpha\beta\gamma\delta} V_{\alpha\beta\gamma\delta} c^{\dagger}_{\alpha} c^{\dagger}_{\beta} c_{\delta} c_{\gamma} \qquad (1)$$

$$|\Psi_0\rangle = \frac{1}{\sqrt{N_1!}} \times |\phi_1 \ldots \phi_{N_1}| \times \frac{1}{\sqrt{N_2!}} \times |\chi_1 \ldots \chi_{N_2}| \qquad (2)$$

$$|\Psi_0\rangle = c^{\dagger}_1 c^{\dagger}_2 \ldots c^{\dagger}_{N_1} c'^{\dagger}_1 c'^{\dagger}_2 \ldots c'^{\dagger}_{N_2} |0\rangle \qquad (3)$$

Here $|0\rangle$ represents the core space of inert nucleons

$$|\alpha m\rangle = \sum_j C_j^{\alpha m} |jm\rangle \tag{4}$$

$$H = \sum_j \epsilon_j a_{jm}^\dagger a_{jm} + \sum_{\substack{j_1 j_2 j_3 j_4 \\ m_1 m_2 m_3 m_4}} V(j_1 m_1 j_2 m_2; j_3 m_3 j_4 m_4) a_{j_1 m_1}^\dagger a_{j_2 m_2}^\dagger a_{j_4 m_4} a_{j_3 m_3} \tag{5}$$

in the uncoupled representation and the Hartree-Fock equations can be written as

$$(\epsilon_j - e_{\alpha m}) C_j^{\alpha m} + \sum_{j_1 j_2 j_4 m_2} V(j_1 m j_2 m_2; j m j_4 m_2) \rho_{j_4 m_2 j_2 m_2} C_{j_1}^{\alpha m} = 0 \tag{6}$$

In the Hartree-Fock approximation there are the occupied orbits (the lowest orbits) and the unoccupied orbits (Fig.1) which lie higher in energy. The Hartree-Fock solution is determined by the occupied orbits.

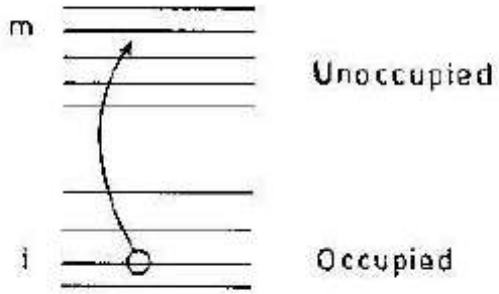

Figure 1: The occupied and unoccupied orbits of Hartree-Fock Theory. Excited configurations are obtained by particle-hole excitations.

The occupied orbits determine the density matrix

$$\rho_{j_4 m_2 j_2 m_2} = \langle \Phi_{HF} | a^{\dagger}_{j_2 m_2} a_{j_4 m_2} | \Phi_{HF} \rangle \tag{7}$$

is the density matrix. $|\Phi_{HF}\rangle$ is the Slater determinant of the lowest energy deformed orbits and the density matrix becomes

$$\rho_{j_4 m_2 j_2 m_2} = \sum_{\substack{\alpha \\ (occupied)}} C^{\alpha m_2}_{j_2} C^{\alpha m_2}_{j_4} \tag{8}$$

Equations (6) and (8) are solved by iteration to obtain the deformed single-particle states and $|\Phi_{HF}\rangle$.
One has the Hartree-Fock onebody potential

$$\Gamma = V\rho \tag{9}$$

Thus eqn (6) can be symbolically written as

$$(\epsilon + \Gamma)|\alpha m\rangle = e|\alpha m\rangle \tag{10}$$

A convergent Hartree-Fock solution means self-consistency between occupation of orbits (density matrix ρ) and the Hartree-Fock Hamiltonian h or W ($h \equiv W = \epsilon + \Gamma$).

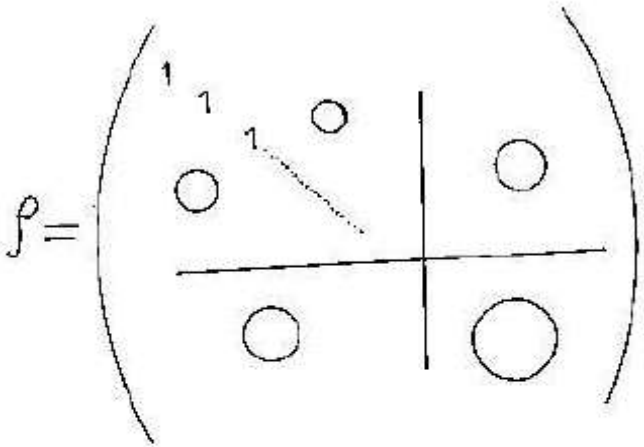

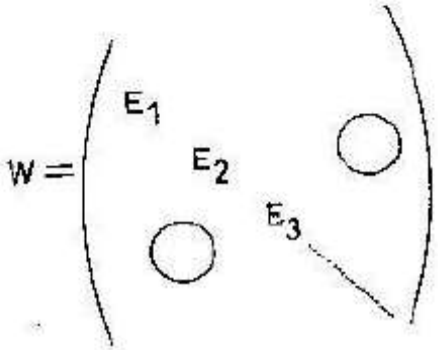

Thus in the representation where the eigenstates are the HF single-particle states both ρ and W are simultaneously diagonal.

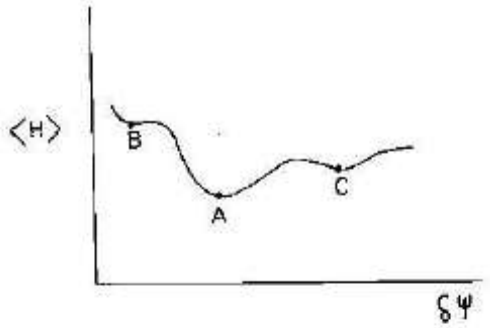

Figure 2: Energy surface (schematic) with a number of local minima.

For a converged Hartree-Fock solution we have the Hartree-Fock energy as the expectation value of H

$$\begin{aligned} E_{HF} &= \langle H \rangle \\ &= \sum_i \epsilon_i \rho_{ii} + \sum_{ijkl} V(ij,kl)\rho_{lj}\rho_{ki} \end{aligned} \tag{11}$$

The energy of the αth Hartree-Fock orbit is

$$\begin{aligned} e_\alpha &= \sum_i \epsilon_i C_i^{\alpha *} C_i^\alpha + \sum_{\beta(occupied)} C_i^{\alpha *} C_k^\alpha C_j^{\beta *} C_l^\beta V(ij,kl) \\ &= \sum_i \epsilon_i |C_i^\alpha|^2 + \sum V(ijkl)\rho_{ki}\rho_{lj} \end{aligned} \tag{12}$$

The energy of a Hartree-Fock orbit is to be identified with the single-nucleon removal energy (Koopman's Theorem).

RESIDUAL INTERACTIONS

(i). Rosenfeld mixture:– This is a Yukawa potential with appropriate spin, isospin exchange components and has the form

$$V = V_0 \times \frac{1}{3} \times (\vec{\tau_1} \cdot \vec{\tau_2}) \times (0.3 + 0.7\vec{\sigma_1} \cdot \vec{\sigma_2}) \times \frac{\exp(-\frac{r}{a})}{\frac{r}{a}} \tag{14}$$

This interaction is attractive for (T = 0, S = 1) and (T = 1, S = 0) combinations of spin and isospin and thus embodies some of the essential features of the two-nucleon force[57].

(ii). Pairing and Quadrupole Interaction ("the Copenhagen Interaction"):–

This interaction contains a pairing term and a quadrupole deformation- producing term and has been often used for nuclear structure studies[6,55]. It can be written as:

$$V = -G \sum_{jmj'm'} c^{\dagger}_{jm} c^{\dagger}_{j\bar{m}} c_{j'\bar{m}'} c_{j'm'} - \chi Q(1).Q(2) \tag{15}$$

(iii). Surface delta interaction[61]:– The interaction is confined to the nuclear surface (radius R_0) and has the form

$$V(\vec{r_{12}}) = -2F \times (R_0 u_0)^{-4} \times \delta(\cos w_{12} - 1) \tag{16}$$

The above can be written in the form

$$V(\vec{r_{12}}) = -V_0 \sum_{lm} Y^*_{lm}(\Omega) Y_{lm}(\Omega) \tag{17}$$

SYMMETRIES OF HARTREE-FOCK POTENTIAL

See Ripka in Adv Nucl Phys vol 2

The nuclear Hamiltonian has some of the familiar symmetries (three dimensional rotational symmetry, reflection symmetry, time reversal symmetry etc). But the resulting Hartree-Fock orbits, the HF density ρ and the HF potential $\Gamma = V\rho$ need not have the symmetries of the original Hamiltonian. For example, three dimensional rotational symmetry of Γ is very rare in HF and is possible only if complete spherical j shells are being filled with (2j+1) nucleons.

The question of the symmetry of the Hartree-Fock field Γ is related to the mixing among shell model orbits that is chosen and is often at our disposal while starting a HF iteration . Axial symmetry in Hartree-Fock (mixing among orbits with same m values) is always possible. Also one can always choose orbits of a definite parity, thus preserving reflection symmetry. However when the nuclear system prefers parity mixing, the parity-mixed solution will have a lower energy than the solution with good parity. A gross way to visualise a symmetry is to draw the equipotential surface obtained with the Hartree-Fock potential. Thus for spherical Hartree-Fock solution the equipotential surface is spherical, for an axially symmetric deformed solution the equipotential surface is deformed, but axially symmetric. Examples of such equipotential surfaces (with and without reflection symmetry) are shown in Figure 3.

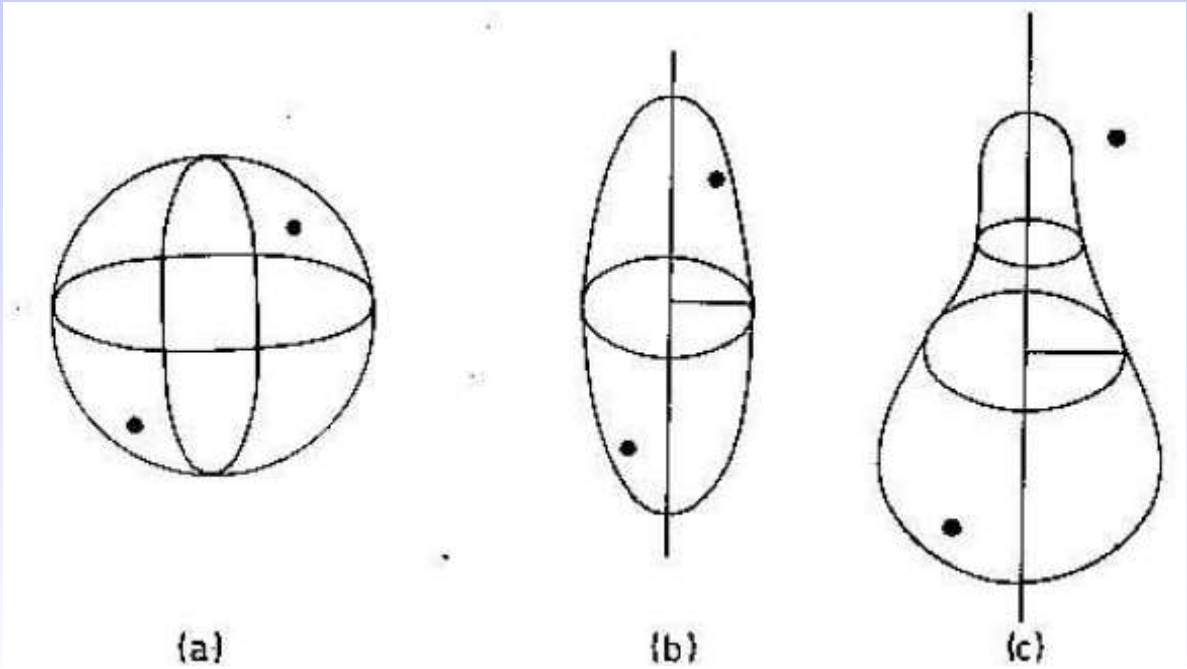

Figure 3: Equipotential surfaces for spherical symmetry (a), axial symmtry (b), (c). While (a) and (b) possess reflection symmetry, (c) lacks reflection symmetry.

When is a symmetry, originally present in the nuclear Hamiltonian H, still survives in the Hartree-Fock Hamiltonian $h = \epsilon + \Gamma$? Since the Hartree-Fock potential $\Gamma = V\rho$ depends on the HF orbits occupied, the matter of the symmetry of h is related to the nature of the occupied orbits. This condition is expressed by[4]:

The operator U commutes with h only if it leaves the set of occupied orbits invariant, ie, if it does not mix-up the occupied and unoccupied orbits.

Hartree-Fock Solutions without Reflection Symmetry

Superdeformed HF solutions in 84Zr

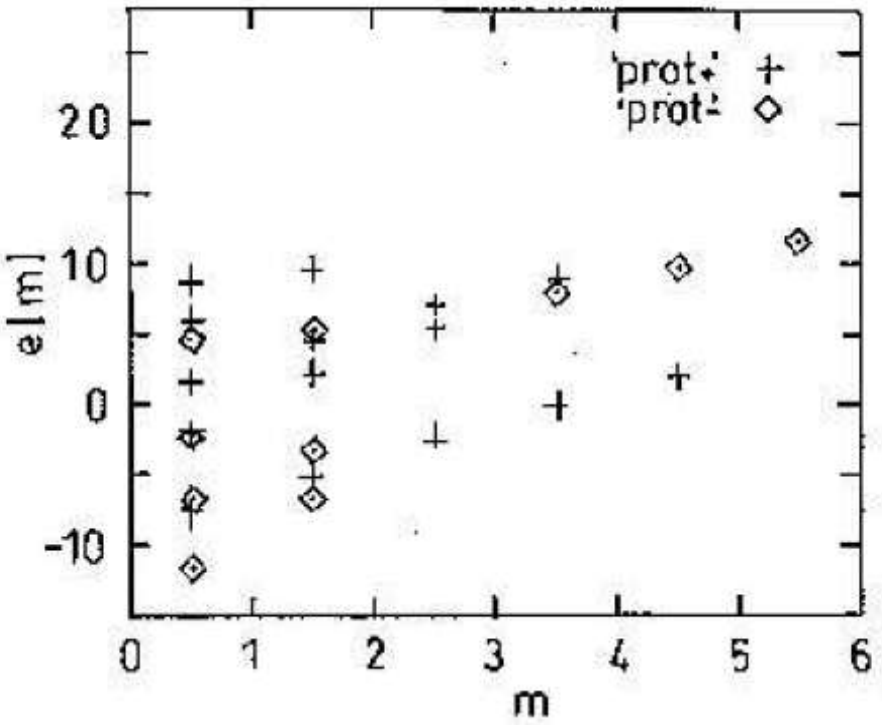

Figure 5(a): Proton HF orbits of superdeformed solution of ^{84}Zr.

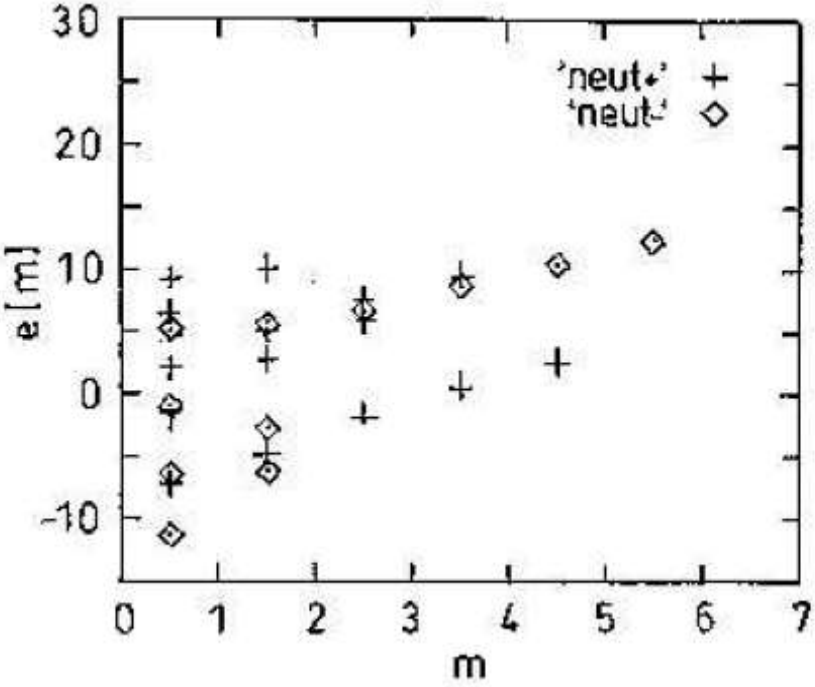

Figure 5(b): Neutron HF orbits of superdeformed solution of ^{84}Zr.

In Figure 6 the energy surface of the superdeformed configuration with respect to octupole deformation is shown, allowing for parity mixing in the Hartree-Fock solution and with an octupole driving term in the Hamiltonian.

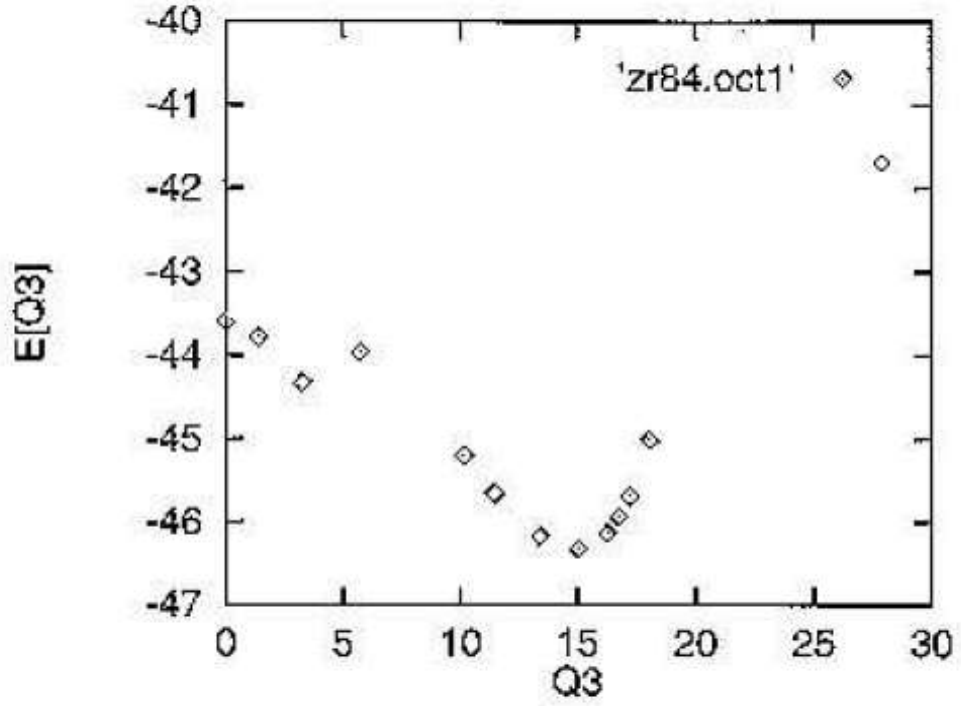

Figure 6: E_{HF} versus octupole deformation for ^{84}Zr

One sees that, among the superdeformed solutions, the lowest solution is a parity-mixed one with considerable octupole deformation. Such calculations showing the role of parity mixing in superdeformed configurations assume significance in view of the experimental discovery of superdeformed bands in the $N, Z \approx 40$ region[13].

RESTORATION OF ROTATIONAL SYMMETRY:

ANGULAR MOMENTUM PROJECTION:-

It is well-known that a deformed intrinsic state is a superposition of various states of good angular momentum

$$|\Phi_K\rangle = \sum_I C_{IK} |\Psi_{IK}\rangle \tag{18}$$

and one needs a projection operator to project out states of good angular momenta from the intrinsic state Φ_K. The angular momentum projection operator is[16,4,17,18]

$$P^{IM}_K = \frac{2I+1}{8\pi^2} \int d\Omega D^{I*}_{MK}(\Omega) R(\Omega) \tag{19}$$

Ω denotes the Euler angles α, θ, γ. $R(\Omega)$ is the rotation operator and D's are the D-functions (irreducible representations of the rotation group[89,90,85–87]).

The normalised state with angular momentum I and z-component M is

$$|\Psi_{IM}\rangle = \frac{1}{\sqrt{N^I_{KK}}} P^{IM}_K |\Phi_K\rangle \tag{20}$$

$$N^I_{K'K} = \langle \Phi_{K'} | P^{IK'}_K | \Phi_K \rangle = \frac{2I+1}{2} \int_0^\pi d\theta sin\theta d^I_{K'K}(\theta) \langle \Phi_{K'} | e^{-i\theta J_y} | \Phi_K \rangle \quad (21)$$

$$N^I_{KK} = \langle \Phi_K | P^{IK}_K | \Phi_K \rangle = (C_{IK})^2 \quad (22)$$

We give below the overlap matrix elements of various operators[4,17,21]

(a) Hamiltonian H=$H_{S.P.}$ + V
Multipole Tensor operators
(b) Q_2 (electric quadrupole),
(c) M_1 (magnetic dipole),
(d) $\vec{J} = \vec{J}_{coll} + \vec{J}_{RAL}$
(angular momenta contributed by collective rotation and by rotation-alignment)

$$\langle \Psi^I_{MK_2} | H | \Psi^I_{MK_1} \rangle = \frac{2I+1}{2} \frac{1}{(N^I_{K_1K_1} N^I_{K_2K_2})^{1/2}} \int_0^\pi d\theta sin\theta d^I_{K_2K_1}(\theta)$$
$$\times \langle \Phi_{K_2} | H e^{-i\theta J_y} | \Phi_{K_1} \rangle \quad (23)$$

For a multipole operator T^L of spherical rank L we have the reduced matrix element

$$\langle \Psi^{I_2}_{K_2} || T^L || \Psi^{I_1}_{K_1} \rangle = \frac{1}{2} \frac{(2I_1+1)(2I_2+1)^{1/2}}{(N^I_{K_1K_1} N^I_{K_2K_2})^{1/2}} \sum_\nu C^{I_1}_{K_2-\nu \ \ \nu \ \ K_2} \times \int_0^\pi d\theta sin\theta d^{I_1}_{K_2-\nu \ K_1}(\theta)$$
$$\times \langle \Phi_{K_2} | T^L_\nu e^{-i\theta J_y} | \Phi_{K_1} \rangle \quad (24)$$

66Zn : **Band-crossing and Rotation-Alignment :-**

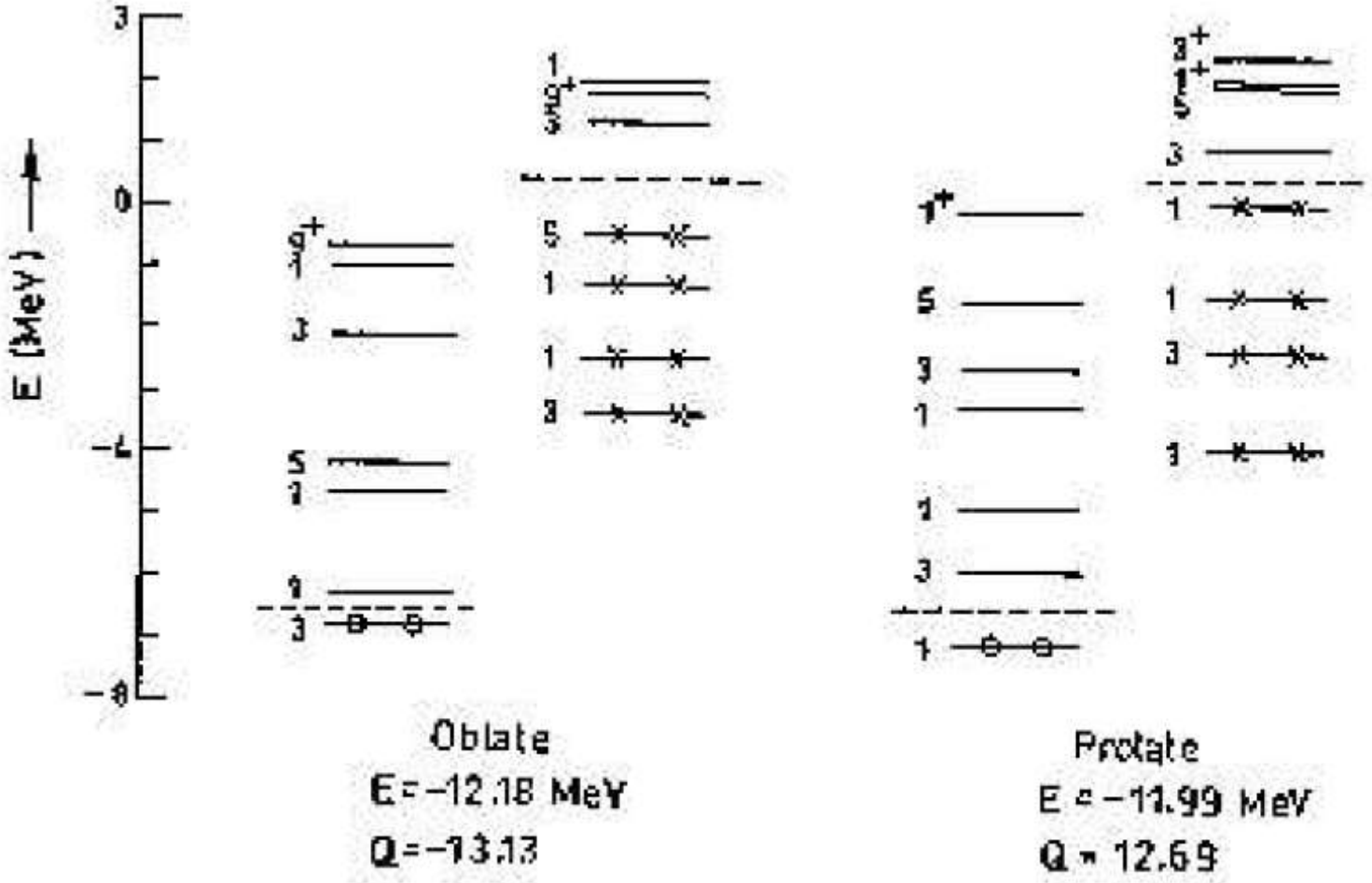

Fig. 8 Hartree-Fock orbits of ^{66}Zn.

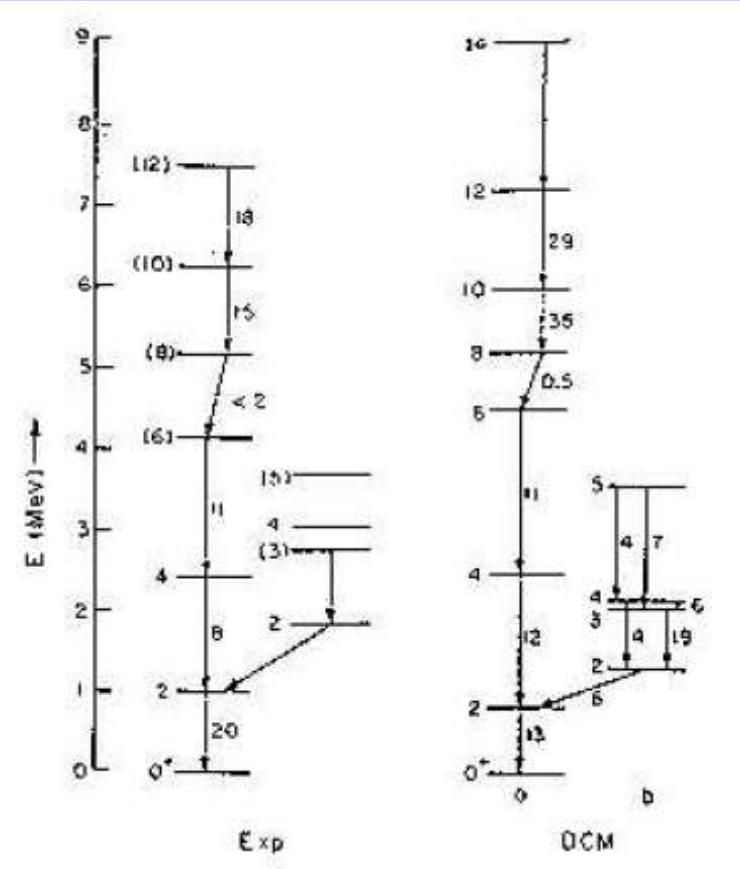

Fig. 9 Positive parity bands of ^{66}Zn. The numbers near arrows indicate $B(E2)$ values in W.u.

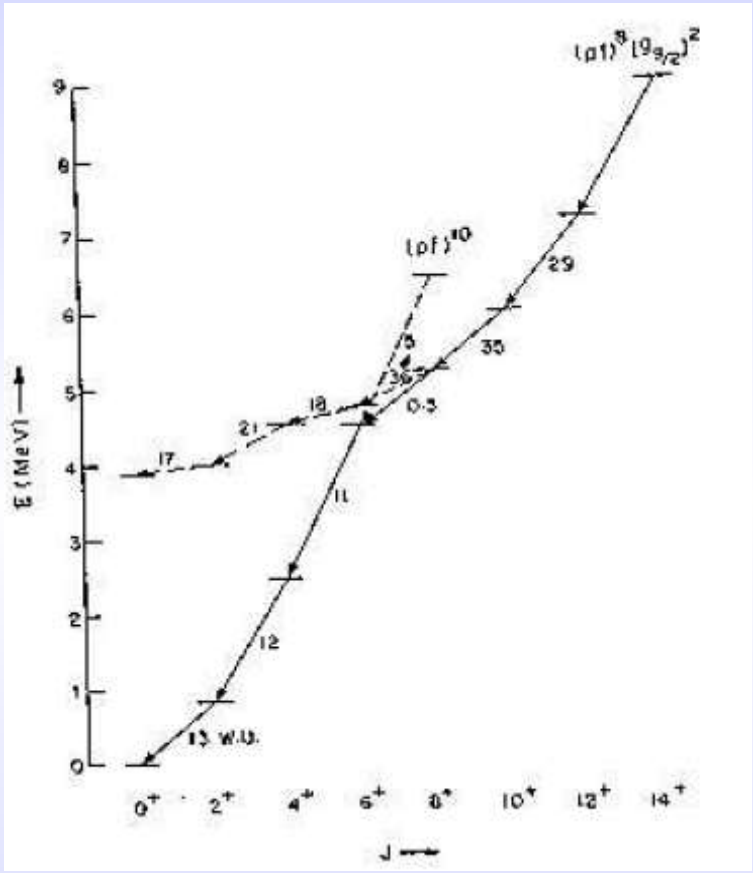

Figure 10: Crossing of the ground and RAL bands in ^{66}Zn.

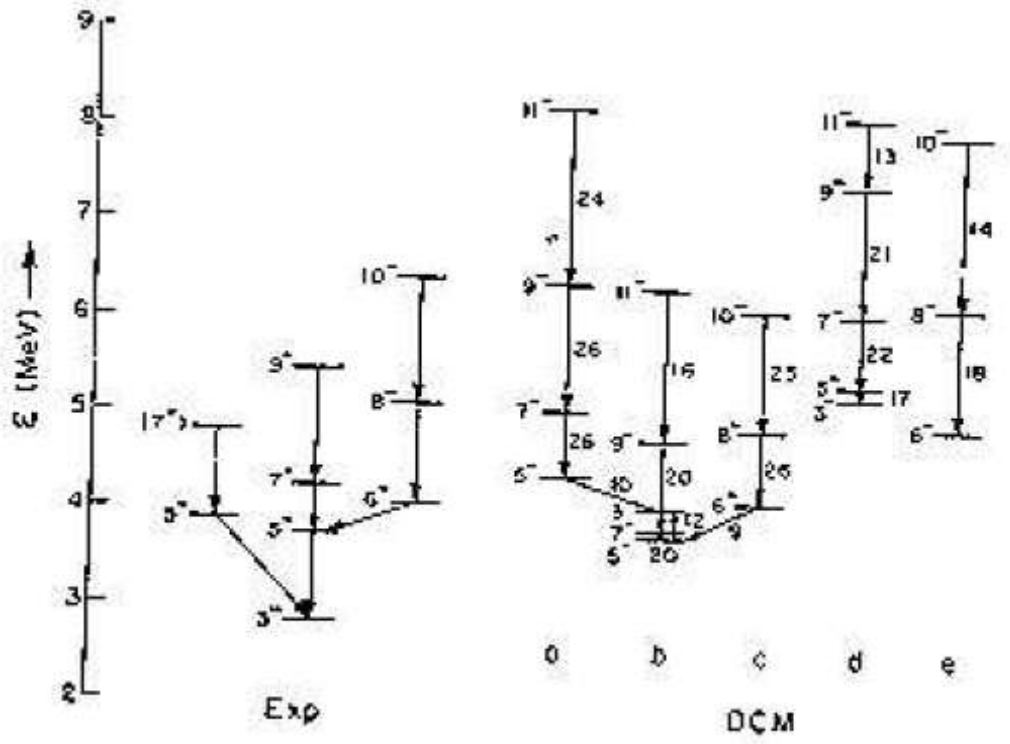

Figure 11: Negative parity bands of ^{66}Zn.

Angular momentum intensities in (a) K=0+ and RAL band (b,c).

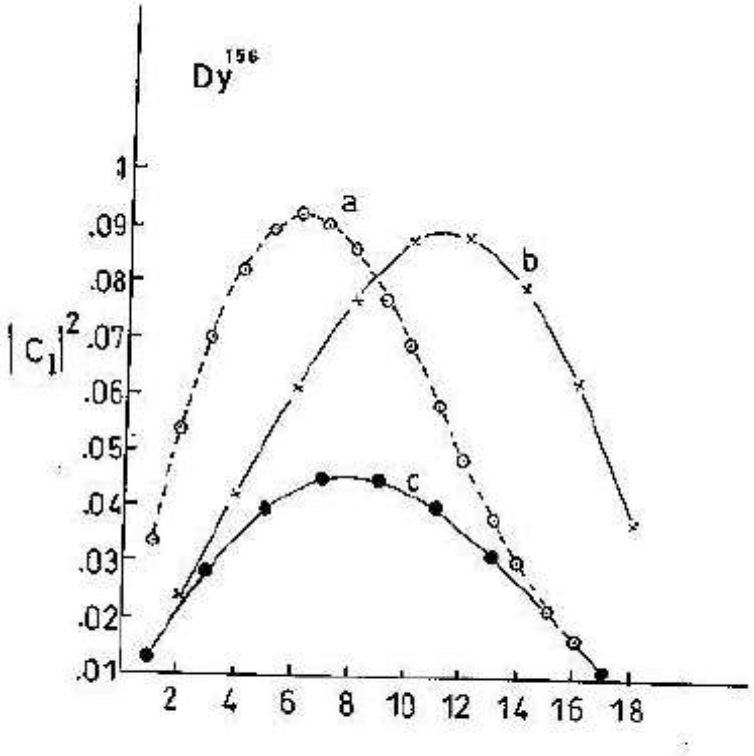

Figure 12: Intensities of angular momentum values for two $K = 1^+$ bands of ^{156}Dy. Note the staggering in C_I values (for even and odd I) for the RAL band and the significantly large intensity in the RAL even branch for high spins.

Bandcrossing andneutron RAL in 198Hg CRP and Khadkikar PRL 50, 1254 (1983)

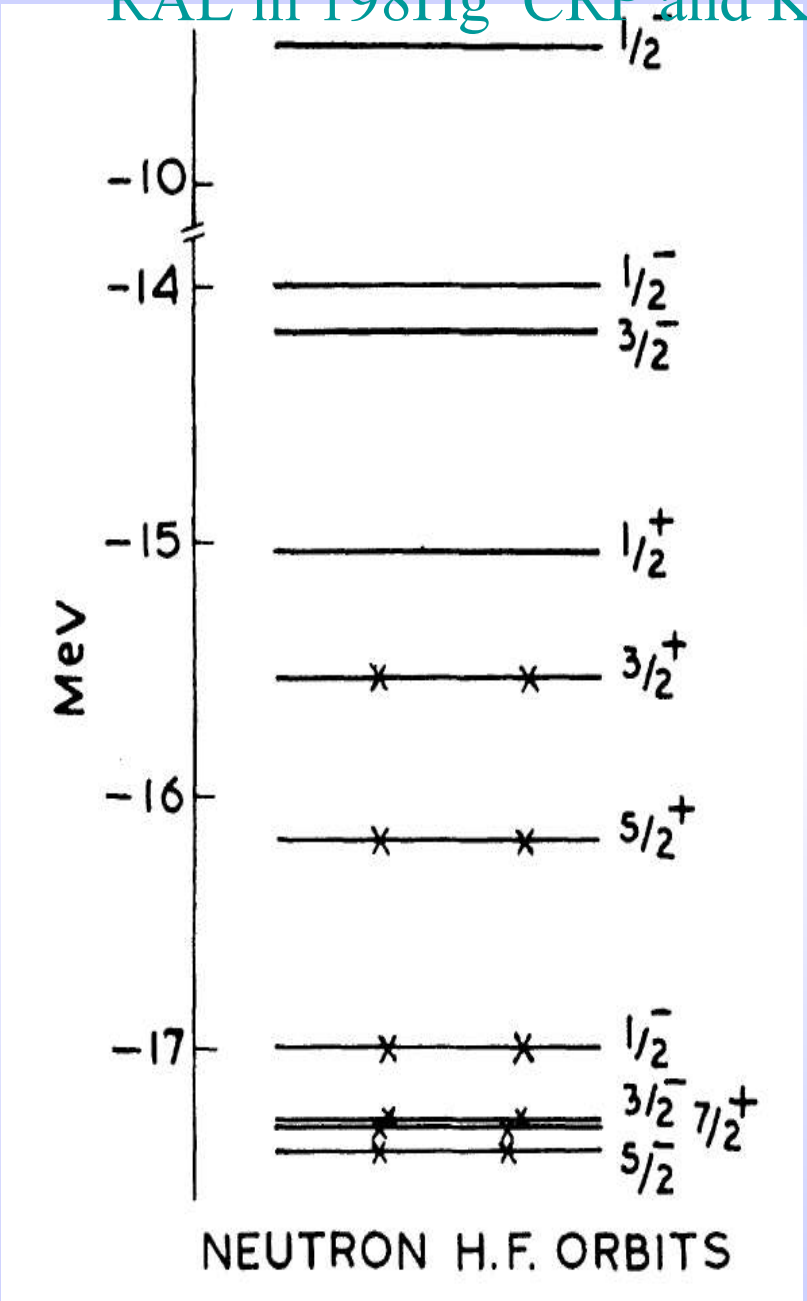

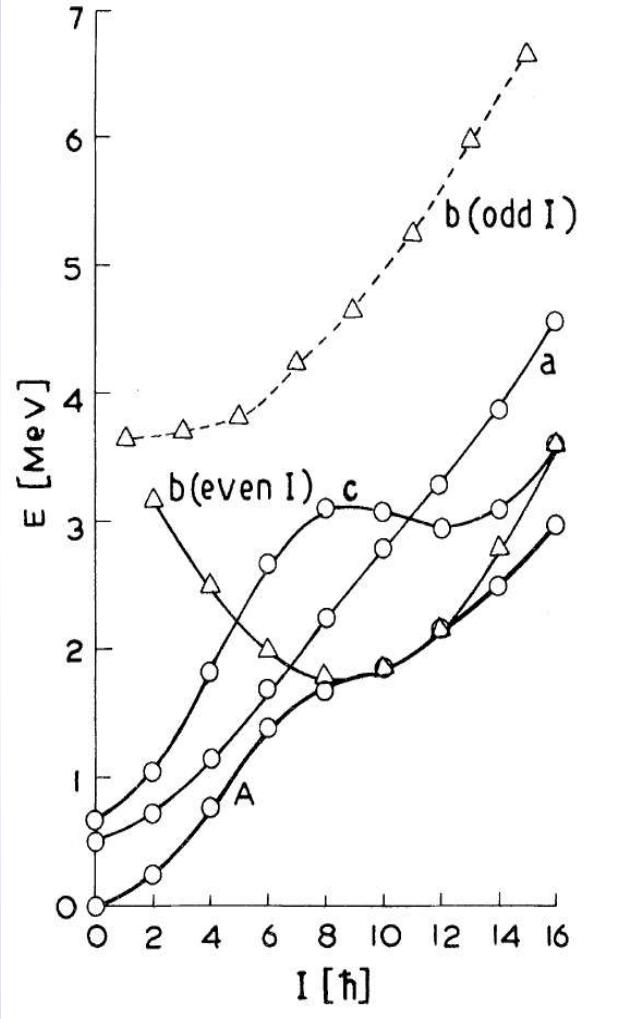
E [MeV]
I [ħ]
b (odd I)
b(even I)
a
c
A

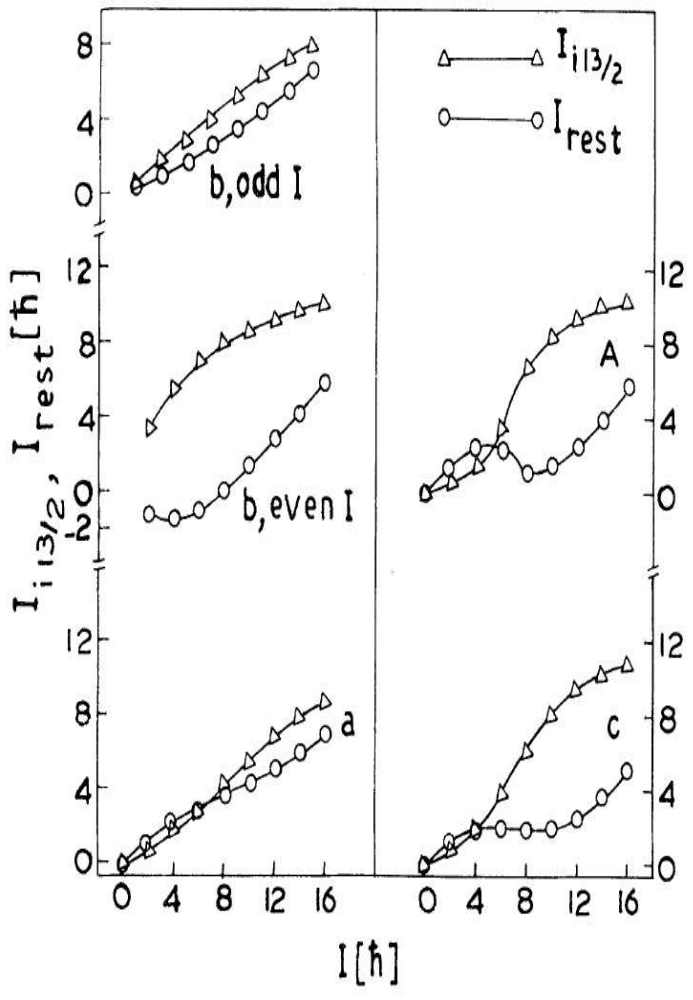
$I_{i13/2}$
I_{rest}
b,odd I
b,even I
a
A
c
$I_{i13/2}$, I_{rest}[ħ]
I[ħ]

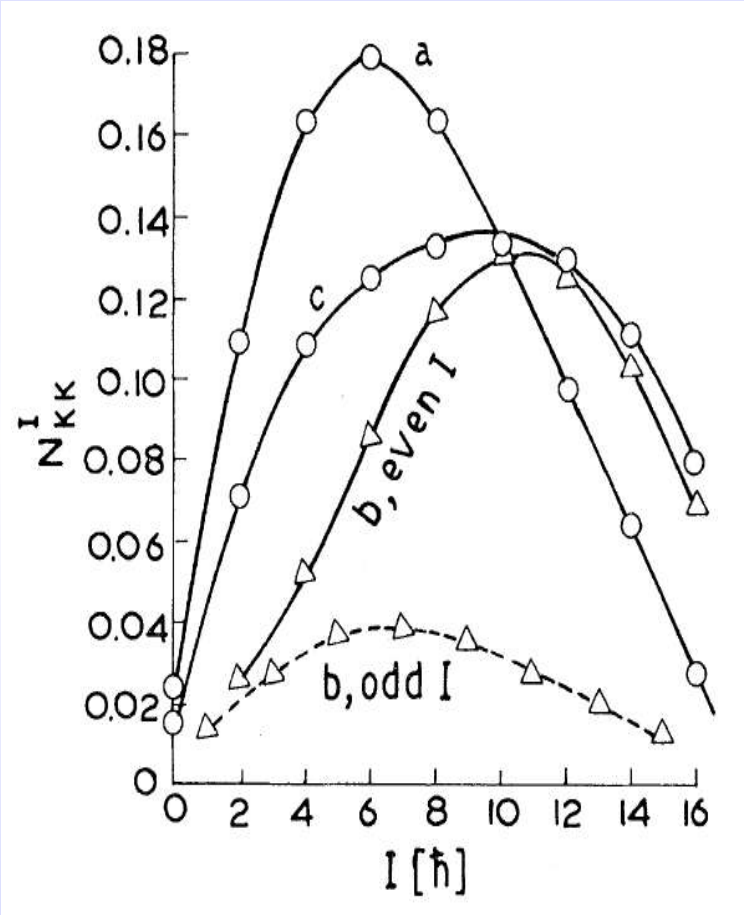
0.18
0.16
0.14
0.12
0.10
0.08
0.06
0.04
0.02
0
N^I_{KK}
a
c
b, even I
b, odd I
0 2 4 6 8 10 12 14 16
I [ħ]

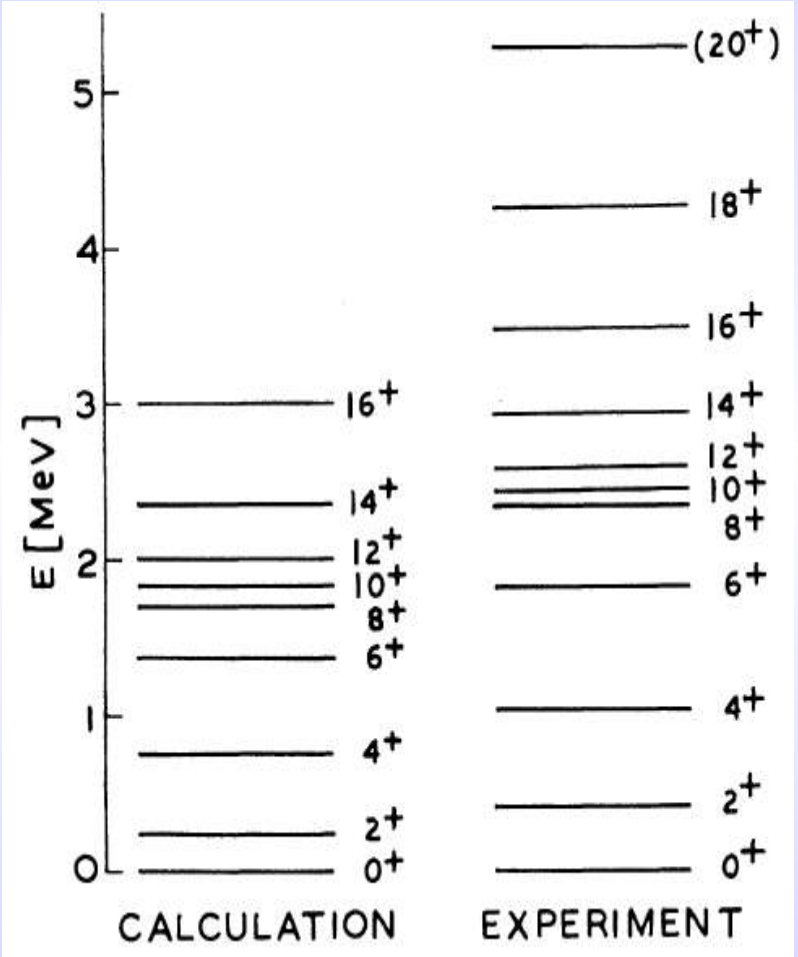
5
4
3
2
1
0
E [MeV]
16+
14+
12+
10+
8+
6+
4+
2+
0+
CALCULATION
(20+)
18+
16+
14+
12+
10+
8+
6+
4+
2+
0+
EXPERIMENT

Model Space in Rare-earth Region

- Orbits for protons are $3s_{1/2}$, $2d_{3/2}$, $2d_{5/2}$, $1g_{7/2}$, $1h_{9/2}$, $1h_{11/2}$ and orbits for neutrons are $3p_{1/2}$, $3p_{3/2}$, $2f_{5/2}$, $2f_{7/2}$, $1h_{9/2}$, $1i_{13/2}$.
- ^{132}Sn is considered as spherical inert core.

Table 1: Single Particle Energies of Protons and Neutrons.

Proton	$g_{7/2}$	$d_{5/2}$	$s_{1/2}$	$d_{3/2}$	$h_{11/2}$	$h_{9/2}$
[MeV]	0	0.731	3.654	3.288	2.305	7.1
Neutron	$f_{7/2}$	$p_{3/2}$	$f_{5/2}$	$h_{9/2}$	$p_{1/2}$	$i_{13/2}$
[MeV]	0	2.974	3.432	0.686	4.462	1.487

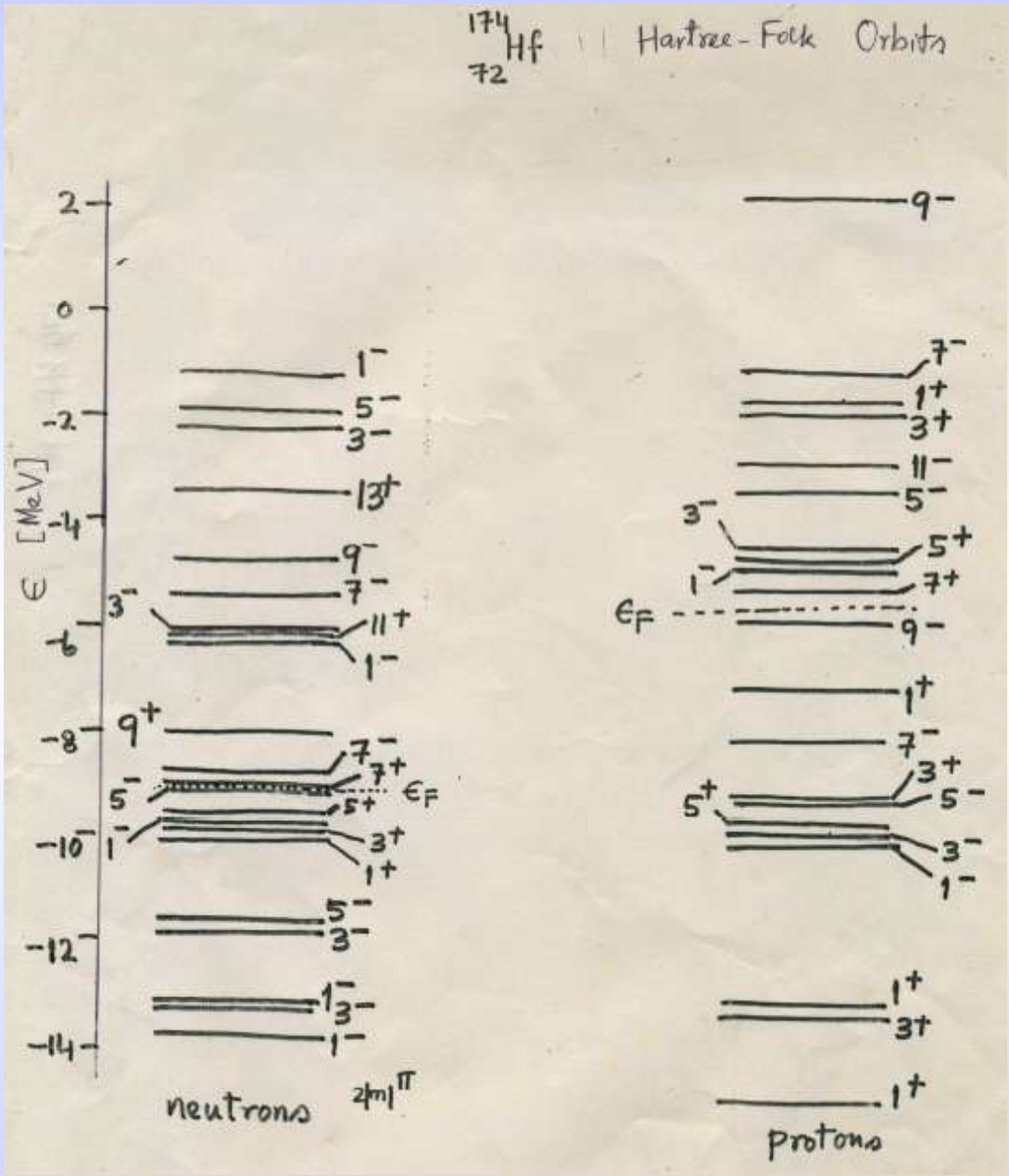
174 72 Hf
Hartree-Fock Orbits
ε [MeV]
2
0
-2
-4
-6
-8
-10
-12
-14
1⁻
5⁻
3⁻
13⁺
9⁻
7⁻
3⁻
11⁺
1⁻
9⁺
7⁻
7⁺
5⁻
5⁺
εF
1⁻
3⁺
1⁺
5⁻
3⁻
1⁻
3⁻
1⁻
neutrons
2hω
9⁻
7⁻
1⁺
3⁺
11⁻
5⁻
3⁻
5⁺
1⁻
7⁺
εF
9⁻
1⁺
7⁻
5⁺
3⁺
5⁻
3⁻
1⁻
1⁺
3⁺
1⁺
protons

HF orbits for ^{171}Lu

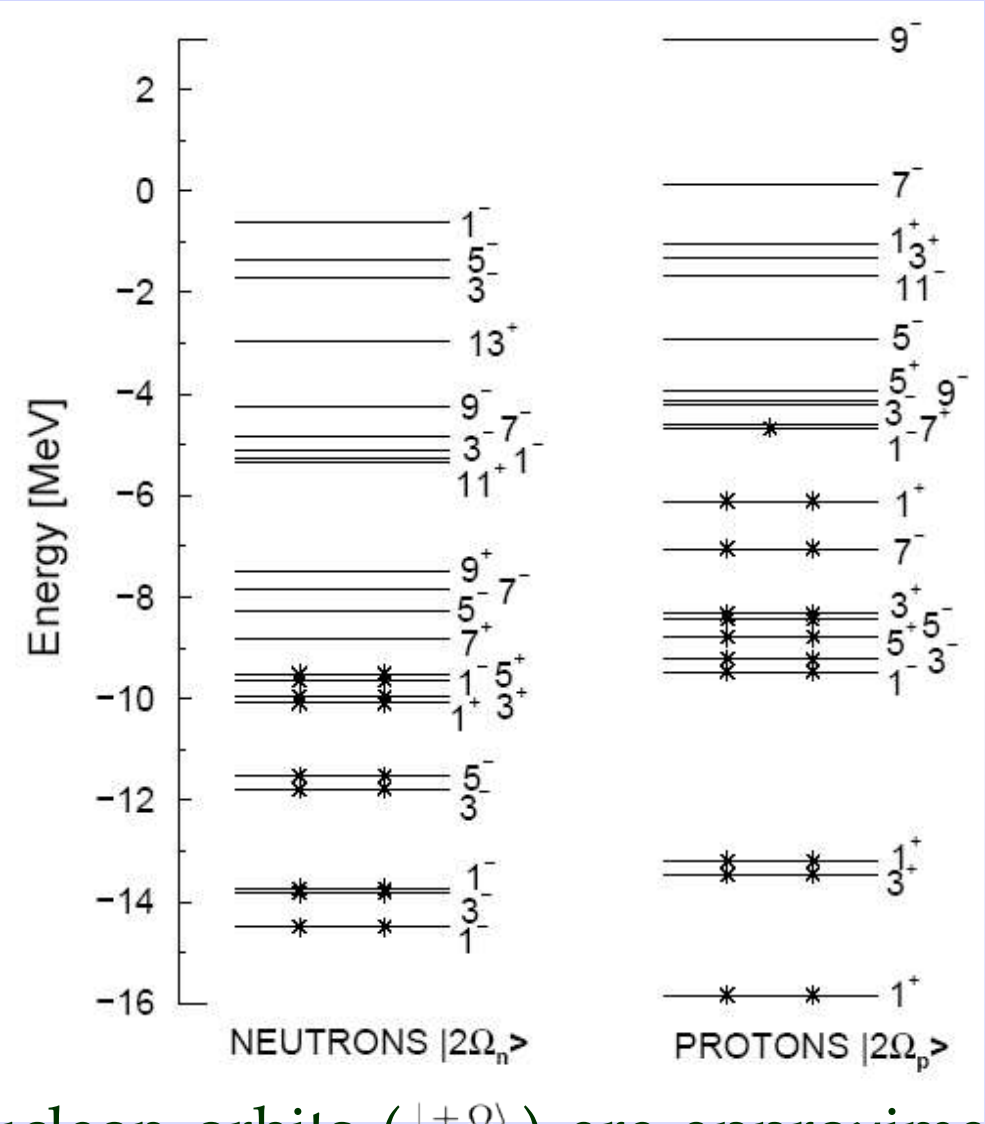

The nucleon orbits ($|\pm\Omega\rangle$) are approximately two fold degenerate.

Angular Momentum (J) Projection

- From the HF single particle orbits, HF intrinsic and particle-hole intrinsic states are constructed by J projection.
- Intrinsic state $|\phi_K\rangle$ does not have a unique J quantum number.

$$|\phi_K\rangle = \sum_J C_K^J |\Psi_{JK}\rangle$$

- By angular momentum projection from intrinsic states the spectra and other spectroscopic properties are obtained.

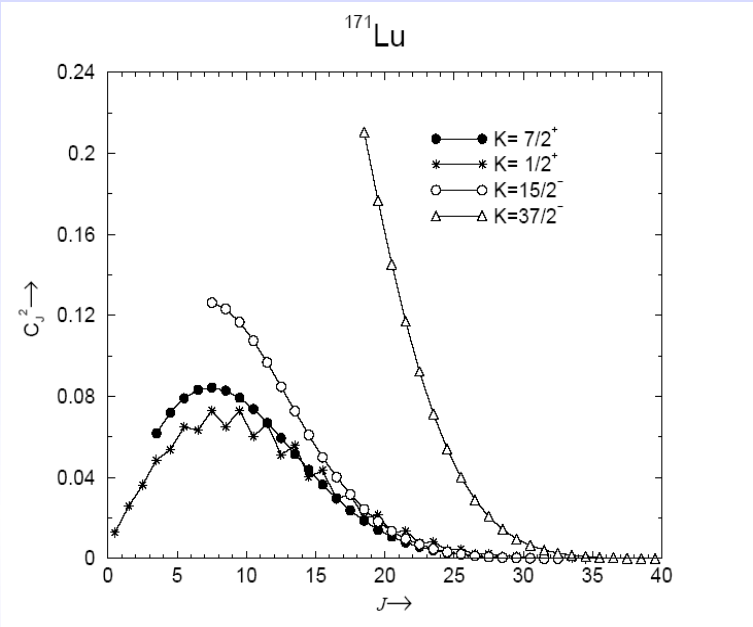

- Angular momentum projection operator is

$$P_K^{JM} = \frac{2J+1}{8\pi^2} \int d\Omega \; D_{MK}^J(\Omega)^* \; R(\Omega)$$

Where $R(\Omega)$ = $e^{-i\alpha J_z} e^{-i\beta J_y} e^{-i\gamma J_z}$

Band-mixing

- In general, two states $|\Psi^{JM}_{K_1}\rangle$ and $|\Psi^{JM}_{K_2}\rangle$ projected from two intrinsic configurations are not orthogonal to each other even if $|\phi_{K_1}\rangle$ and $|\phi_{K_2}\rangle$ are orthogonal.

- Thus, whenever necessary, we do band-mixing using the following equation to get better results.

$$\sum_{K'}(H^J_{KK'} - E_J N^J_{KK'})C^J_{K'} = 0$$

Results for Lu, Re, Nd and K Isomeric bands are given below:

Regular and irregular bands

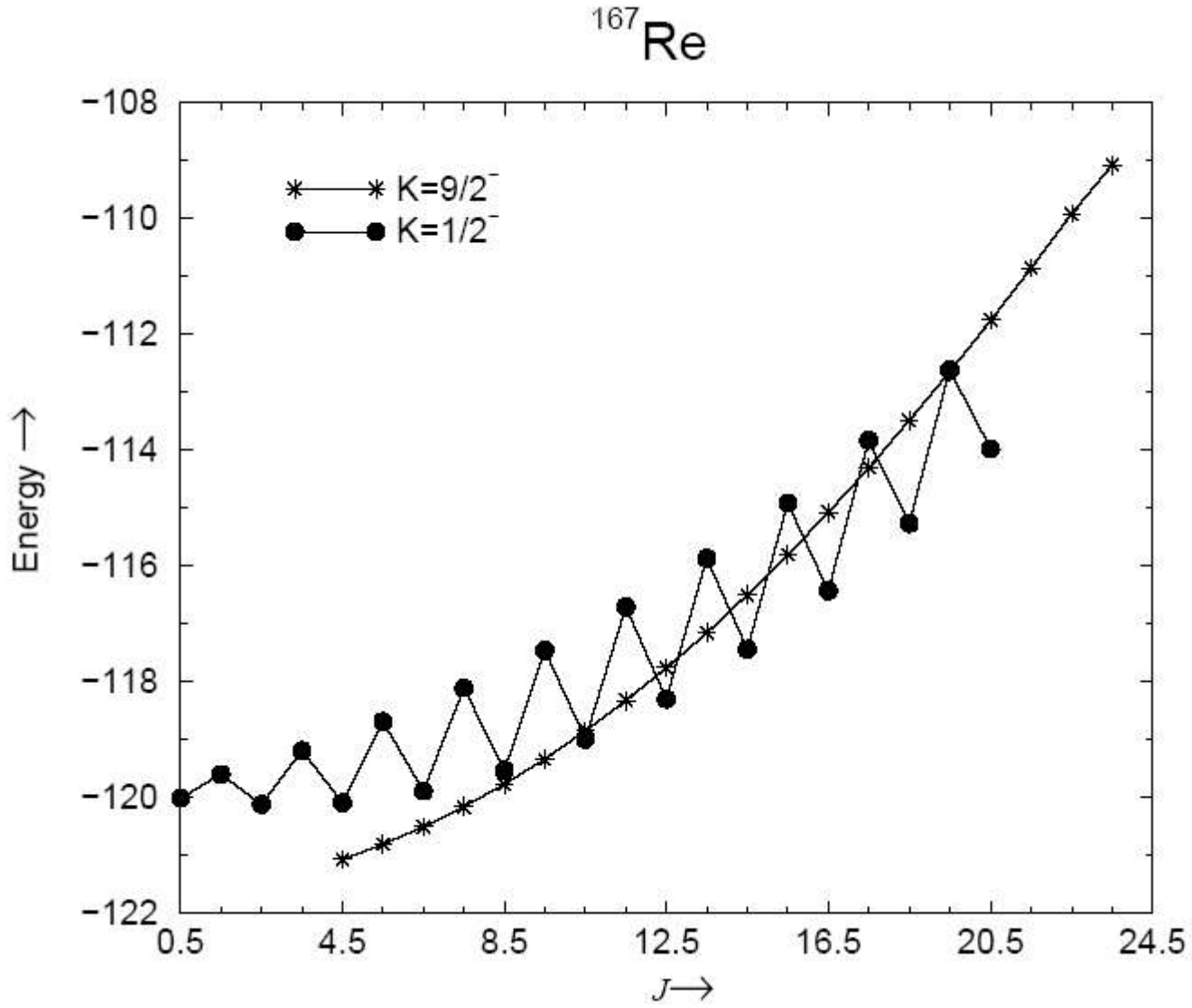

Table 2: Band Head Energies (BHE), Spectroscopic quadrupole moment (Q_S) and Magnetic moment (μ) for ^{169}Lu. Since static quadrupole moment vanishes for J=1/2, the theoretical quadrupole moments are given for J=3/2 and J=5/2 states of K=1/2 bands. The three bands below the dotted line are 3-quasiparticle bands.

		BHE [MeV]		Q_S [eb]		μ [μ_n]	
K^π	Conf.	Th.	Exp.	Th.	Exp.	Th.	Exp.
$1/2^+$	$\pi\frac{1}{2}^+[411]$	0.203	0.0974			0.013	
	(J=3/2)	0.182	0.115	-1.242, -1.776			
$1/2^-$	$\pi\frac{1}{2}^-[541]$	0.327	0.029			$1.13^\dagger$	0.538^{r1}
	(J=5/2)	0.277	0.0429	-1.432, -2.075			
$5/2^+$	$\pi\frac{5}{2}^+[402]$	.638	0.1862	2.356		2.54	
$7/2^+$	$\pi\frac{7}{2}^+[404]$	0	0	3.07	3.48	2.41	2.295^{r1}
$9/2^-$	$\pi\frac{9}{2}^-[514]$	.779	0.4391	3.659		4.599	
.....	.....	.....	.....	.....	.....	.....	.....
$15/2^-$	(a)*	1.646		4.419		2.101	
$9/2^-$	(b)*	1.492		3.732		3.033	
$9/2^+$	(c)*	1.899		3.865		0.091	

* Three quasiparticle configurations a, b and c are given in Subsection 3.3

Table 3: Same as Table 2 for ^{171}Lu.

		BHE [MeV]		Q_S [eb]		μ [μ_n]	
K^π	Conf.	Th.	Exp.	Th.	Exp.	Th.	Exp.
$1/2^+$	$\pi\frac{1}{2}^+[411]$	0.757	0.208			0.084	
	(J=3/2)	0.753	0.221	-1.552, -2.216			
$1/2^-$	$\pi\frac{1}{2}^-[541]$	0.0597	0.071			1.153†	0.585^{r1}
	(J=5/2)	0.016	0.073	-1.483, -2.145			
$5/2^+$	$\pi\frac{5}{2}^+[402]$	0.634	0.295	2.445		2.523	
$7/2^+$	$\pi\frac{7}{2}^+[404]$	0	0	3.186	3.525	2.397	2.293^{r1}, 2.03^{r2}
$9/2^-$	$\pi\frac{9}{2}^-[514]$	0.468	0.469	3.975		4.723	
.....	.....	.....	.....	.....	.....	.....	.....
$15/2^-$	(a)	0.936	1.241	4.589		2.448	
$9/2^-$	(b)	1.666	—*	3.822		3.010	
		$2.287_{(21/2^-)}$**	1.844				
$9/2^+$	(c)	1.182	—*	3.974		0.148	
		$1.353_{(13/2^+)}$**	1.269				

* the bandheads have not been experimentally observed so far

** experimentally observed states

†Inclusion of $f_{7/2}$ proton orbit reduces μ by about 1/2 [29].

^{r1} from ref. [27] and ^{r2} from ref. [17]

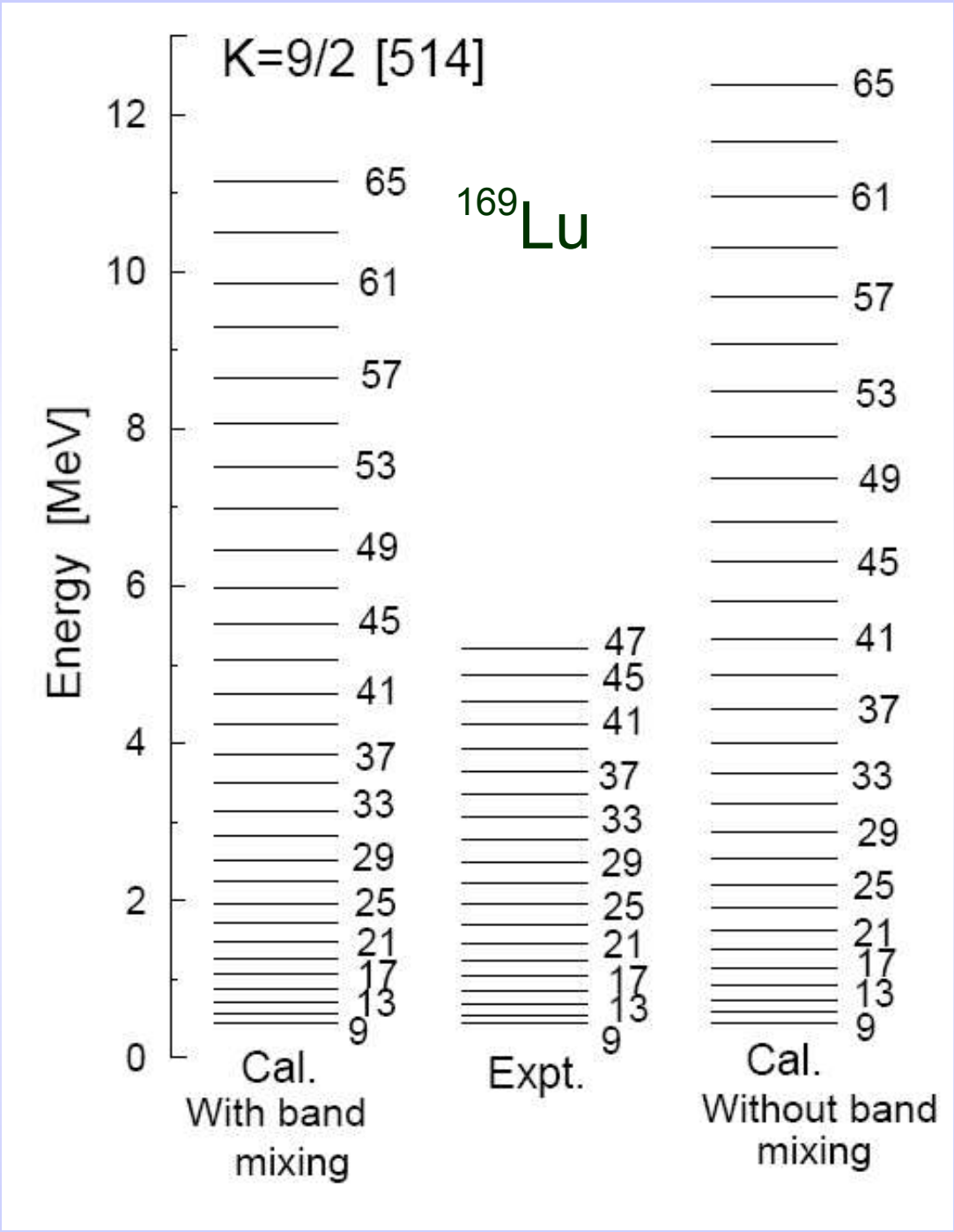
K=9/2 [514]
^{169}Lu
Energy [MeV]
0
2
4
6
8
10
12
65
61
57
53
49
45
41
37
33
29
25
21
17
13
9
Cal.
With band
mixing
47
45
41
37
33
29
25
21
17
13
9
Expt.
65
61
57
53
49
45
41
37
33
29
25
21
17
13
9
Cal.
Without band
mixing

^{169}Lu

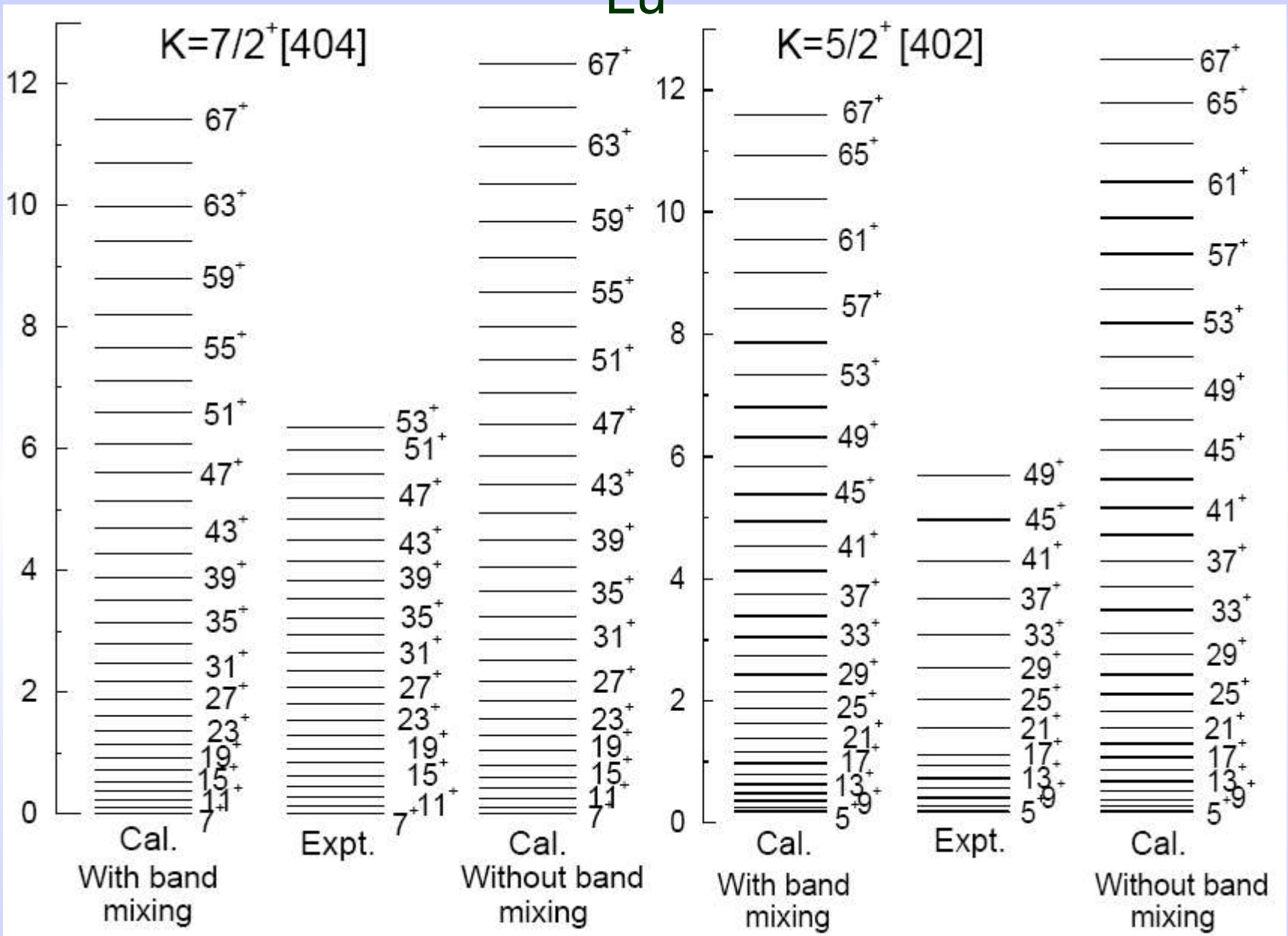
K=7/2+[404]
K=5/2+ [402]
Cal.
With band mixing
Expt.
Cal.
Without band mixing
Cal.
With band mixing
Expt.
Cal.
Without band mixing

^{171}Lu ^{173}Lu

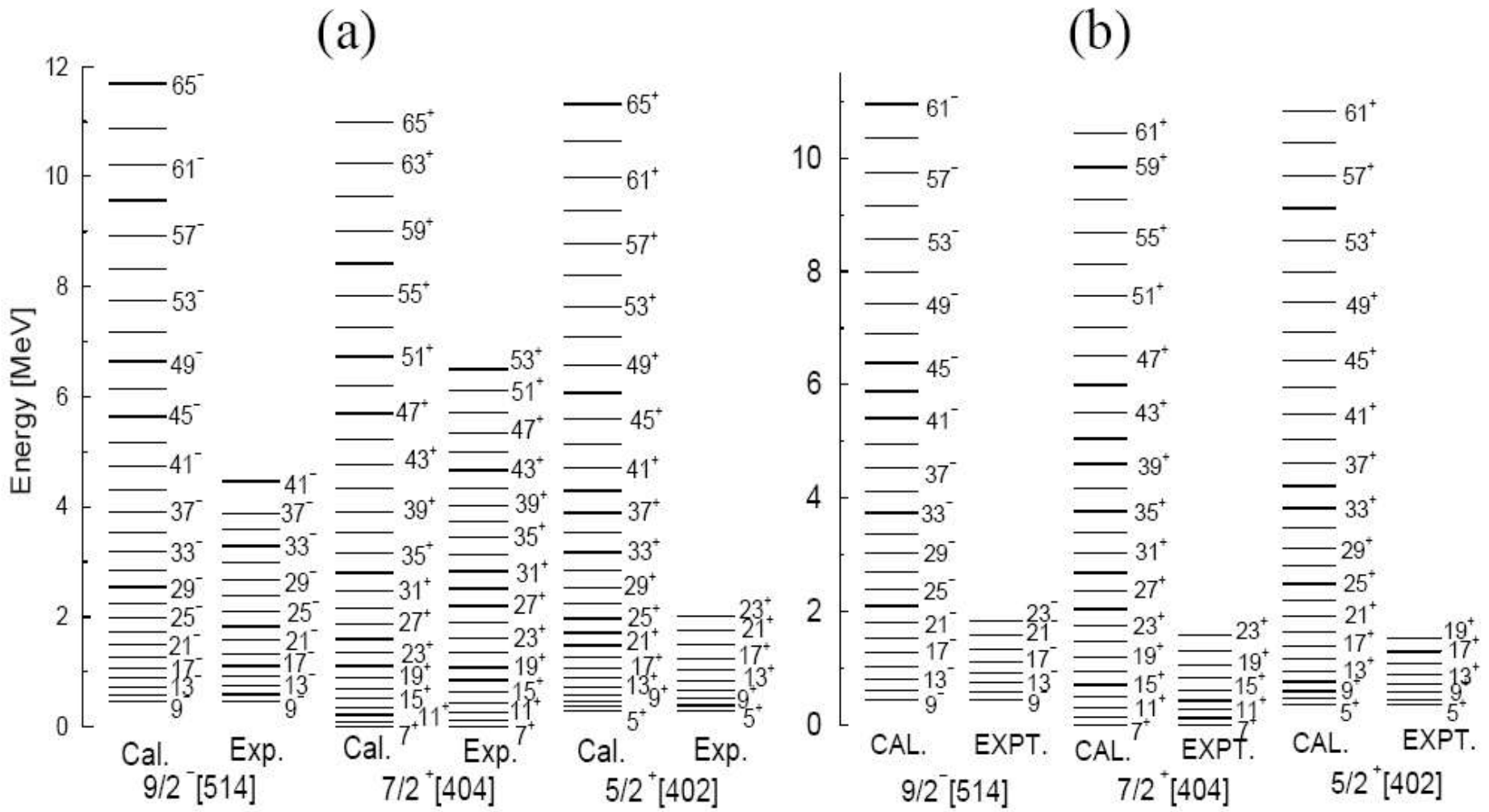

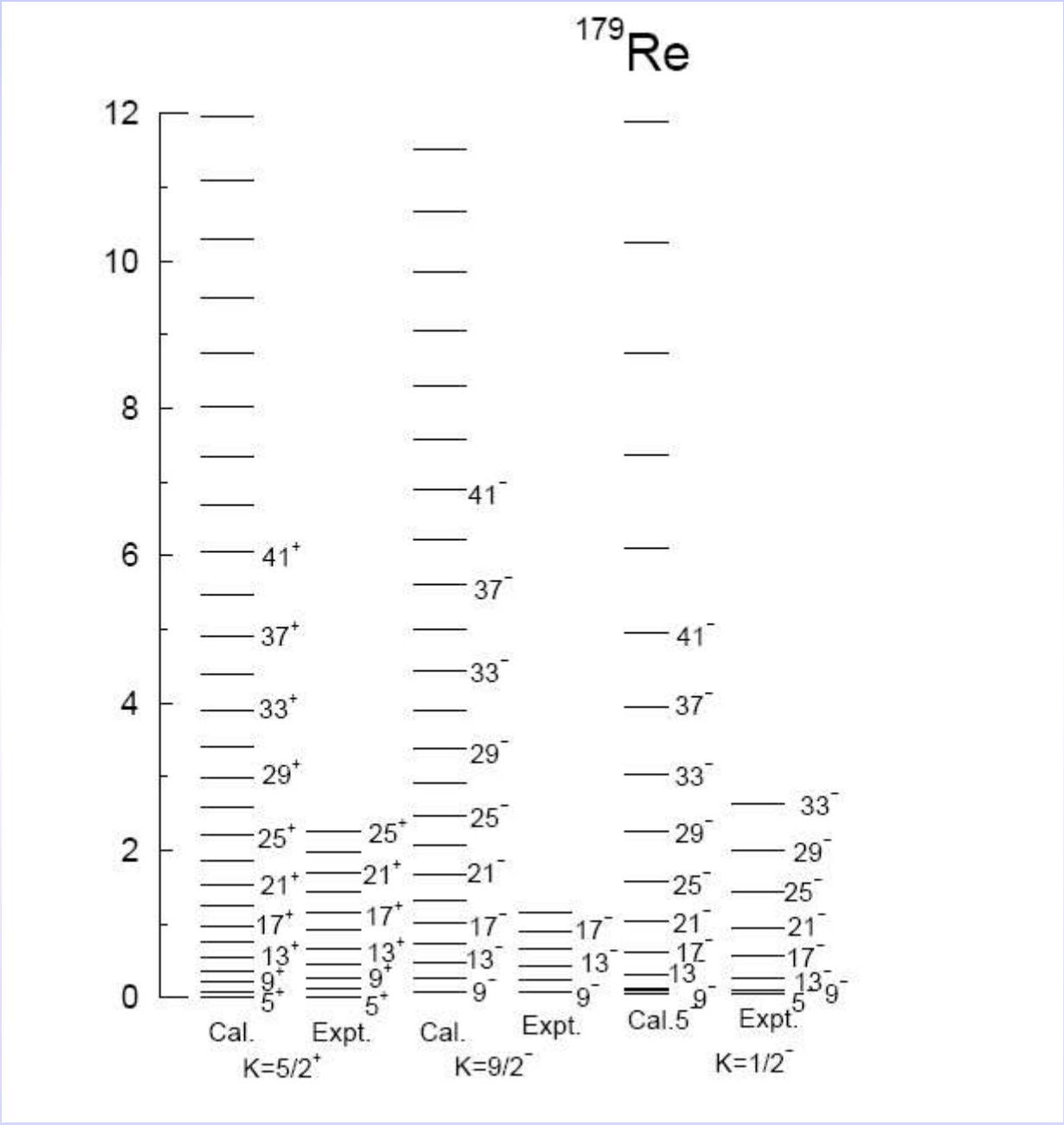
179Re
12
10
8
6
4
2
0
41+
37+
33+
29+
25+
21+
17+
13+
9+
5+
25+
21+
17+
13+
9+
5+
41-
37-
33-
29-
25-
21-
17-
13-
9-
17-
13-
9-
41-
37-
33-
29-
25-
21-
17-
13-
9-
5
33-
29-
25-
21-
17-
13-
9-
5
Cal.
Expt.
Cal.
Expt.
Cal.
Expt.
K=5/2+
K=9/2-
K=1/2-

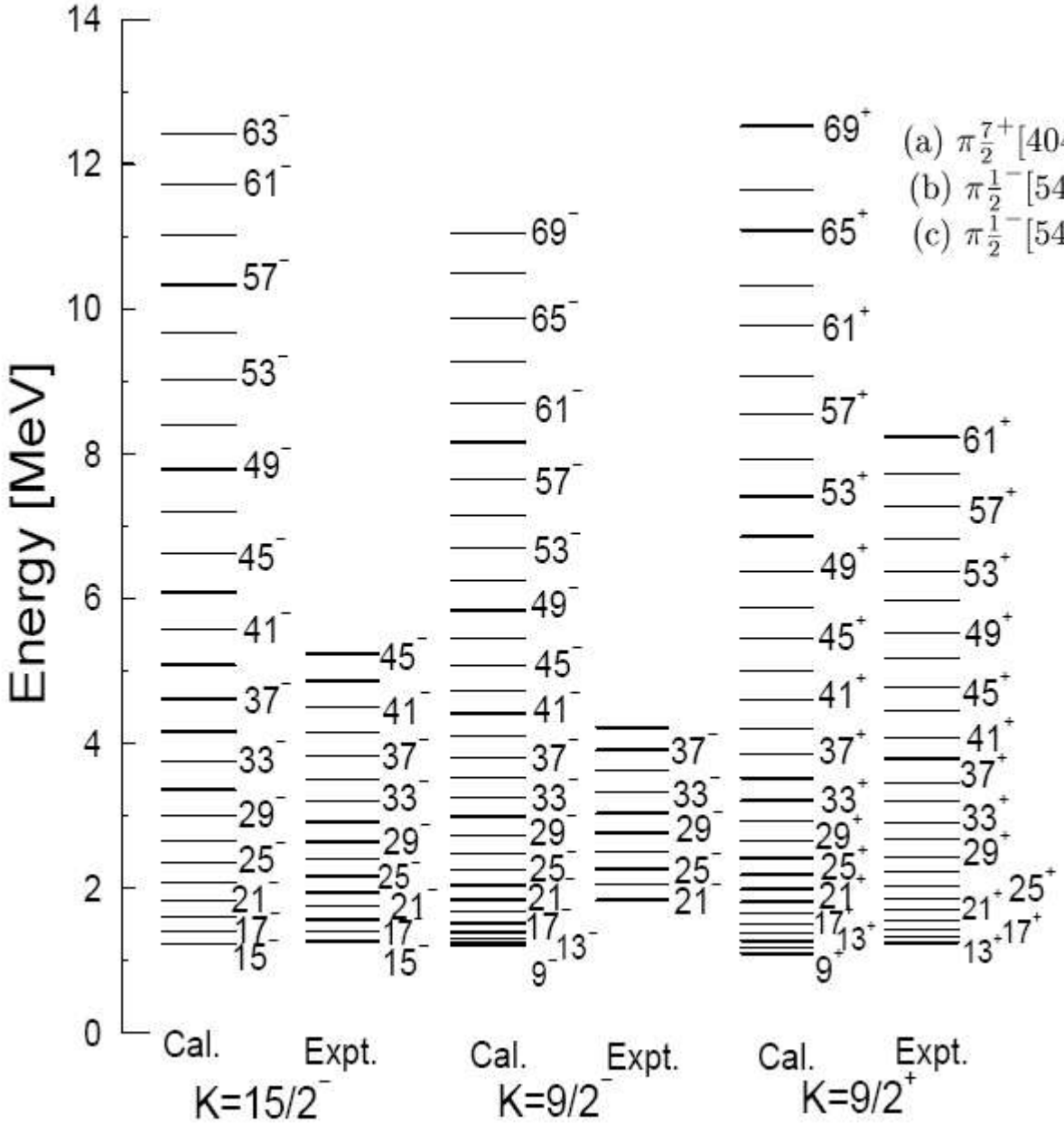

(a) $\pi\frac{7}{2}^{+}[404] \otimes \nu\frac{7}{2}^{+}[633] \otimes \nu\frac{1}{2}^{-}[521]$ $K = \frac{15}{2}^{-}$

(b) $\pi\frac{1}{2}^{-}[541] \otimes \pi\frac{1}{2}^{+}[411] \otimes \pi\frac{7}{2}^{+}[404]$ $K = \frac{9}{2}^{-}$

(c) $\pi\frac{1}{2}^{-}[541] \otimes \nu\frac{7}{2}^{+}[633] \otimes \nu\frac{1}{2}^{-}[521]$ $K = \frac{9}{2}^{+}$

^{171}Lu

3qp bands

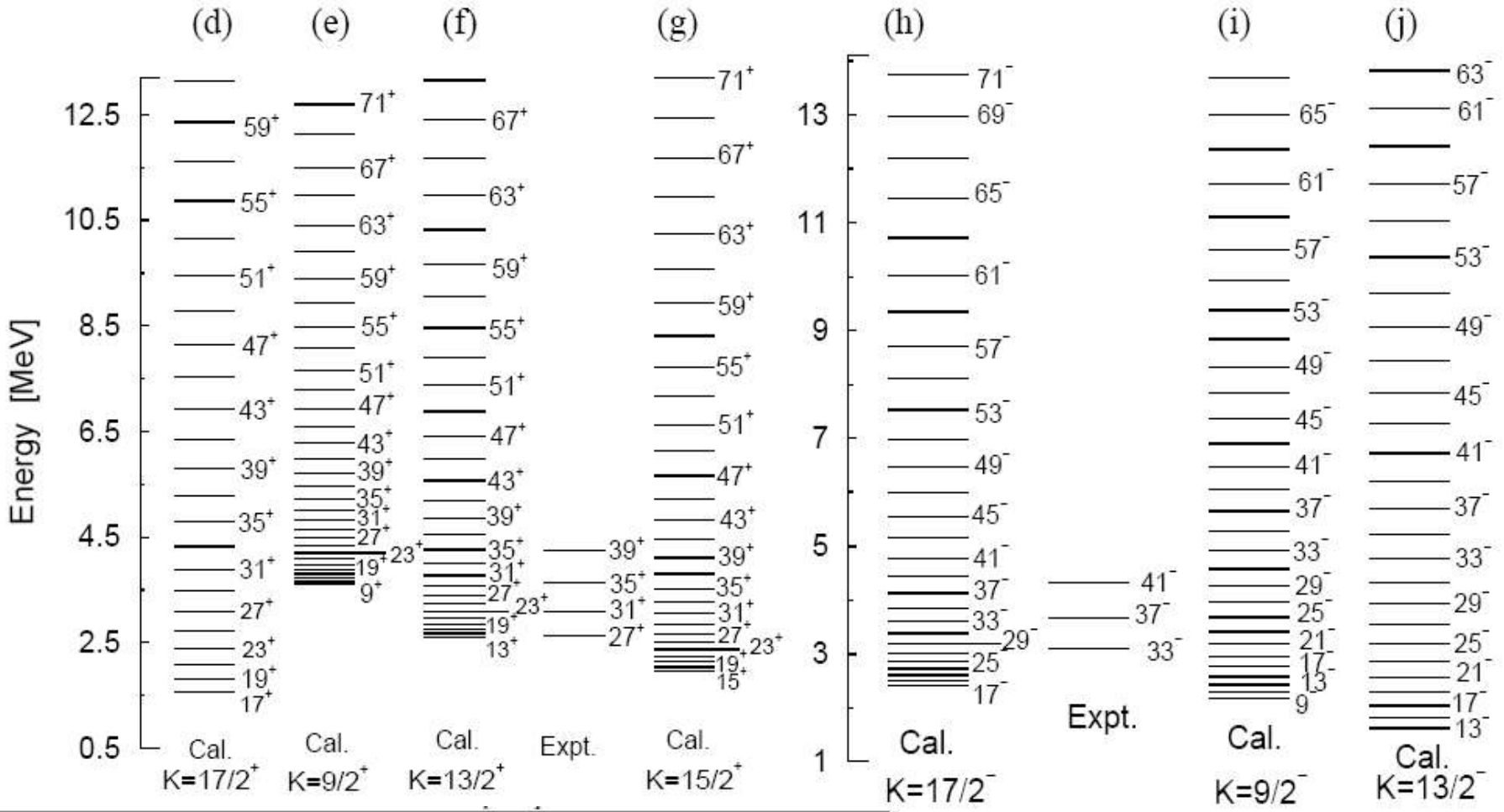

K^π	Conf.	BHF [MeV] Th.	Q_S [eb] Th.	μ [μ_n] Th.
(d) $17/2^+$	$\pi\frac{9}{2}^-[514] \otimes \nu\frac{7}{2}^+[633] \otimes \nu\frac{1}{2}^-[521]$	1.567	4.931	4.571
(e) $9/2^+$	$\pi\frac{1}{2}^+[411] \otimes \nu\frac{7}{2}^+[633] \otimes \nu\frac{1}{2}^+[660]$	3.619	4.151	-0.243
(f) $13/2^+$	$\pi\frac{5}{2}^+[402] \otimes \nu\frac{7}{2}^+[633] \otimes \nu\frac{1}{2}^+[660]$	2.599	4.344	2.419
(g) $15/2^+$	$\pi\frac{7}{2}^+[404] \otimes \nu\frac{7}{2}^+[633] \otimes \nu\frac{1}{2}^+[660]$	1.959	4.574	2.069
(h) $17/2^-$	$\pi\frac{9}{2}^-[514] \otimes \nu\frac{7}{2}^+[633] \otimes \nu\frac{1}{2}^+[660]$	2.409	4.863	4.361
(i) $9/2^-$	$\pi\frac{1}{2}^+[411] \otimes \nu\frac{7}{2}^+[633] \otimes \nu\frac{1}{2}^-[521]$	2.174	4.197	-0.047
(j) $13/2^-$	$\pi\frac{5}{2}^+[402] \otimes \nu\frac{7}{2}^+[633] \otimes \nu\frac{1}{2}^-[521]$	1.629	4.406	2.622

^{171}Lu

quasiparticle bands (d)−(j) of Table VIII. Inspection of level spacings suggests that the positive and negative parity bands could be of $K=13/2^+$ [band (f)] and $K=17/2^-$ [band (h)] origin, respectively.

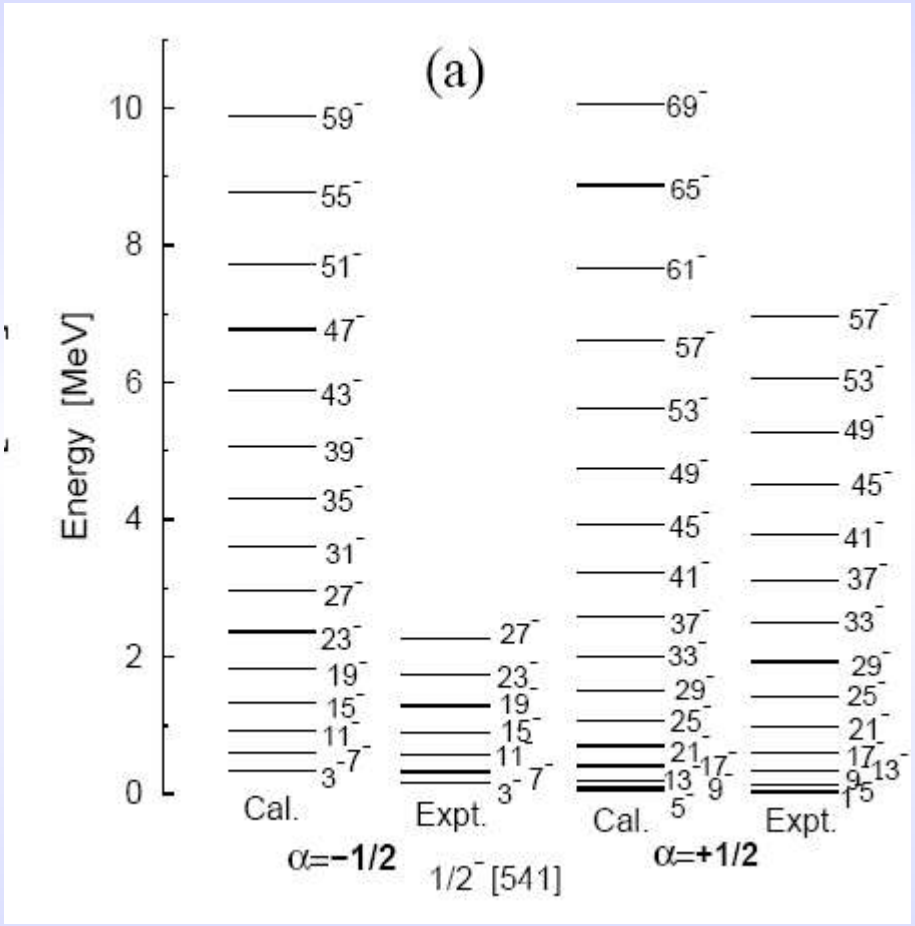
(a)
Energy [MeV]
Cal.
Expt.
Cal.
Expt.
α=−1/2
1/2⁻ [541]
α=+1/2

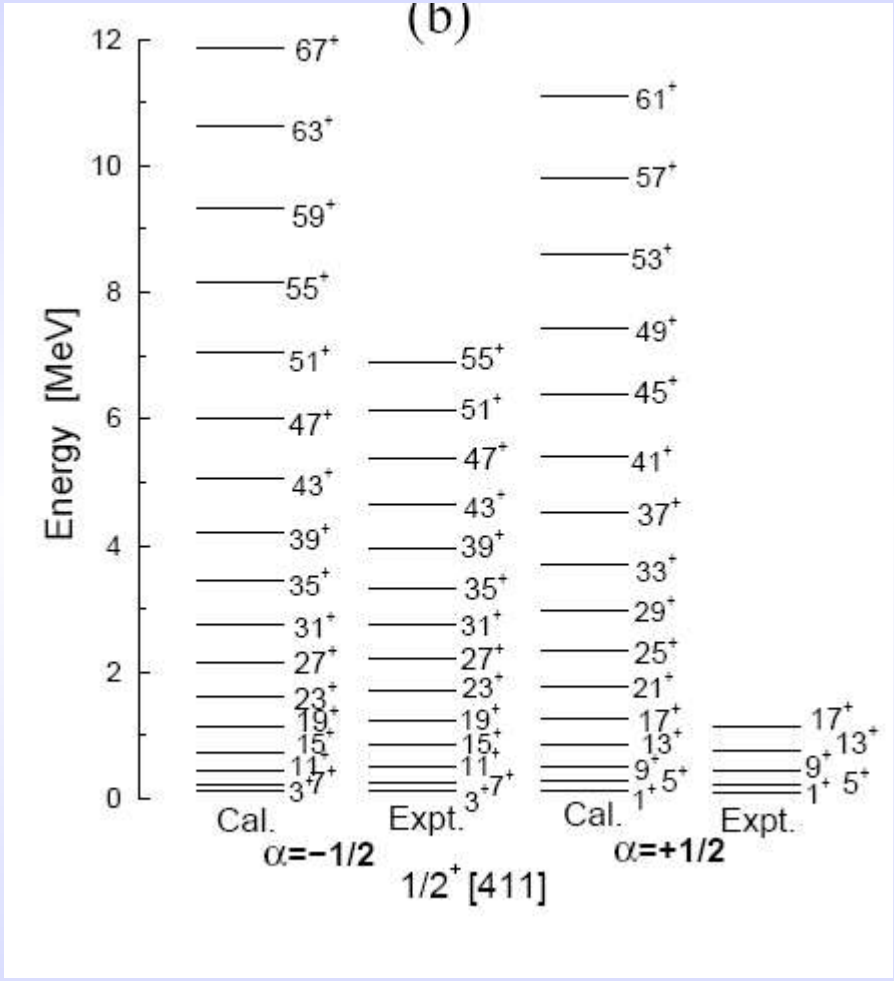
(b)
Energy [MeV]
Cal.
Expt.
Cal.
Expt.
α=−1/2
1/2⁺ [411]
α=+1/2

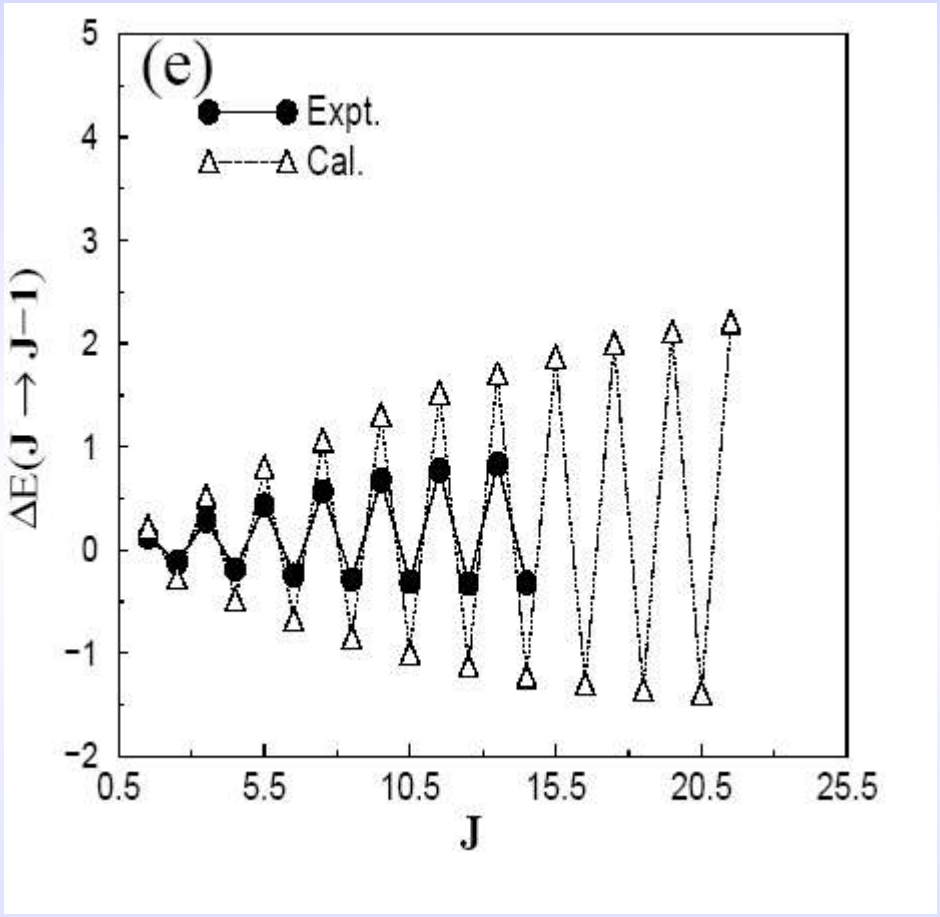
(e)
Expt.
Cal.
ΔE(J → J−1)
J
5
4
3
2
1
0
−1
−2
0.5
5.5
10.5
15.5
20.5
25.5

$1/2^-[541]$

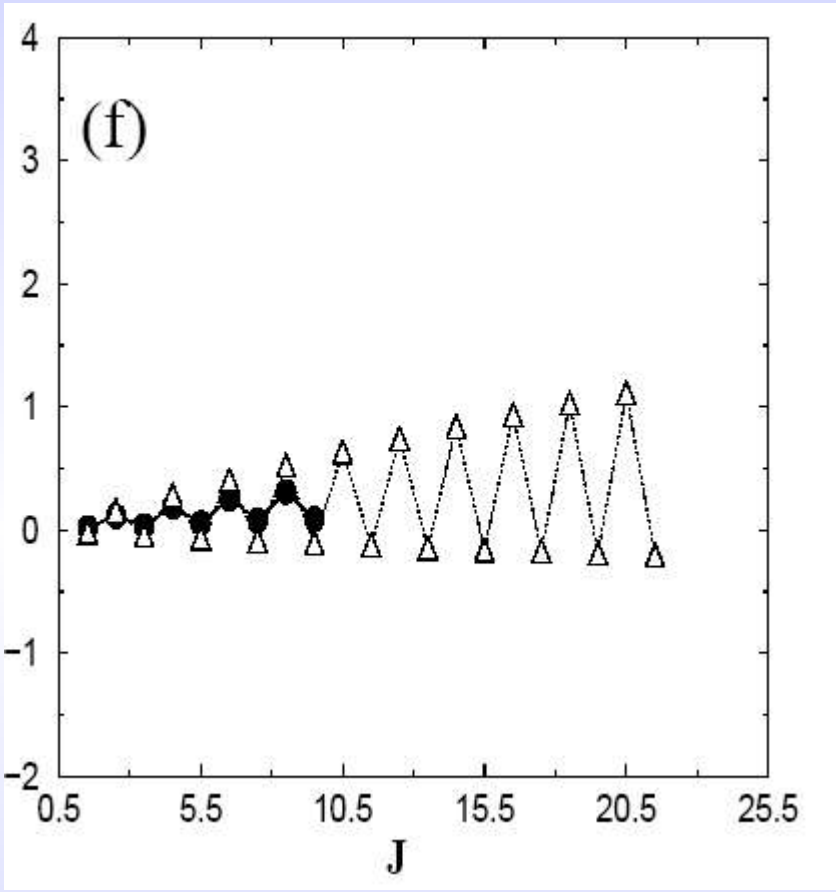
(f)
J
4
3
2
1
0
−1
−2
0.5
5.5
10.5
15.5
20.5
25.5

$1/2^+[411]$

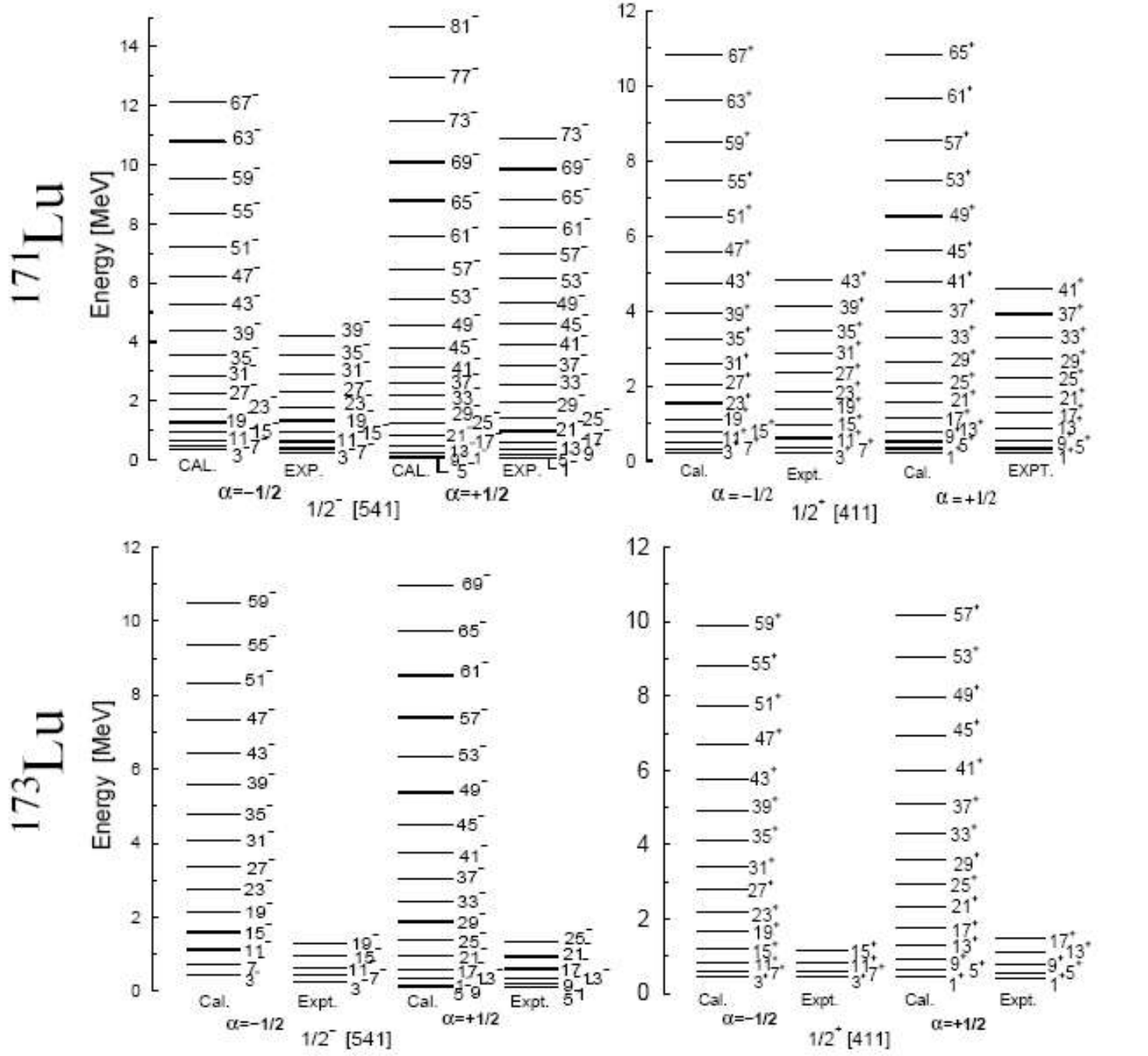
^{171}Lu
^{173}Lu
Energy [MeV]
CAL.
EXP.
Cal.
Expt.
α=−1/2
α=+1/2
1/2⁻ [541]
1/2⁺ [411]

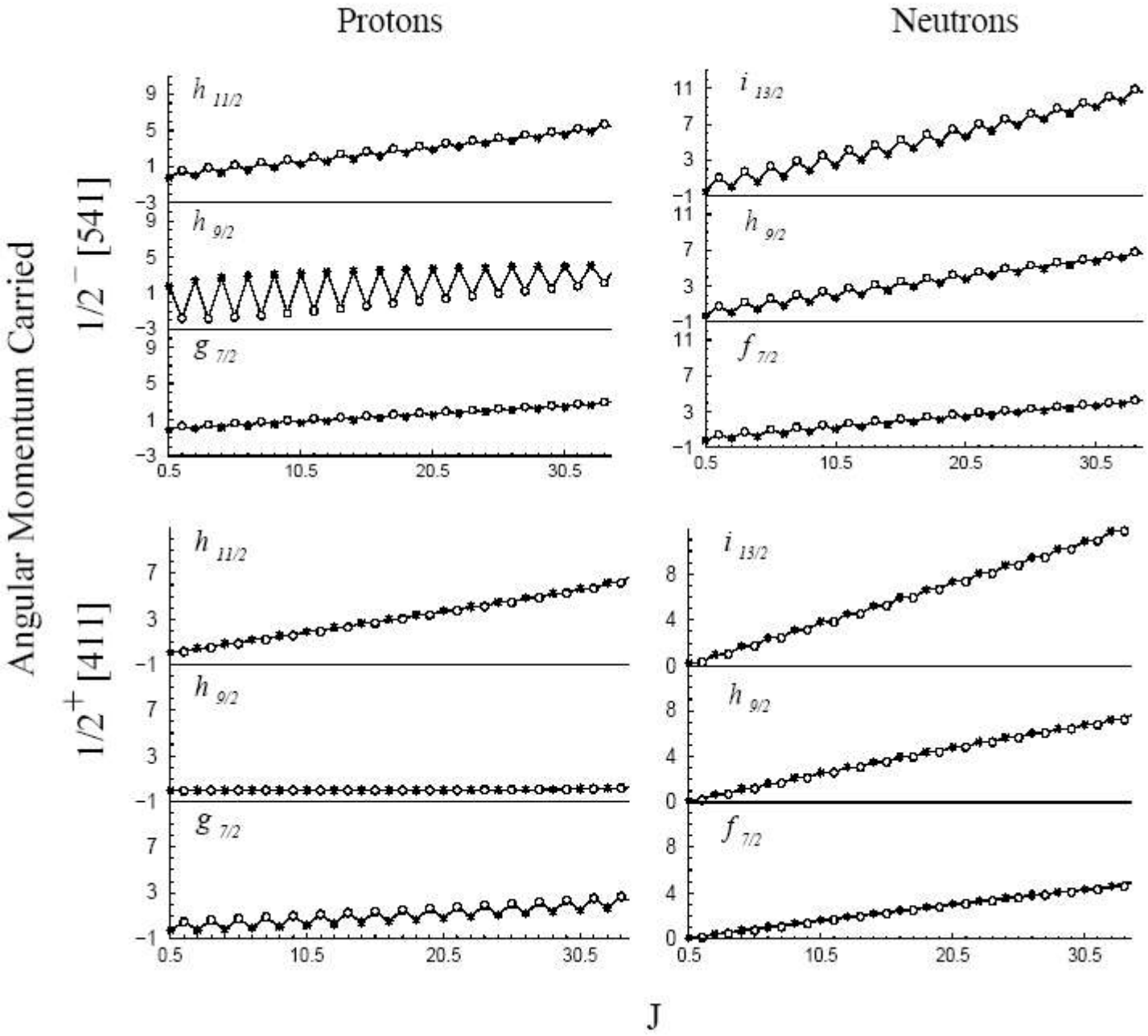
Protons
Neutrons
Angular Momentum Carried
1/2⁻ [541]
1/2⁺ [411]
h 11/2
h 9/2
g 7/2
i 13/2
f 7/2
J
0.5
10.5
20.5
30.5

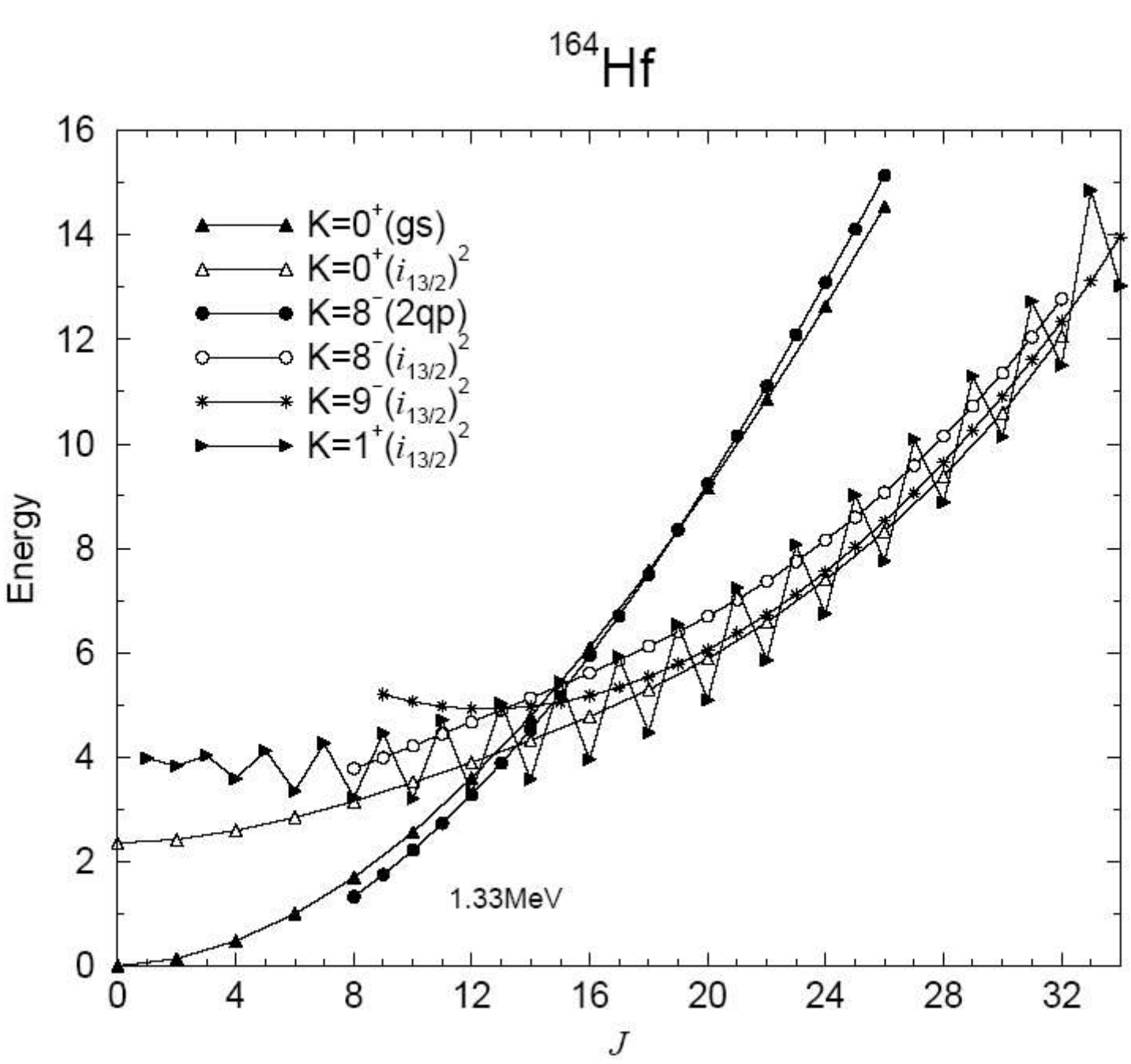
^{164}Hf
Energy
J
K=0$^+$(gs)
K=0$^+$($i_{13/2}$)^2
K=8$^-$(2qp)
K=8$^-$($i_{13/2}$)^2
K=9$^-$($i_{13/2}$)^2
K=1$^+$($i_{13/2}$)^2
1.33MeV
0
2
4
6
8
10
12
14
16
0
4
8
12
16
20
24
28
32

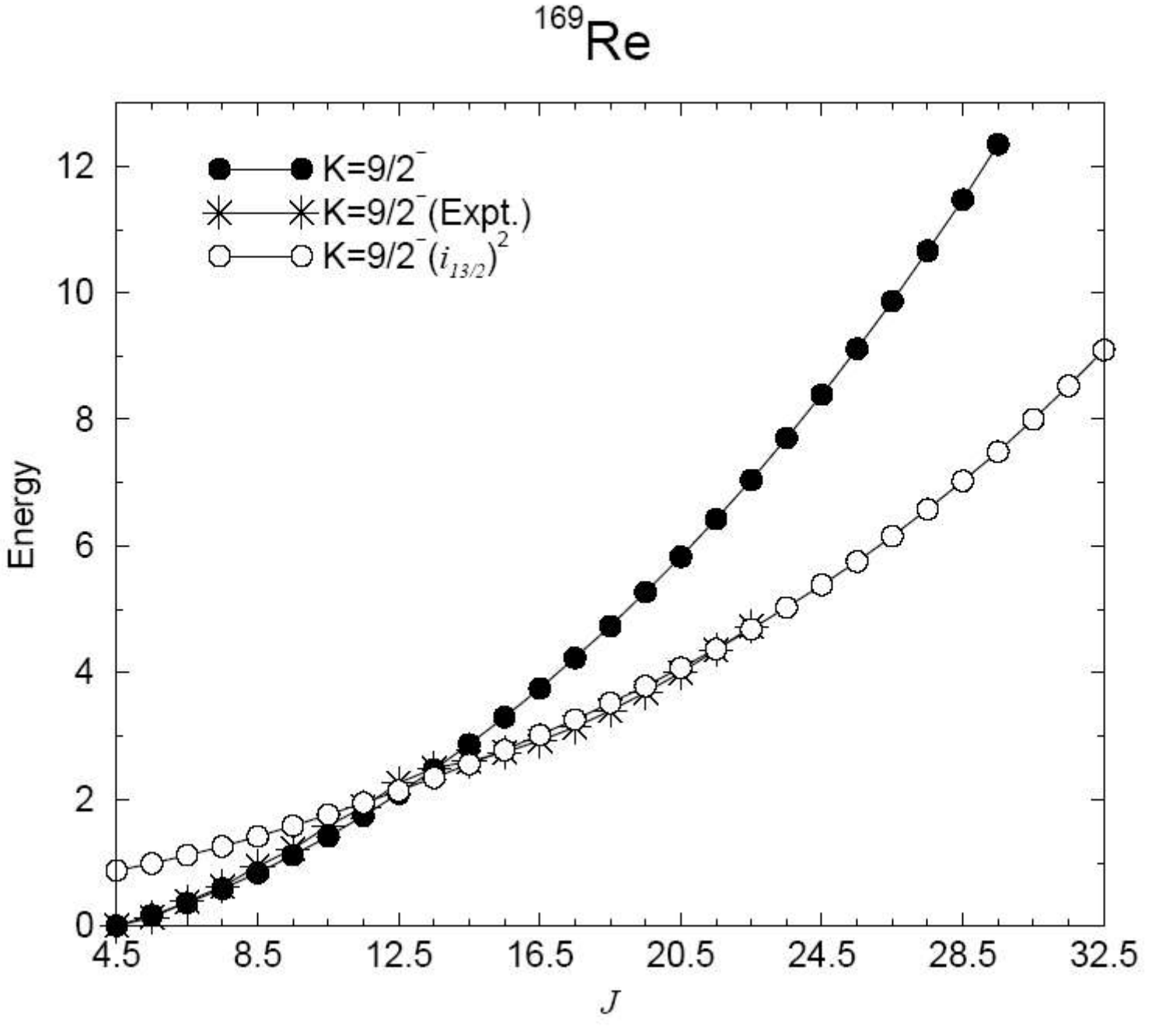
^{169}Re
K=9/2$^-$
K=9/2$^-$(Expt.)
K=9/2$^-$($i_{13/2}$)^2
Energy
J
0
2
4
6
8
10
12
4.5
8.5
12.5
16.5
20.5
24.5
28.5
32.5

HF orbits for ^{150}Nd

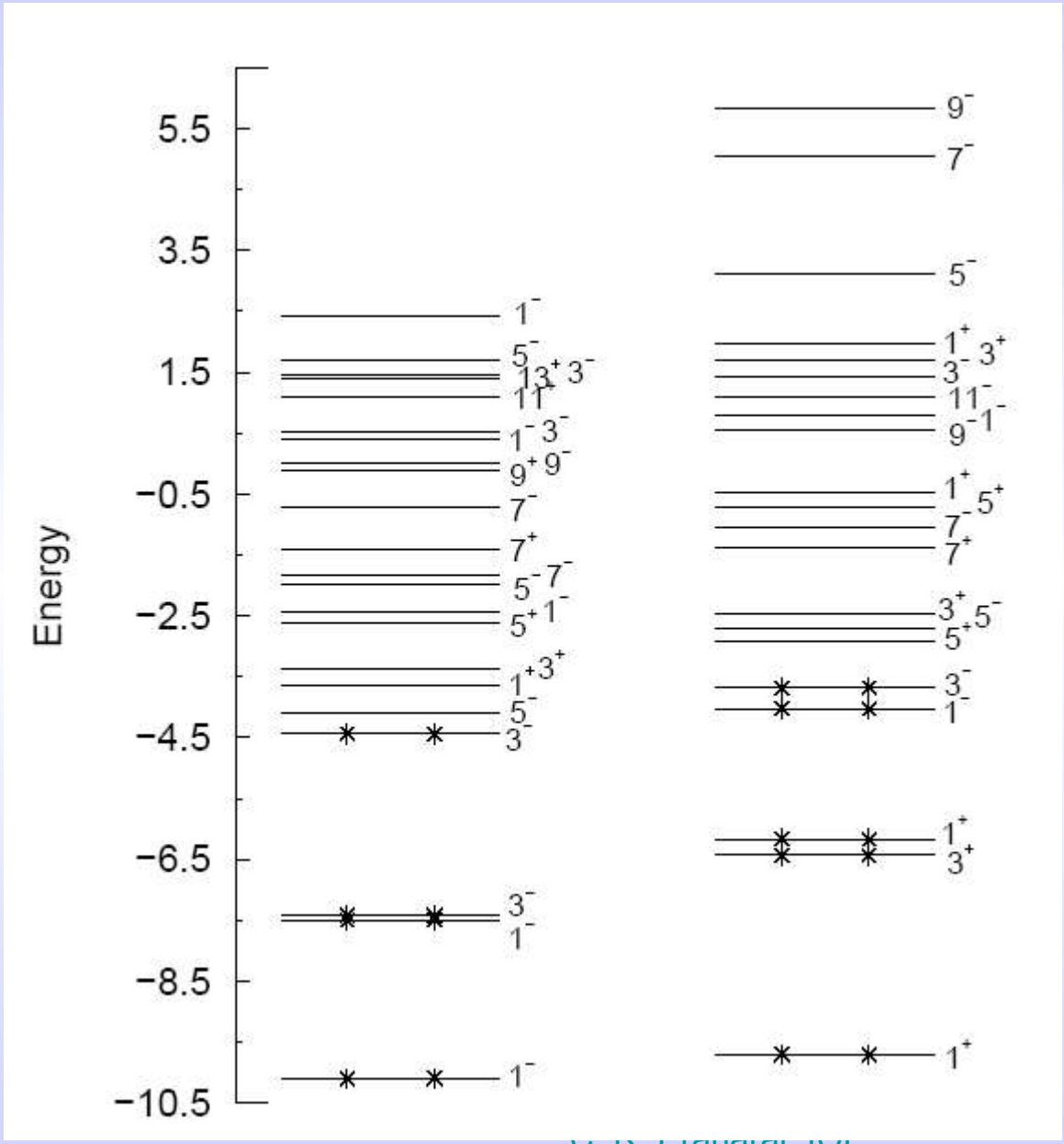

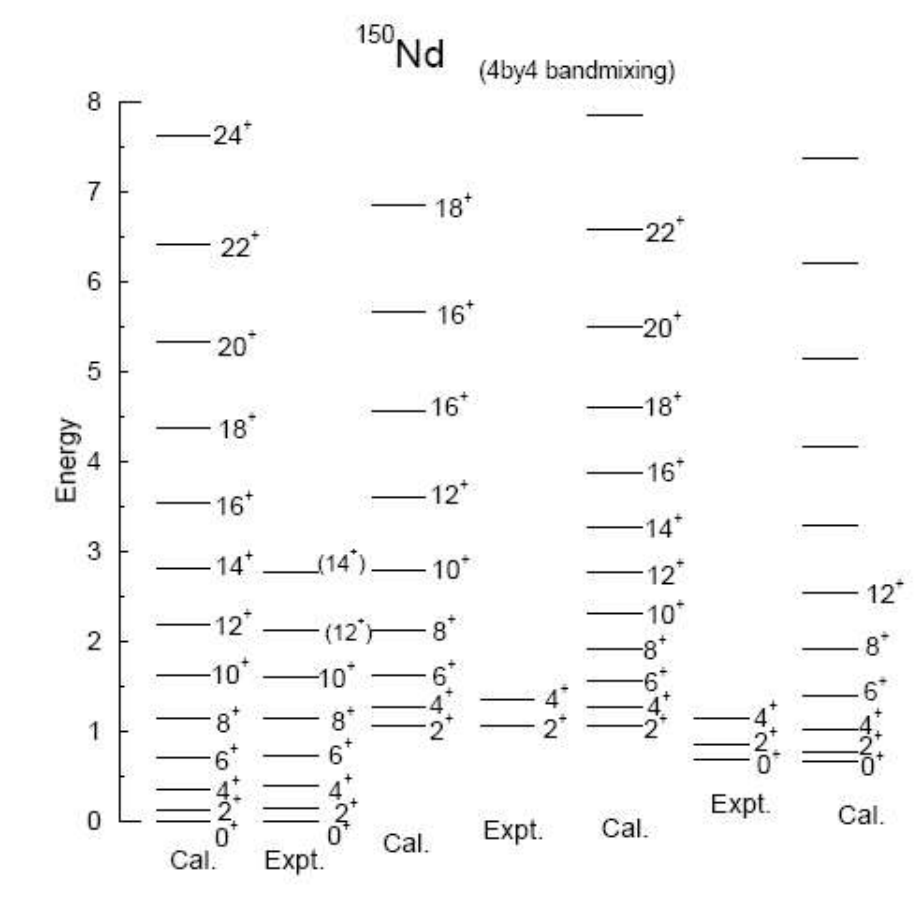
150Nd
(4by4 bandmixing)
Energy
Cal.
Expt.
Cal.
Expt.
Cal.
Expt.
Cal.

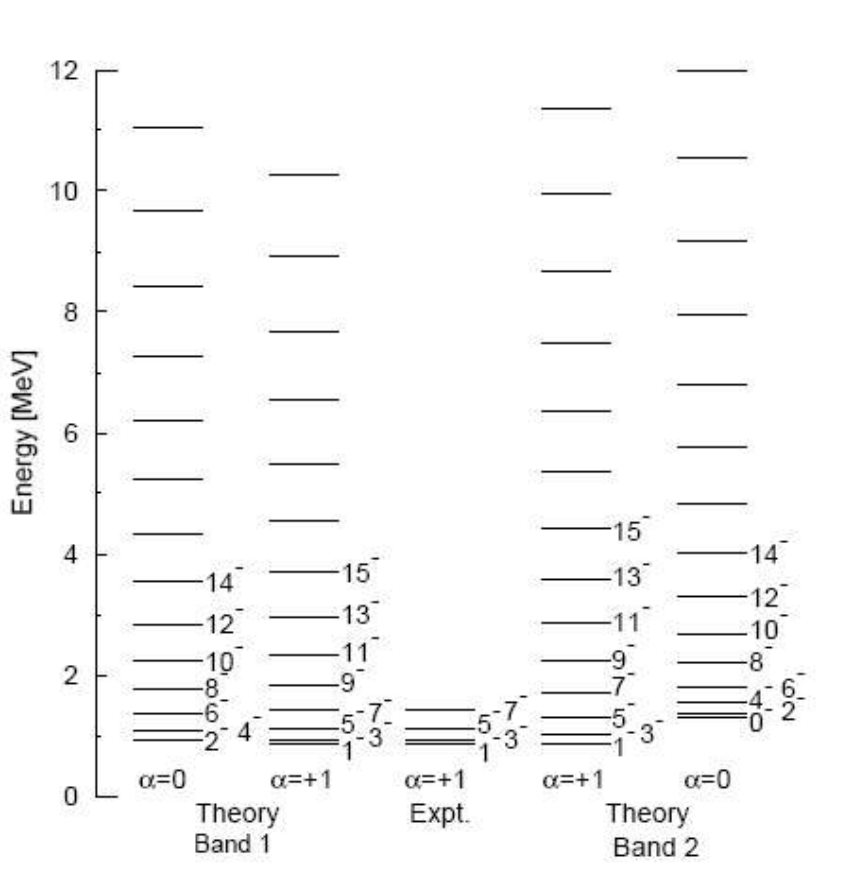
Energy [MeV]
α=0
α=+1
α=+1
α=+1
α=0
Theory
Band 1
Expt.
Theory
Band 2

Multi-quasi particle Large K bands

Table 1: Bandhead Energy, Quadrupole moment and Magnetic moment

Isotope	K^π	BHE		Q_S [eb]		μ [μ_N]	
		Th.	Expt.	Th.	Expt.	Th.	Expt.
^{172}Hf	6^+	1.210	1.685	3.29		5.4726	$5.59^{\pm.61}$
^{172}Hf	8^-	1.311	2.006	3.55		7.63	$7.955^{\pm.065}$
^{173}Hf	$\frac{23}{2}^-$	0.494	1.982	4.17		7.0858	$6.63^{\pm.23}$
^{178}Hf	8^-	1.097	1.479	4.651		7.542	
^{178}Hf	8^-	1.189	1.147	4.767		-0.010	1.4 to 5.3
^{178}Hf	16^+	2.001	2.446	5.54		7.712	$7.36^{\pm.10}$
^{177}Lu	$\frac{23}{2}^-$			5.335	5.71	2.616	$2.93^{\pm.17}$
^{179}W	$\frac{35}{2}^-$		3.535	5.314	4.73	6.076	8.31

band crossing due to 113/2 neutrons (prolate).

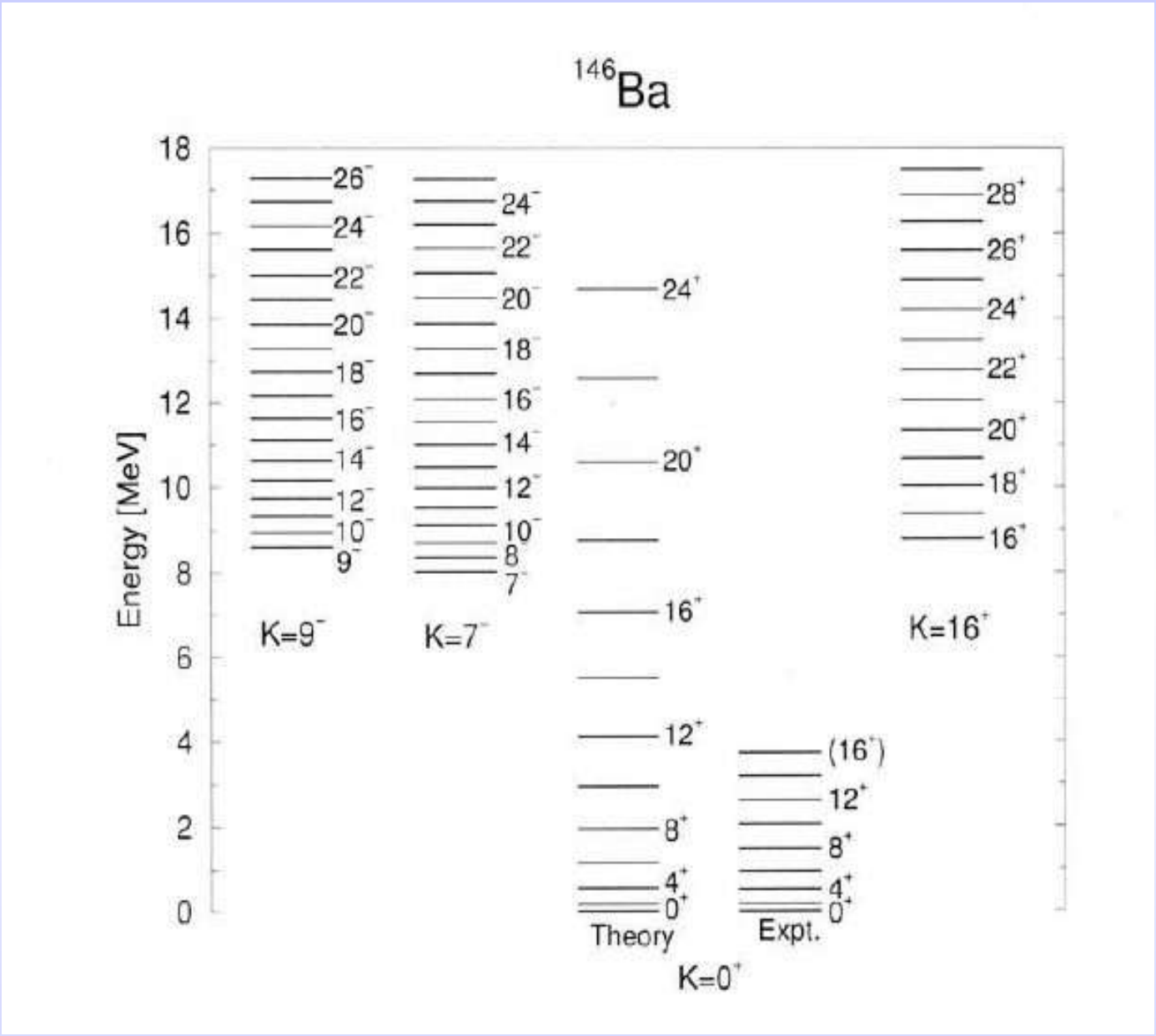

Table 5: Configurations for large K three quasiparticle bands of ^{169}Lu (upper part), ^{171}Lu (middle part) and ^{173}Lu (lower part)

		BHE [MeV]	Q_S [eb]	μ [μ_n]
K^π	Conf.	Th.	Th.	Th.
$23/2^-$	$(\pi)\frac{7}{2}^+ \otimes (\nu)\frac{9}{2}^+\frac{7}{2}^-$	3.28	4.907	1.63
$23/2^-$	$(\pi)\frac{9}{2}^- \otimes (\nu)\frac{9}{2}^+\frac{5}{2}^+$	3.558	5.04	4.064
.....	.....	.....	.....	.....
$23/2^-$	$(\pi)\frac{7}{2}^+ \otimes (\nu)\frac{9}{2}^+\frac{7}{2}^-$	3.674	5.003	2.422
$23/2^-$	$(\pi)\frac{9}{2}^- \otimes (\nu)\frac{9}{2}^+\frac{5}{2}^+$	3.163	5.242	4.075
.....	.....	.....	.....	.....
$23/2^-$	$(\pi)\frac{7}{2}^+ \otimes (\nu)\frac{9}{2}^+\frac{7}{2}^-$	2.739	5.196	2.426
$23/2^-$	$(\pi)\frac{9}{2}^- \otimes (\nu)\frac{9}{2}^+\frac{5}{2}^+$	3.388	5.35	4.038

(b1) K= $35/2^+$ $(\pi)\frac{9}{2}^-\frac{7}{2}^+\frac{5}{2}^+ \otimes (\nu)\frac{7}{2}^+\frac{7}{2}^-$
(b2) K= $37/2^+$ $(\pi)\frac{9}{2}^-\frac{7}{2}^+\frac{5}{2}^+ \otimes (\nu)\frac{9}{2}^+\frac{7}{2}^-$
(b3) K= $37/2^-$ $(\pi)\frac{9}{2}^-\frac{7}{2}^+\frac{5}{2}^+ \otimes (\nu)\frac{9}{2}^+\frac{7}{2}^+$

Table 6: Configurations for five quasiparticle bands of ^{169}Lu (upper part), ^{171}Lu (middle part) and ^{173}Lu (lower part)

		BHE [MeV]	Q_S [eb]	μ [μ_n]
Sl. No.	K^π	Th.	Th.	Th.
(b1)	$35/2^+$	6.294	4.858	10.692
(b2)	$37/2^+$	7.23	4.874	10.675
(b3)	$37/2^-$	6.712	4.941	9.812
.....	.....	.....	.....	.....
(b1)	$35/2^+$	6.988	5.08	10.708
(b2)	$37/2^+$	7.903	5.094	10.678
(b3)	$37/2^-$	7.298	5.161	9.811
.....	.....	.....	.....	.....
(b1)	$35/2^+$	5.695	5.34	10.889
(b2)	$37/2^+$	7.186	5.26	10.646
(b3)	$37/2^-$	6.041	5.407	9.948

(c1) K=$47/2^+$ $(\pi)\frac{9}{2}^-\frac{7}{2}^+\frac{5}{2}^+ \otimes (\nu)\frac{5}{2}^+\frac{7}{2}^+\frac{5}{2}^-\frac{9}{2}^+$
(c2) K=$49/2^+$ $(\pi)\frac{9}{2}^-\frac{7}{2}^+\frac{5}{2}^+ \otimes (\nu)\frac{5}{2}^+\frac{7}{2}^+\frac{7}{2}^-\frac{9}{2}^+$
(c3) K=$45/2^-$ $(\pi)\frac{9}{2}^-\frac{7}{2}^+\frac{5}{2}^+ \otimes (\nu)\frac{5}{2}^+\frac{7}{2}^+\frac{5}{2}^-\frac{7}{2}^-$
(c4) K=$47/2^-$ $(\pi)\frac{9}{2}^-\frac{7}{2}^+\frac{5}{2}^+ \otimes (\nu)\frac{5}{2}^+\frac{5}{2}^-\frac{7}{2}^-\frac{9}{2}^+$
(c5) K=$47/2^-$ $(\pi)\frac{9}{2}^-\frac{7}{2}^+\frac{5}{2}^+ \otimes (\nu)\frac{7}{2}^+\frac{5}{2}^-\frac{7}{2}^-\frac{9}{2}^+$

		BHE [MeV]	Q_S [eb]	μ [μ_n]
Sl. No.	K^π	Th.	Th.	Th.
(c1)	$47/2^+$	8.243	4.903	9.242
(c2)	$49/2^+$	8.188	4.909	9.874
(c3)	$45/2^-$	7.181	4.863	10.191
(c4)	$47/2^-$	8.484	4.782	9.964
(c5)	$47/2^-$	8.841	4.812	9.978
.....	.....	.....	.....	.....
(c1)	$47/2^+$	8.691	5.136	9.233
(c2)	$49/2^+$	8.691	5.136	9.233
(c3)	$45/2^-$	7.732	5.095	10.189
(c4)	$47/2^-$	9.04	5.017	9.974
(c5)	$47/2^-$	9.265	5.046	9.975
.....	.....	.....	.....	.....
(c1)	$47/2^+$	7.09	5.447	9.358
(c2)	$49/2^+$	7.038	5.454	10.016
(c3)	$45/2^-$	6.179	5.4	10.307
(c4)	$47/2^-$	7.6252	5.304	10.061
(c5)	$47/2^-$	8.106	5.292	9.943

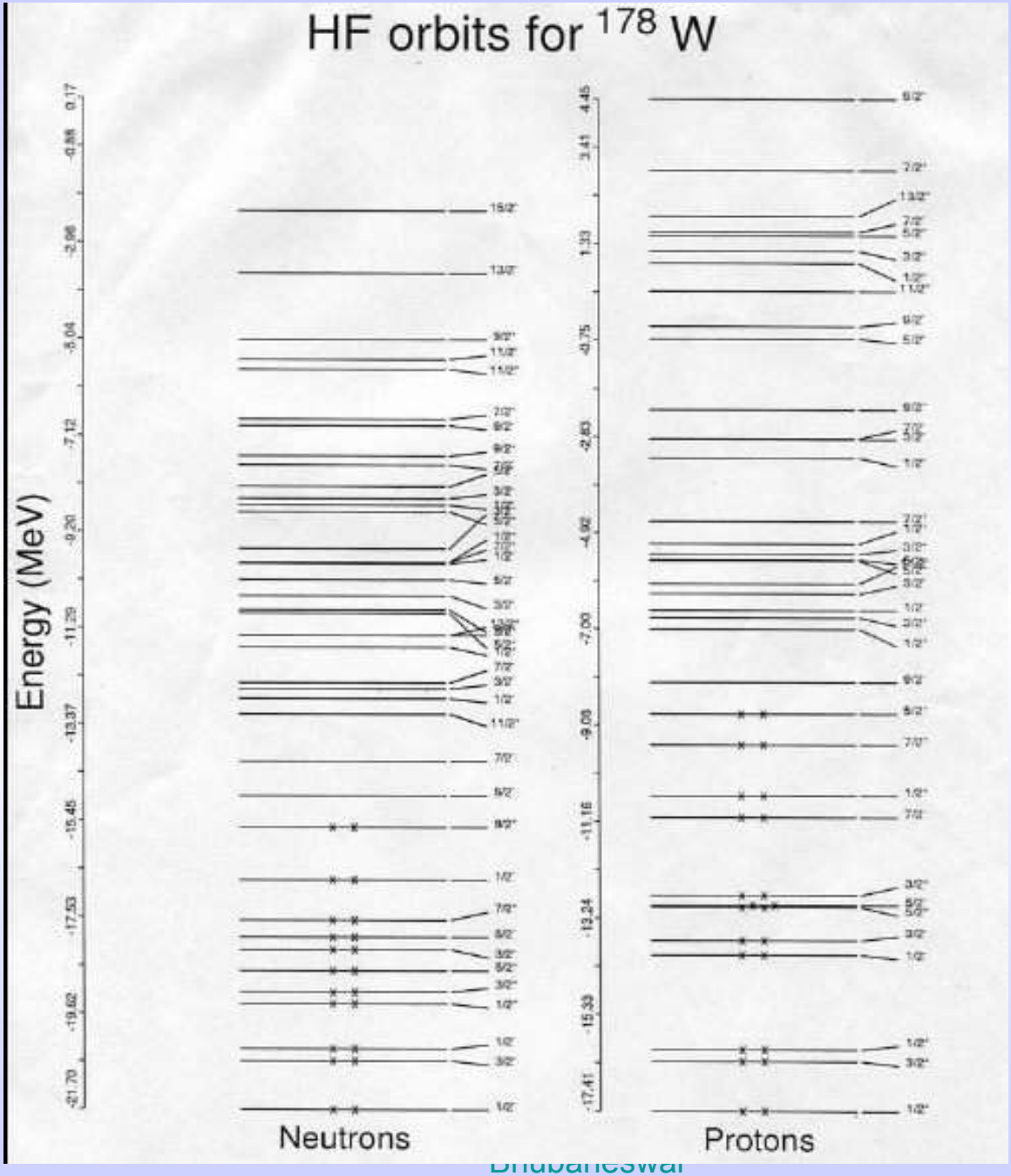
HF orbits for ^{178}W
Energy (MeV)
Neutrons
Protons

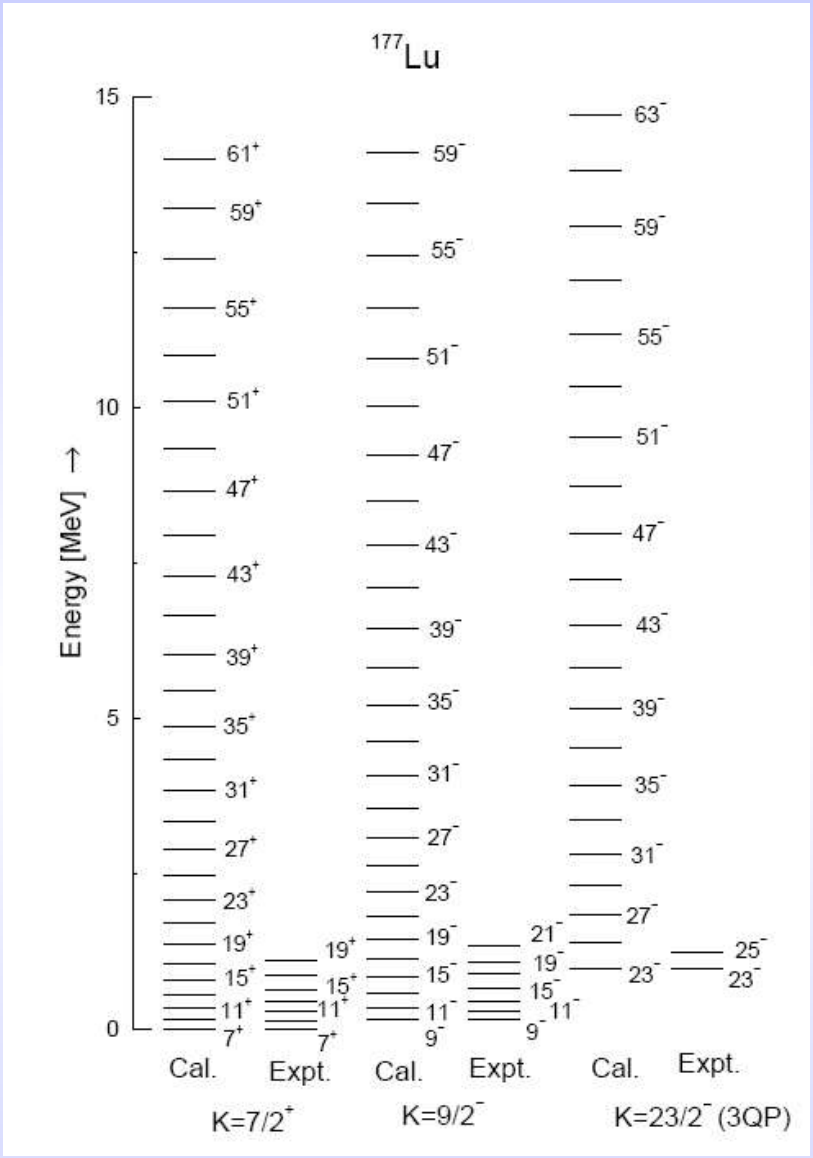
177Lu
Energy [MeV] →
15
10
5
0
61+
59+
55+
51+
47+
43+
39+
35+
31+
27+
23+
19+
15+
11+
7+
19+
15+
11+
7+
59-
55-
51-
47-
43-
39-
35-
31-
27-
23-
19-
15-
11-
9-
21-
19-
15-
11-
9-
63-
59-
55-
51-
47-
43-
39-
35-
31-
27-
23-
25-
23-
Cal.
Expt.
Cal.
Expt.
Cal.
Expt.
K=7/2+
K=9/2-
K=23/2- (3QP)

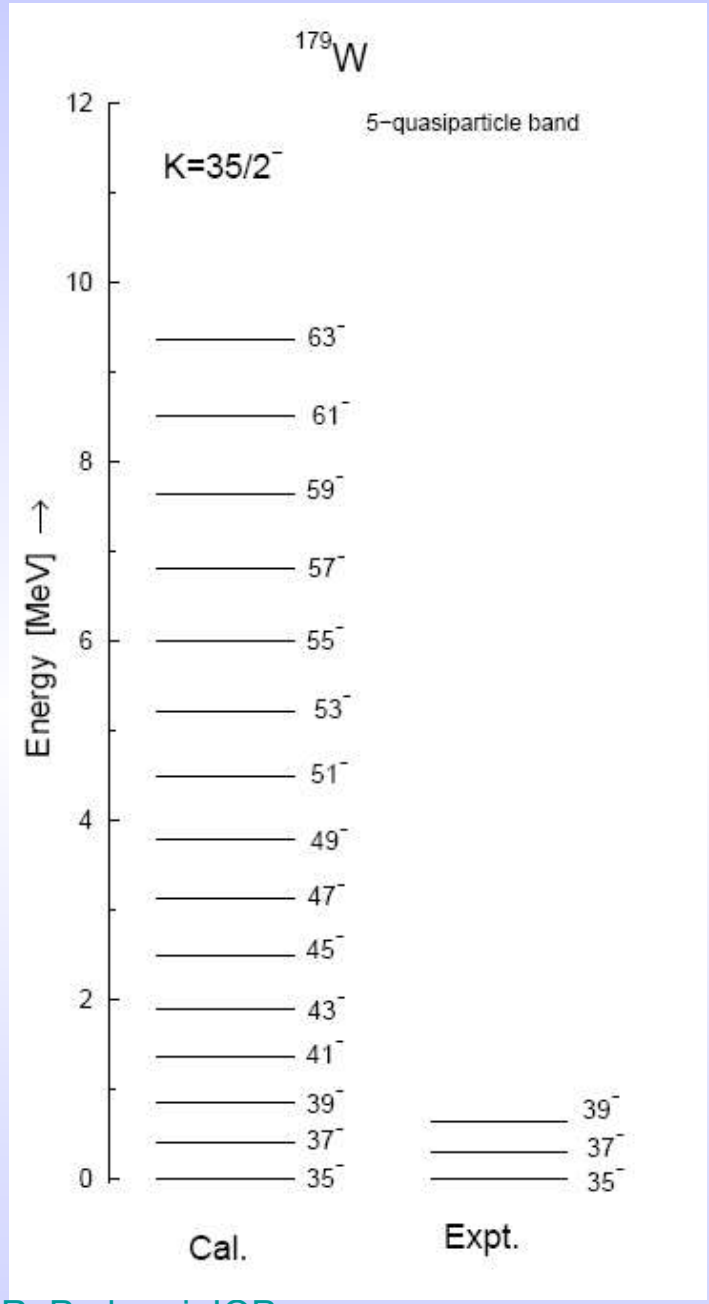
179W
5-quasiparticle band
K=35/2-
Energy [MeV] →
12
10
8
6
4
2
0
63-
61-
59-
57-
55-
53-
51-
49-
47-
45-
43-
41-
39-
37-
35-
39-
37-
35-
Cal.
Expt.

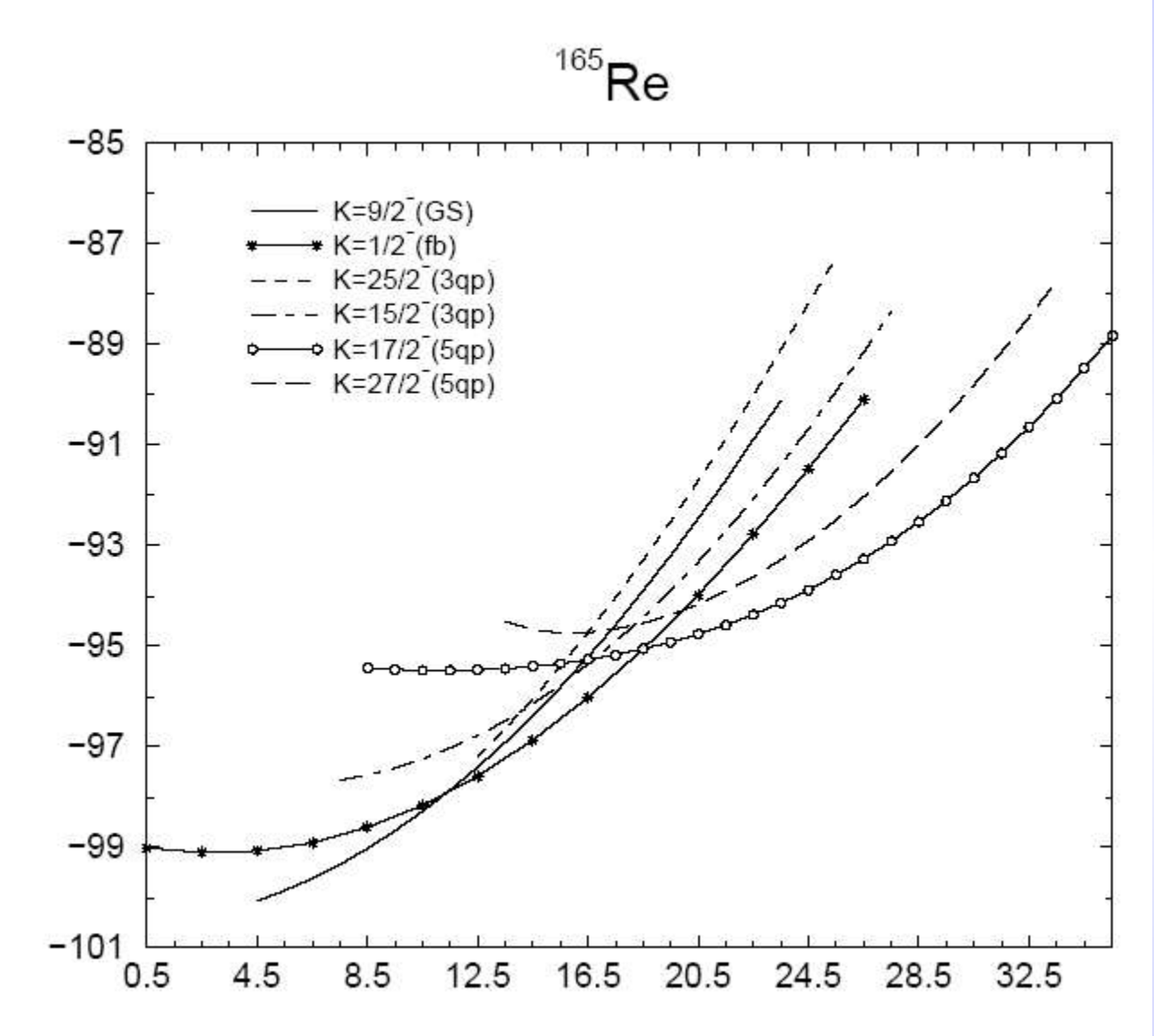
^{165}Re
K=9/2⁻(GS)
K=1/2⁻(fb)
K=25/2⁻(3qp)
K=15/2⁻(3qp)
K=17/2⁻(5qp)
K=27/2⁻(5qp)
−85
−87
−89
−91
−93
−95
−97
−99
−101
0.5
4.5
8.5
12.5
16.5
20.5
24.5
28.5
32.5

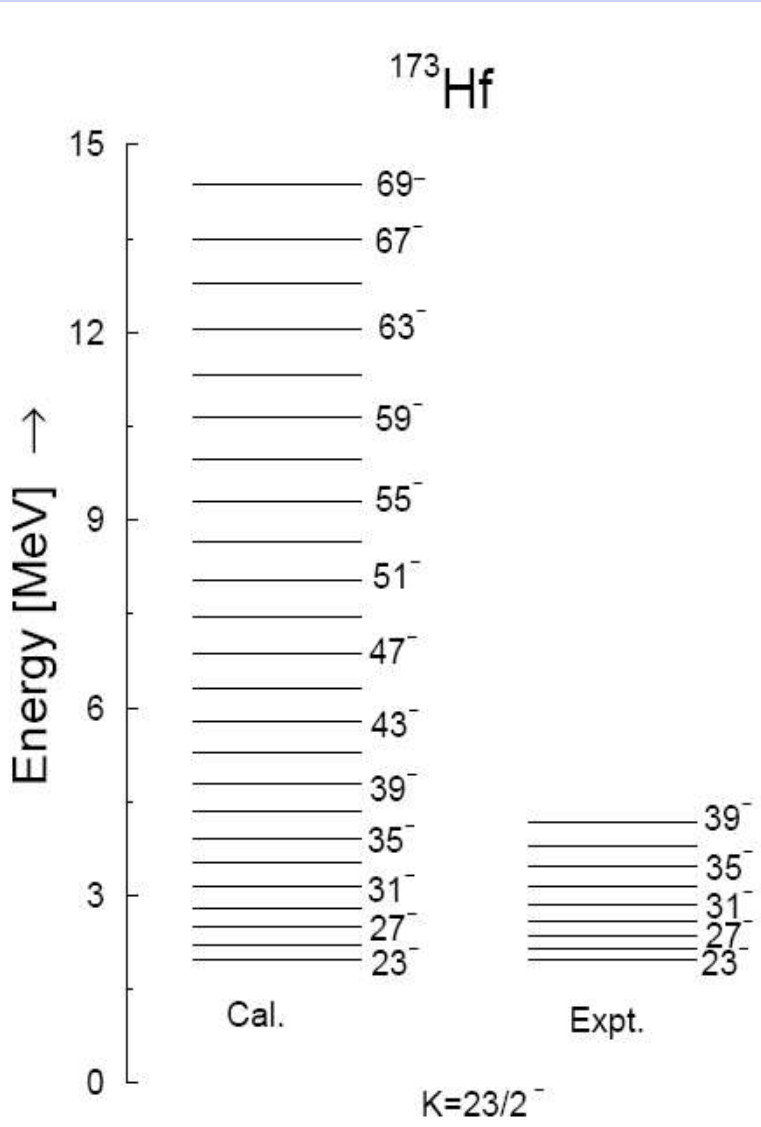
^{173}Hf
Energy [MeV] →
15
12
9
6
3
0
69⁻
67⁻
63⁻
59⁻
55⁻
51⁻
47⁻
43⁻
39⁻
35⁻
31⁻
27⁻
23⁻
39⁻
35⁻
31⁻
27⁻
23⁻
Cal.
Expt.
K=23/2⁻

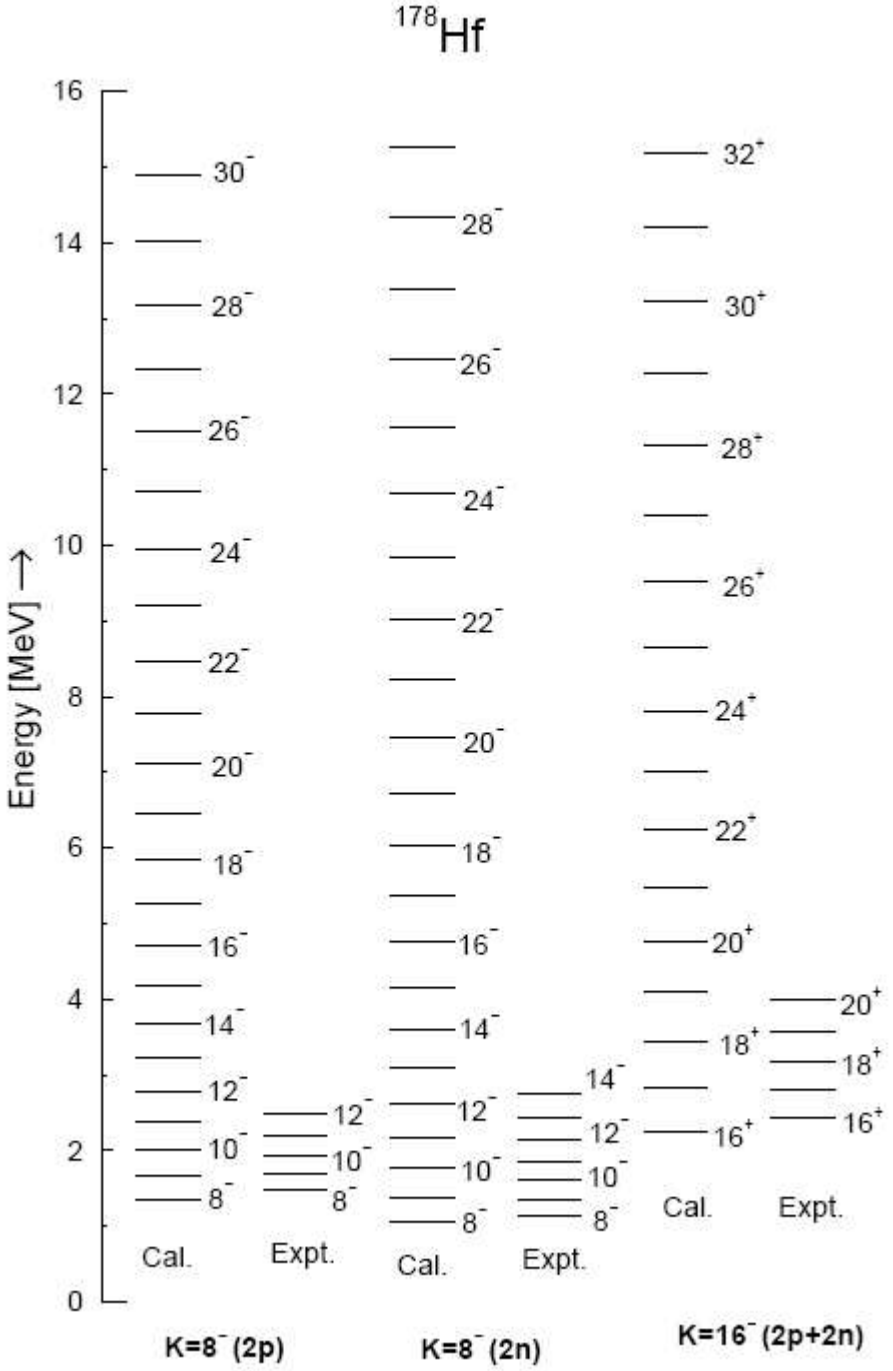
^{178}Hf
Energy [MeV] →
16
14
12
10
8
6
4
2
0
30⁻
28⁻
26⁻
24⁻
22⁻
20⁻
18⁻
16⁻
14⁻
12⁻
10⁻
8⁻
12⁻
10⁻
8⁻
28⁻
26⁻
24⁻
22⁻
20⁻
18⁻
16⁻
14⁻
12⁻
10⁻
8⁻
14⁻
12⁻
10⁻
8⁻
32⁺
30⁺
28⁺
26⁺
24⁺
22⁺
20⁺
18⁺
16⁺
20⁺
18⁺
16⁺
Cal.
Expt.
Cal.
Expt.
Cal.
Expt.
K=8⁻ (2p)
K=8⁻ (2n)
K=16⁻ (2p+2n)

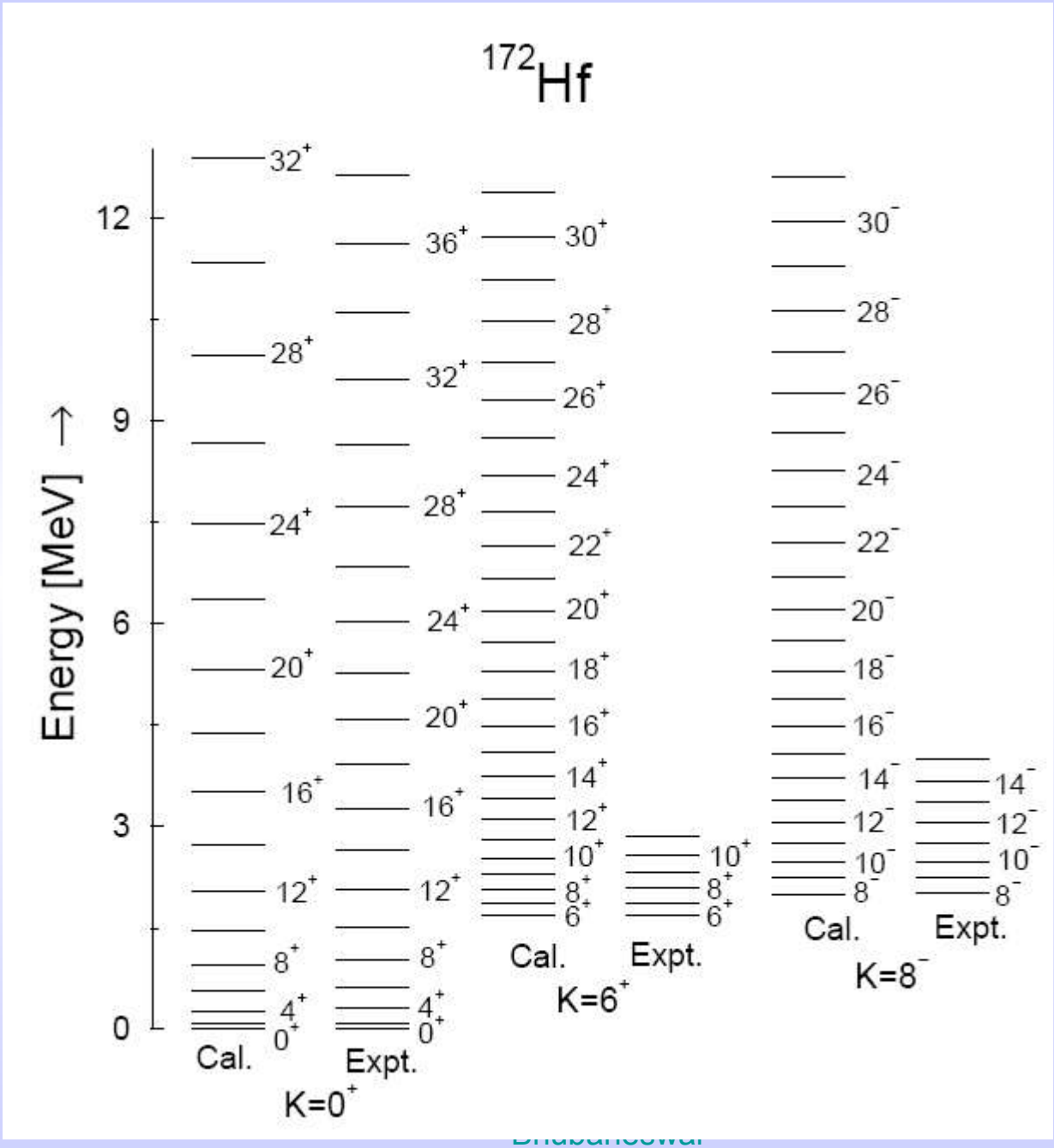
172Hf
Energy [MeV] →
0
3
6
9
12
Cal.
Expt.
K=0+
Cal.
Expt.
K=6+
Cal.
Expt.
K=8-

PHF studies of Chiral and Superdeformed bands

See Ph.D. Thesis of Zashmir Naik
(Institute of Physics, Bhubaneswar) (unpublished)

"Chiral" bands

interaction strength $V_{pp} = V_{np} = V_{nn} = 0.31$ MeV is taken

The deformed HF orbits are calculated with a spherical closed shell core with Z=N=28

Table 1: Single Particle Energies of both Protons and Neutrons.

Proton	$p_{3/2}$	$p_{1/2}$	$f_{5/2}$	$g_{9/2}$	$g_{7/2}$	$d_{5/2}$	$d_{3/2}$	$s_{1/2}$	$h_{11/2}$
(MeV)	0	1.85	0.37	4.44	11.47	8.88	12.21	10.73	13.69
Neutron	$p_{3/2}$	$p_{1/2}$	$f_{5/2}$	$g_{9/2}$	$g_{7/2}$	$d_{5/2}$	$d_{3/2}$	$s_{1/2}$	$h_{11/2}$
(MeV)	0	1.85	0.37	4.44	11.47	8.88	12.21	10.73	13.69

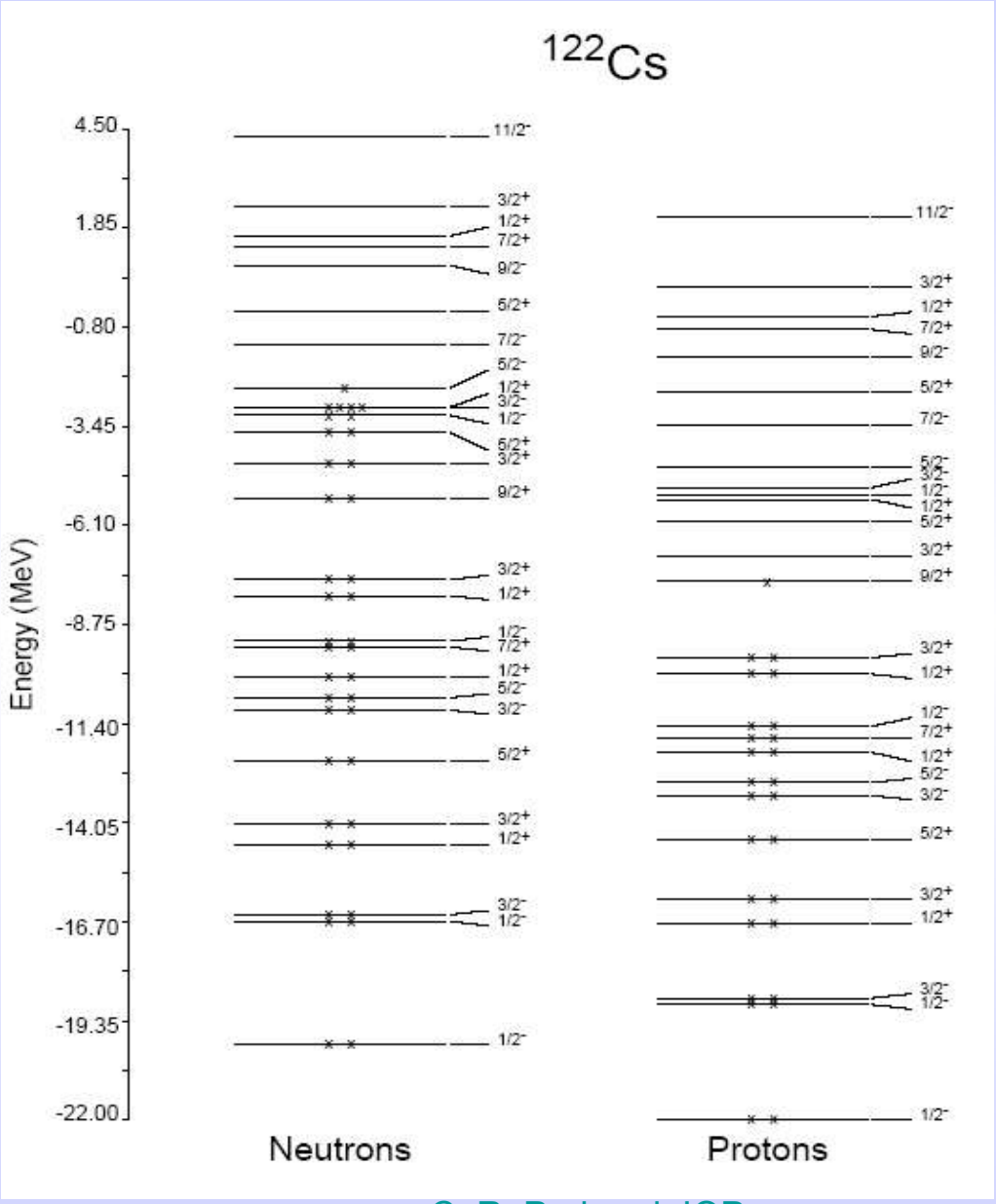
^{122}Cs
Energy (MeV)
4.50
1.85
-0.80
-3.45
-6.10
-8.75
-11.40
-14.05
-16.70
-19.35
-22.00
Neutrons
Protons

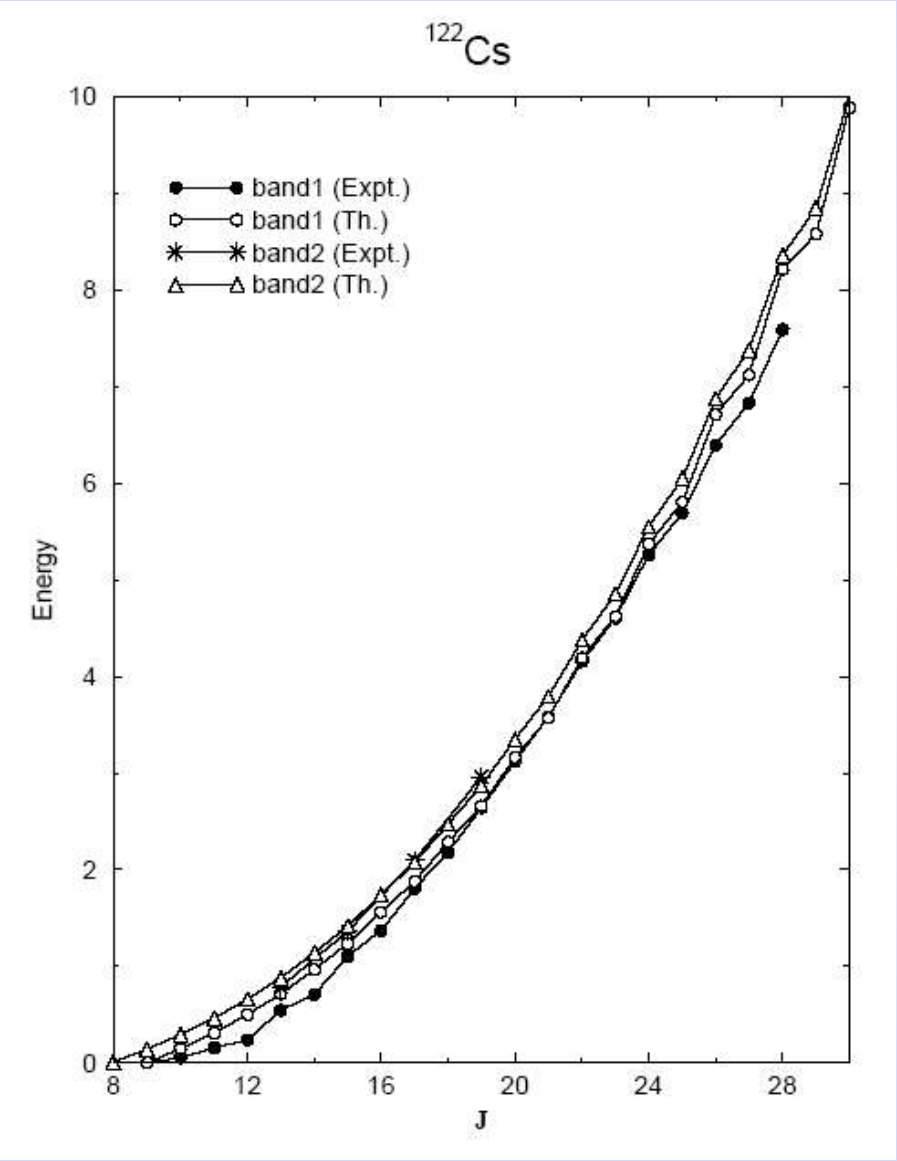
^{122}Cs
band1 (Expt.)
band1 (Th.)
band2 (Expt.)
band2 (Th.)
Energy
J
0
2
4
6
8
10
8
12
16
20
24
28

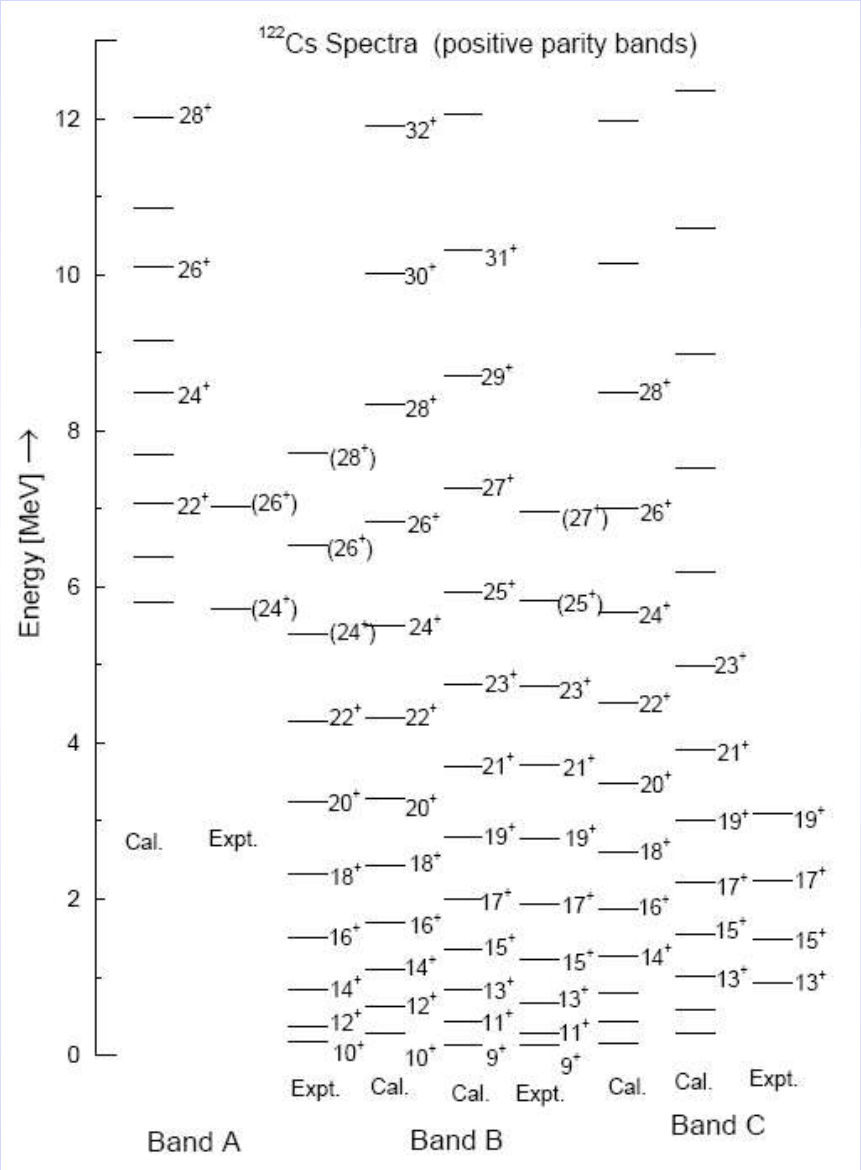
^{122}Cs Spectra (positive parity bands)
Energy [MeV] →
Band A
Band B
Band C
Cal.
Expt.

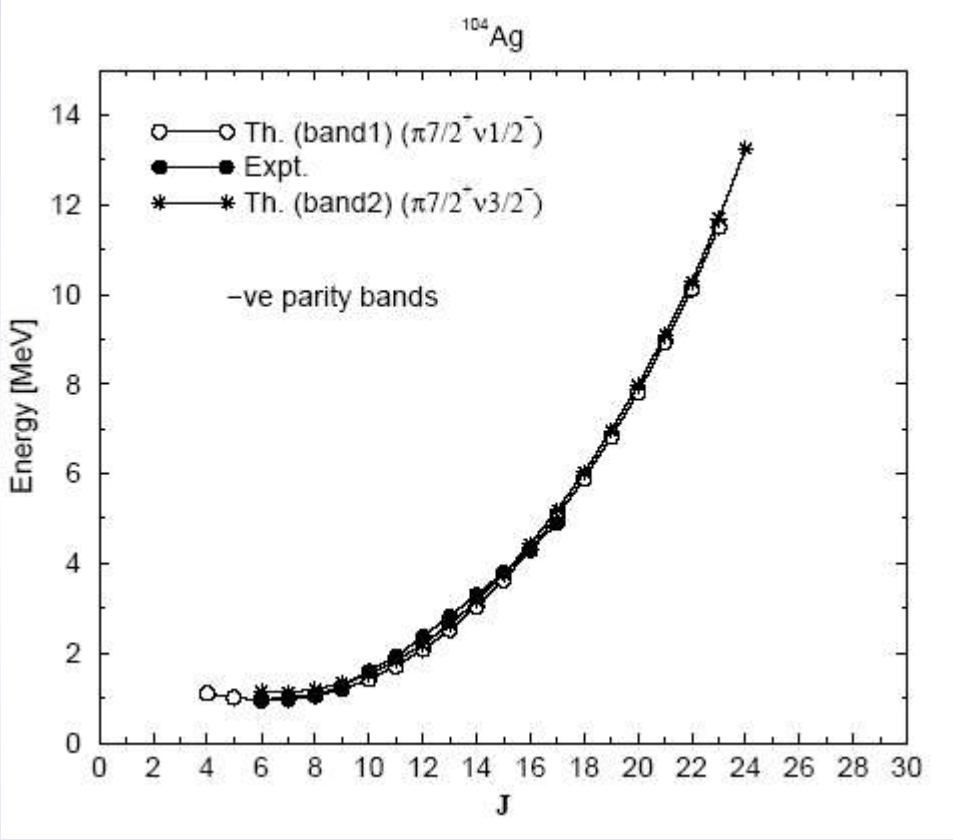
^{104}Ag
Th. (band1) (π7/2⁻ν1/2⁻)
Expt.
Th. (band2) (π7/2⁻ν3/2⁻)
−ve parity bands
Energy [MeV]
J

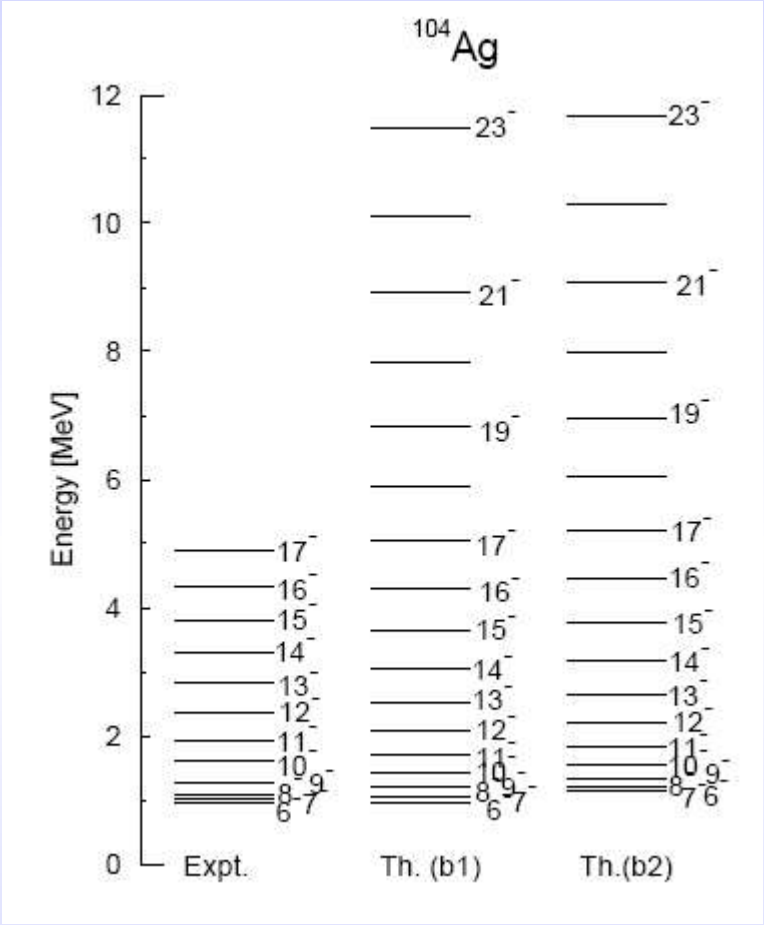
^{104}Ag
Energy [MeV]
Expt.
Th. (b1)
Th.(b2)

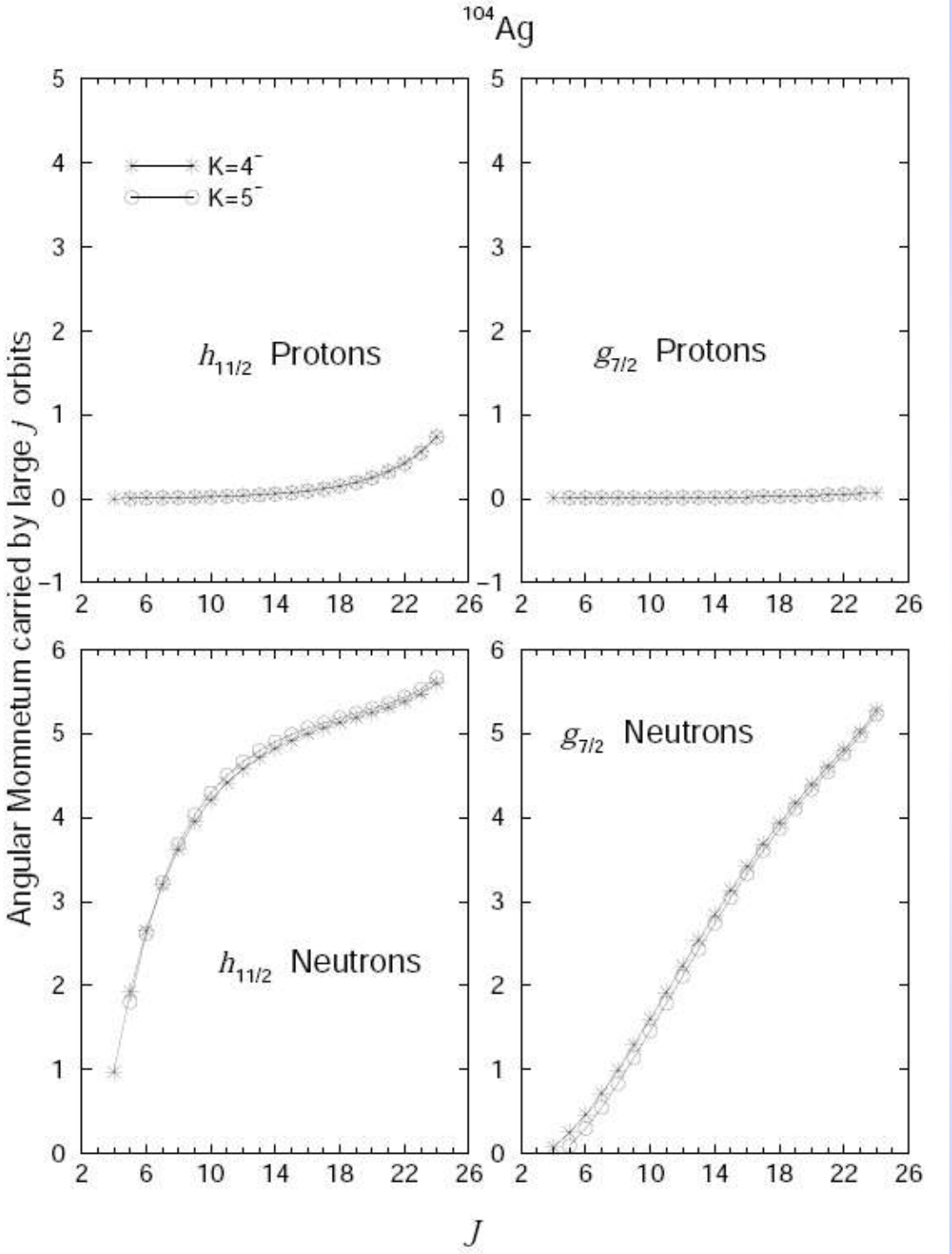
^{104}Ag
K=4$^-$
K=5$^-$
$h_{11/2}$ Protons
$g_{7/2}$ Protons
$h_{11/2}$ Neutrons
$g_{7/2}$ Neutrons
Angular Momnetum carried by large J orbits
J

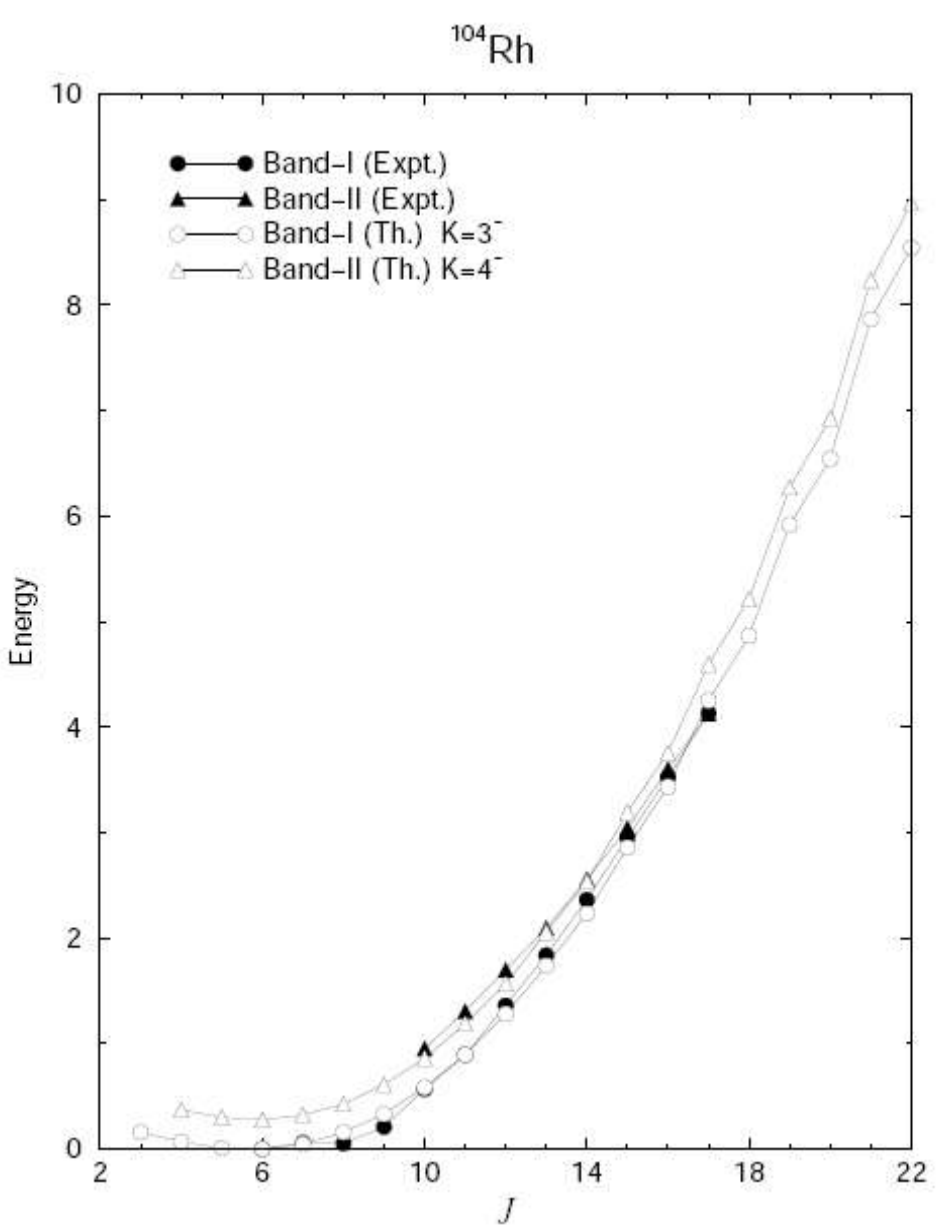
^{104}Rh
Band–I (Expt.)
Band–II (Expt.)
Band–I (Th.) K=3$^-$
Band–II (Th.) K=4$^-$
Energy
J

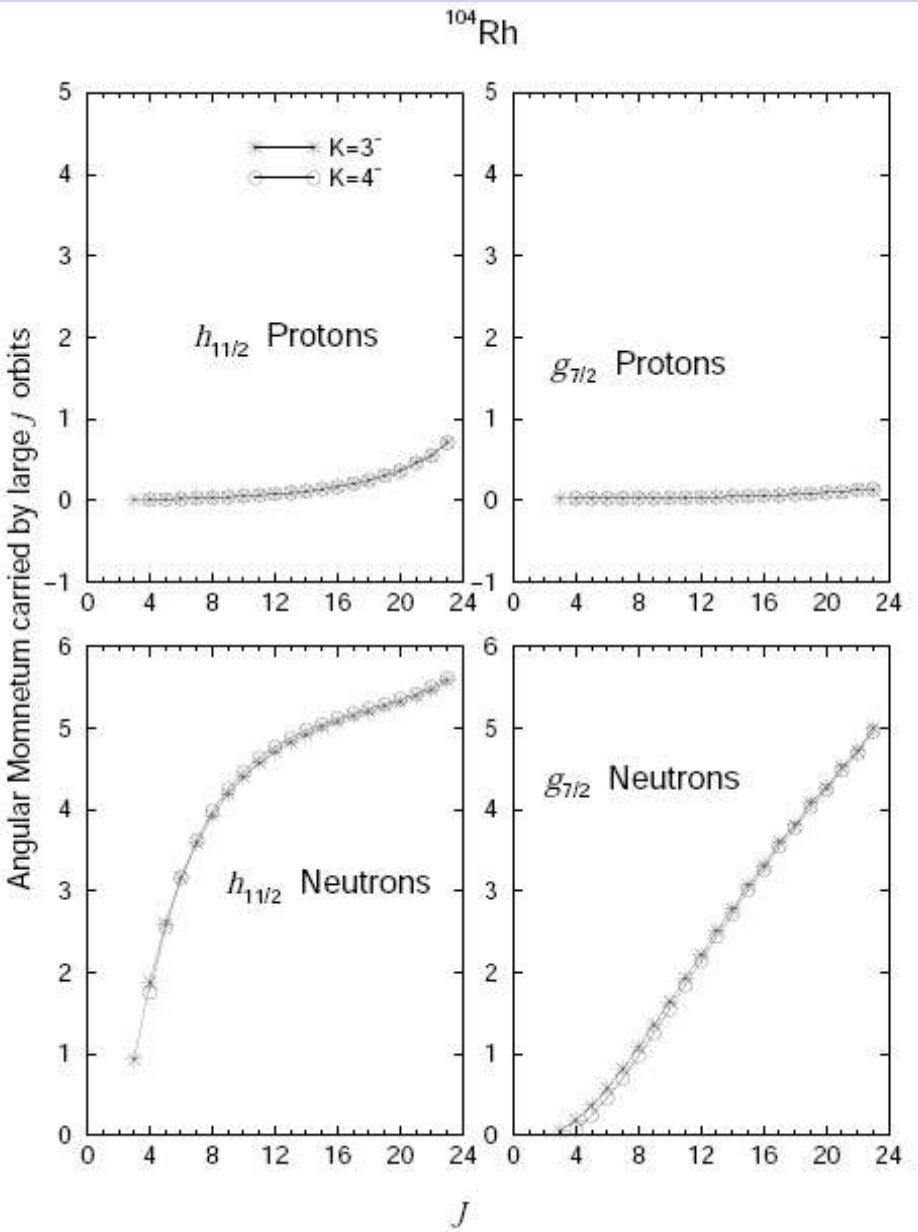
^{104}Rh
K=3$^-$
K=4$^-$
$h_{11/2}$ Protons
$g_{7/2}$ Protons
$h_{11/2}$ Neutrons
$g_{7/2}$ Neutrons
Angular Momnetum carried by large j orbits
J

Superdeformed bands

- Superdeformed band structure of ^{104}Pd is studied
- Model space and interaction are same as ^{122}CS case
- We have performed calculation in two different ways
  - 1st one is by occupying prolate deriving orbits and un-occupying oblate deriving orbits
  - 2nd one is by constraint HF calculation

^{105}Ag

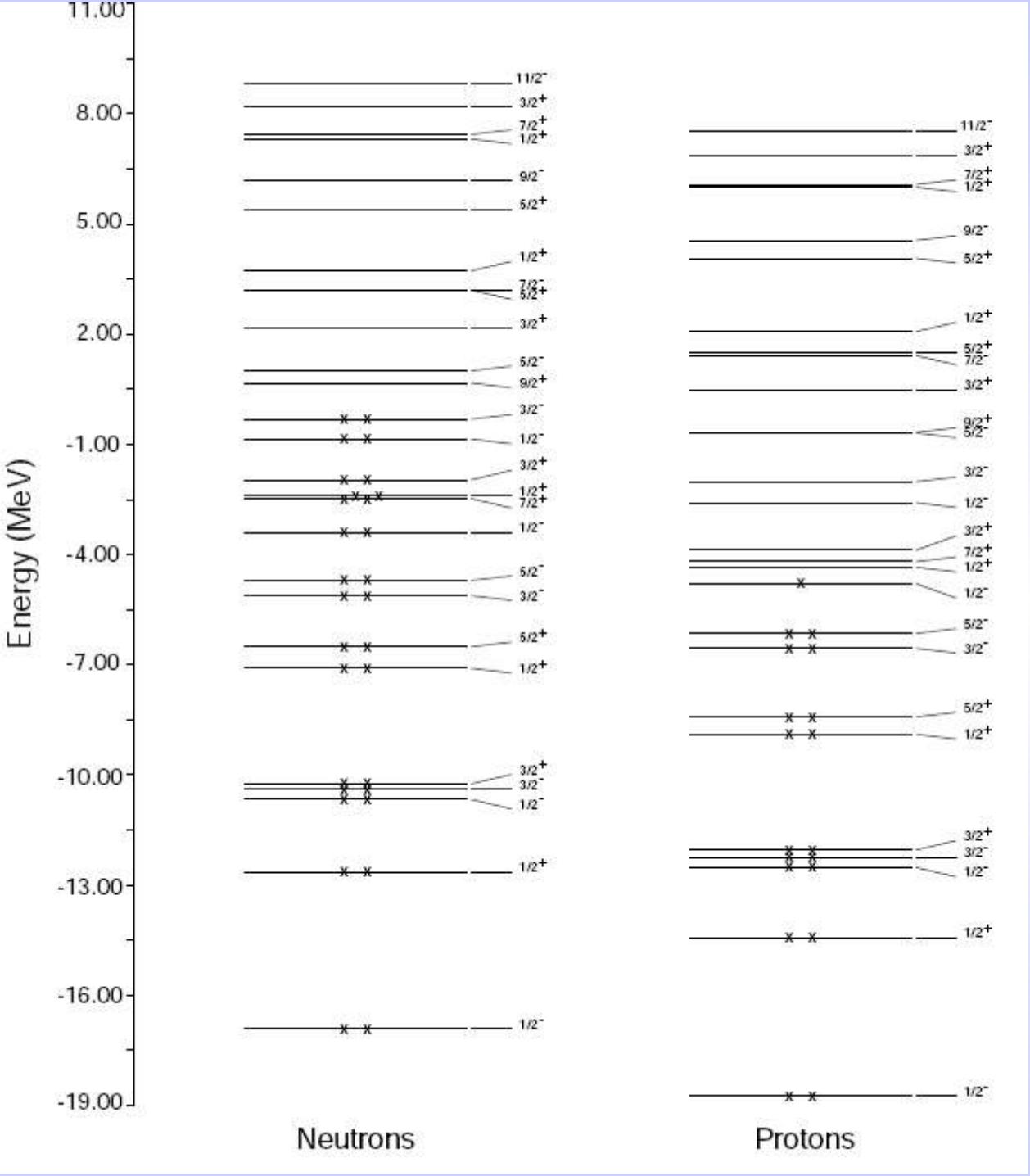
Energy (MeV)
11.00
8.00
5.00
2.00
-1.00
-4.00
-7.00
-10.00
-13.00
-16.00
-19.00
Neutrons
Protons

Table 4.4: Band Head Energies (BHE), Static quadrupole moment (Q_0) and Magnetic moment (μ) of superdeformed bands for ^{105}Ag

Band No.	K	J	BHE	Q_0 [eb]		μ [μ_N]
			Th.	Th.	Expt.	Th.
SD1	$1/2^-$	$1/2^-$	11.79	4.852		-1.134
		$27/2^-$	13.222	5.056	$4.5^{+0.3}_{0.2}$	8.176
SD2	$1/2^-$	$1/2^-$	16.515	5.248		-1.196
		$27/2^-$	17.905	5.452		7.942
SD3	$1/2^+$	$1/2^+$	9.547	4.775		1.127
		$27/2^+$	12.701	4.744		4.044

SD1 : $\pi(h_{11/2})^1 \otimes \nu(h_{11/2})^2$ K=$1/2^-$

SD2 : $\pi(h_{11/2})^1 \otimes \nu(h_{11/2})^4$ K=$1/2^-$

SD3 : $\pi(d_{5/2}g_{7/2})^1 \otimes \nu(h_{11/2})^2$ K=$1/2^+$.

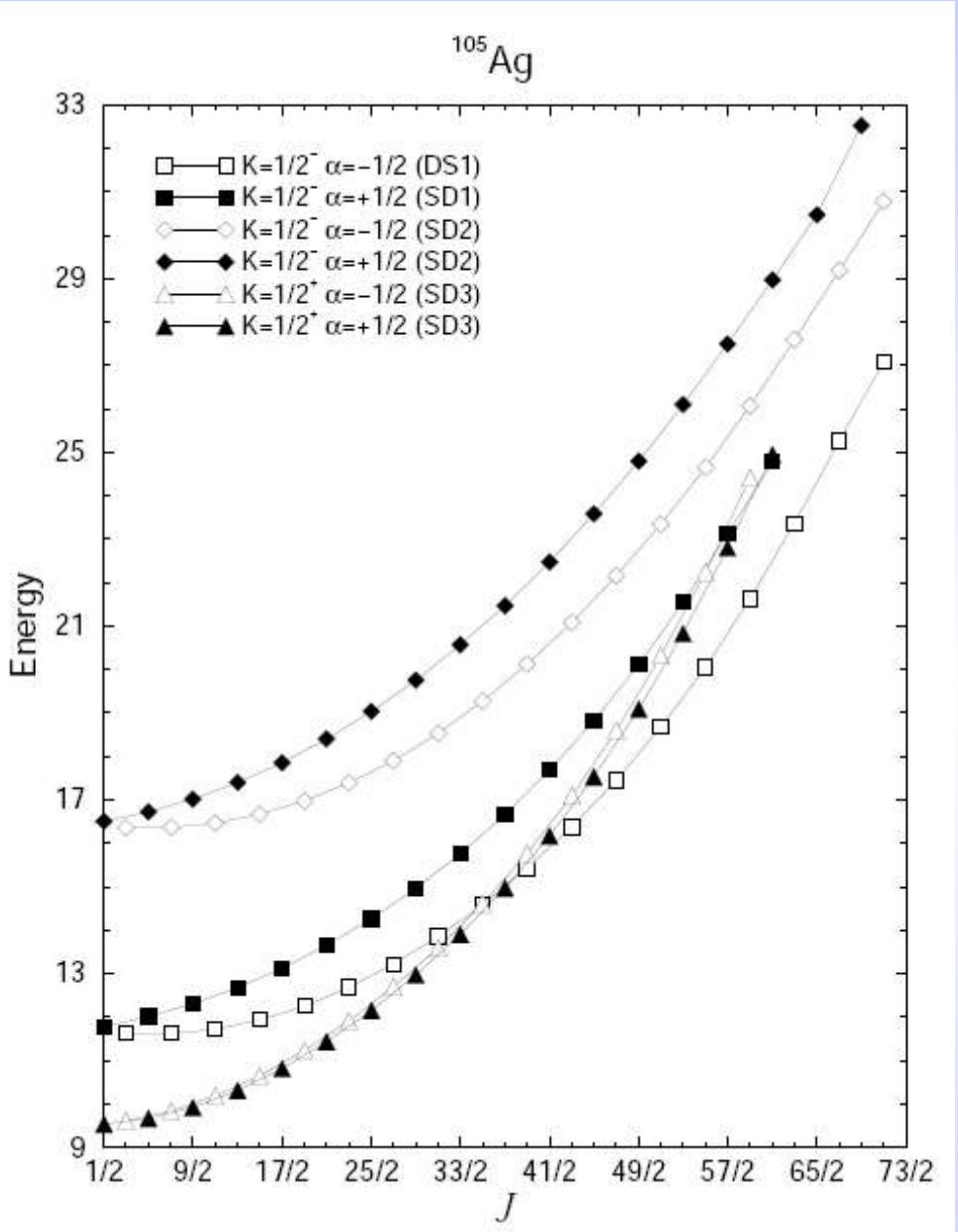
105Ag
K=1/2⁻ α=−1/2 (DS1)
K=1/2⁻ α=+1/2 (SD1)
K=1/2⁻ α=−1/2 (SD2)
K=1/2⁻ α=+1/2 (SD2)
K=1/2⁺ α=−1/2 (SD3)
K=1/2⁺ α=+1/2 (SD3)
Energy
J
33
29
25
21
17
13
9
1/2
9/2
17/2
25/2
33/2
41/2
49/2
57/2
65/2
73/2

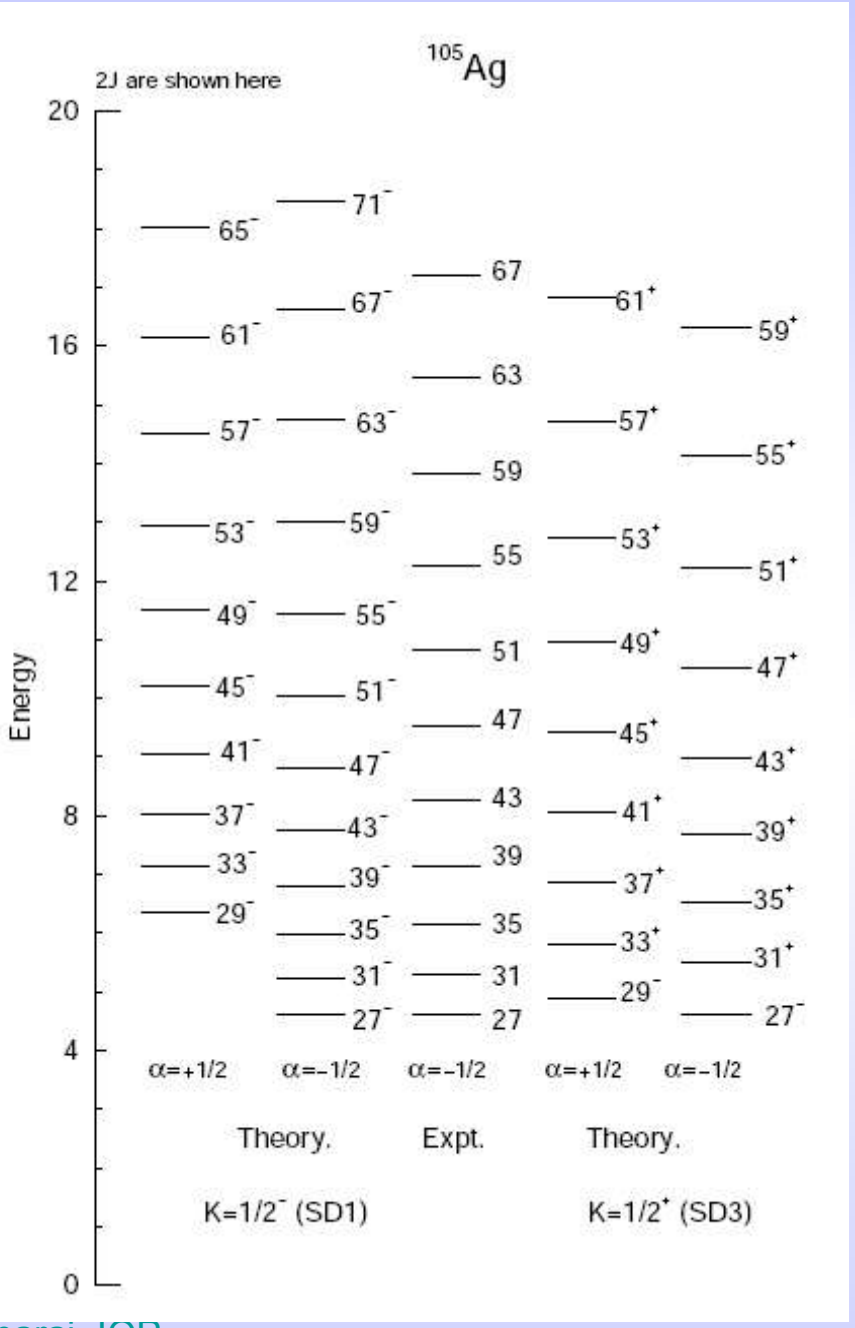
105Ag
2J are shown here
Energy
20
16
12
8
4
0
65⁻
61⁻
57⁻
53⁻
49⁻
45⁻
41⁻
37⁻
33⁻
29⁻
71⁻
67⁻
63⁻
59⁻
55⁻
51⁻
47⁻
43⁻
39⁻
35⁻
31⁻
27⁻
67
63
59
55
51
47
43
39
35
31
27
61⁺
57⁺
53⁺
49⁺
45⁺
41⁺
37⁺
33⁺
29⁻
59⁺
55⁺
51⁺
47⁺
43⁺
39⁺
35⁺
31⁺
27⁻
α=+1/2
α=−1/2
α=−1/2
α=+1/2
α=−1/2
Theory.
Expt.
Theory.
K=1/2⁻ (SD1)
K=1/2⁺ (SD3)

B(E2), B(M1) and B(M1)/B(E2)

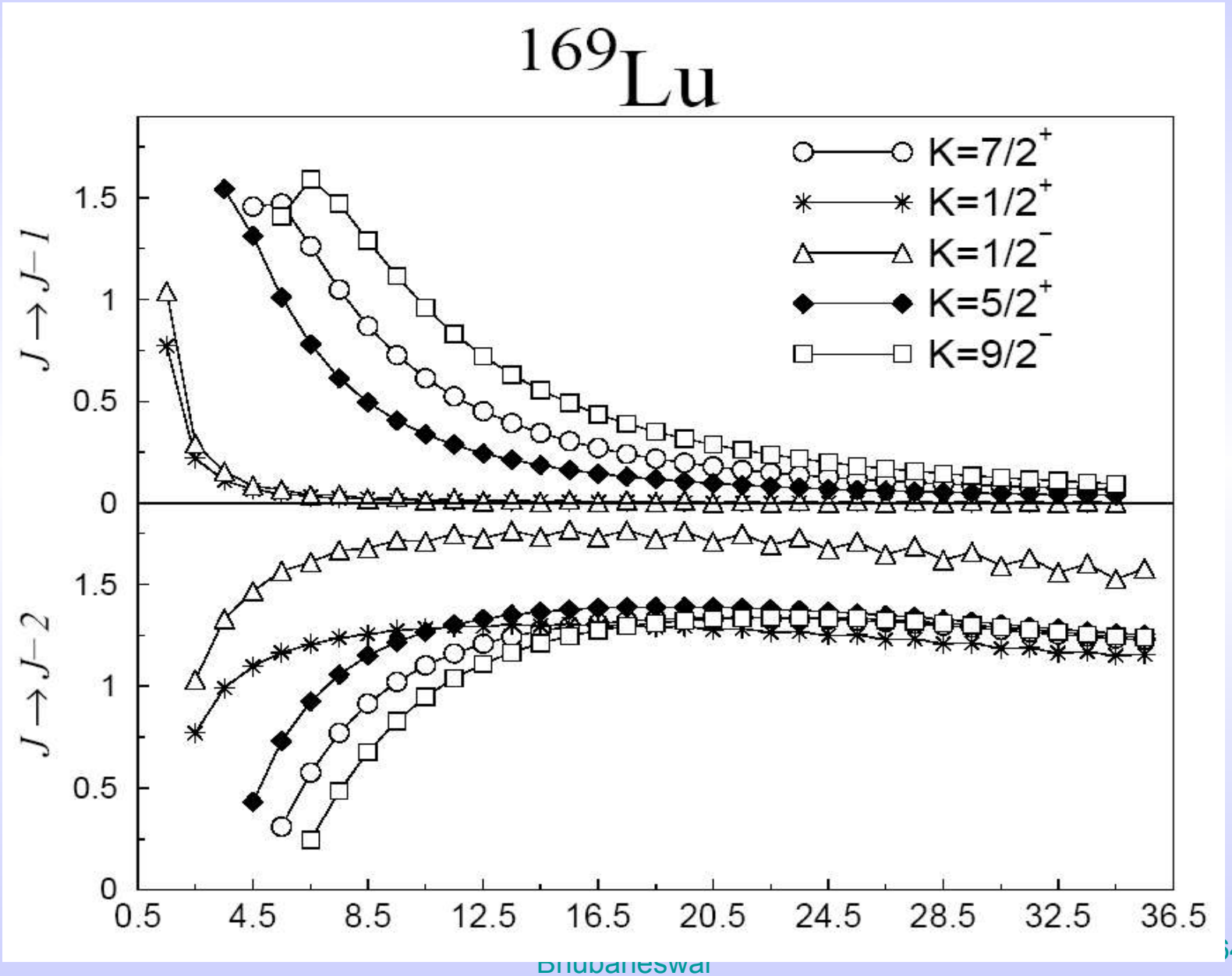

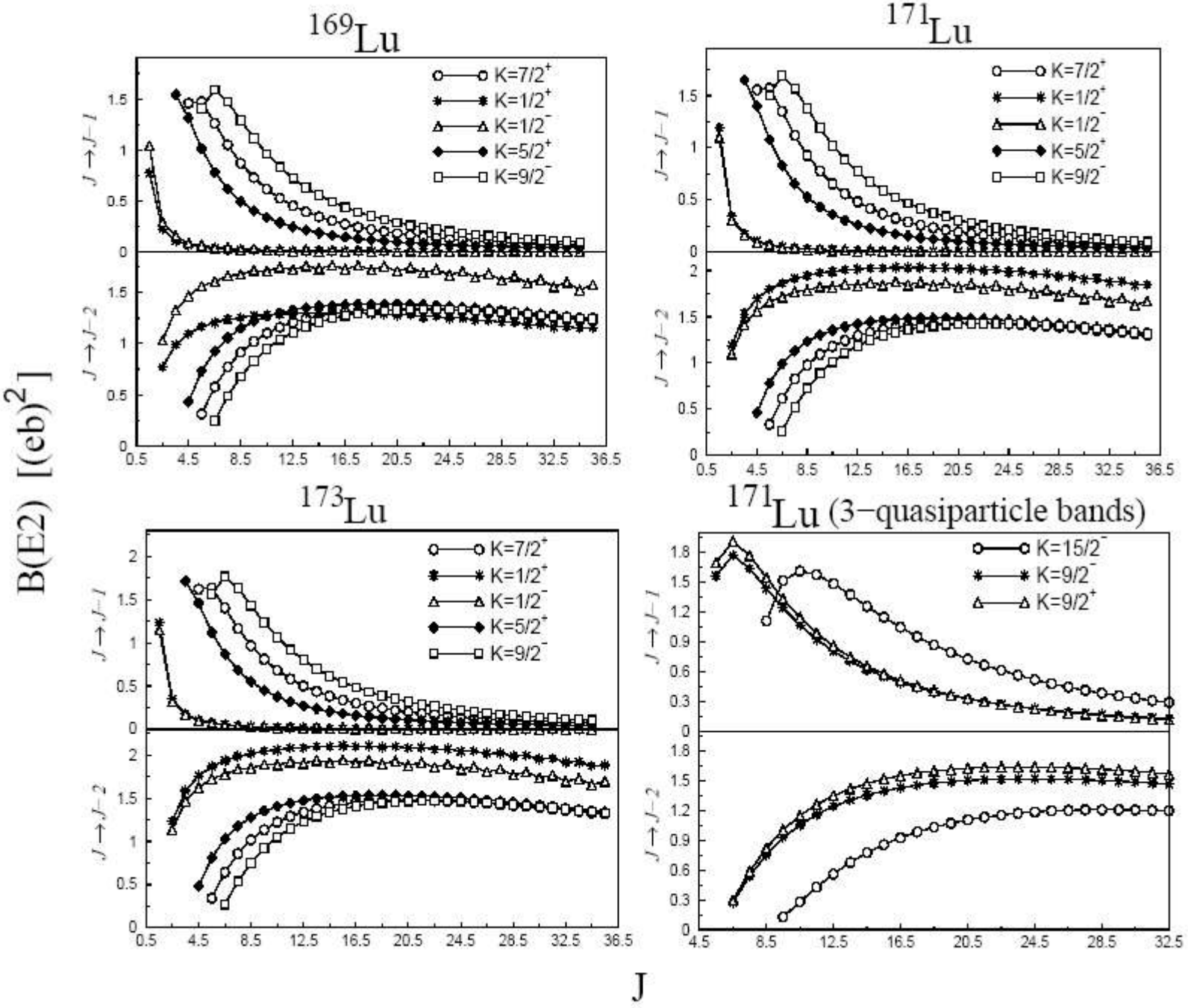
169Lu
171Lu
173Lu
171Lu (3−quasiparticle bands)
K=7/2+
K=1/2+
K=1/2−
K=5/2+
K=9/2−
K=15/2−
K=9/2+
J→J−1
J→J−2
B(E2) [(eb)2]
J

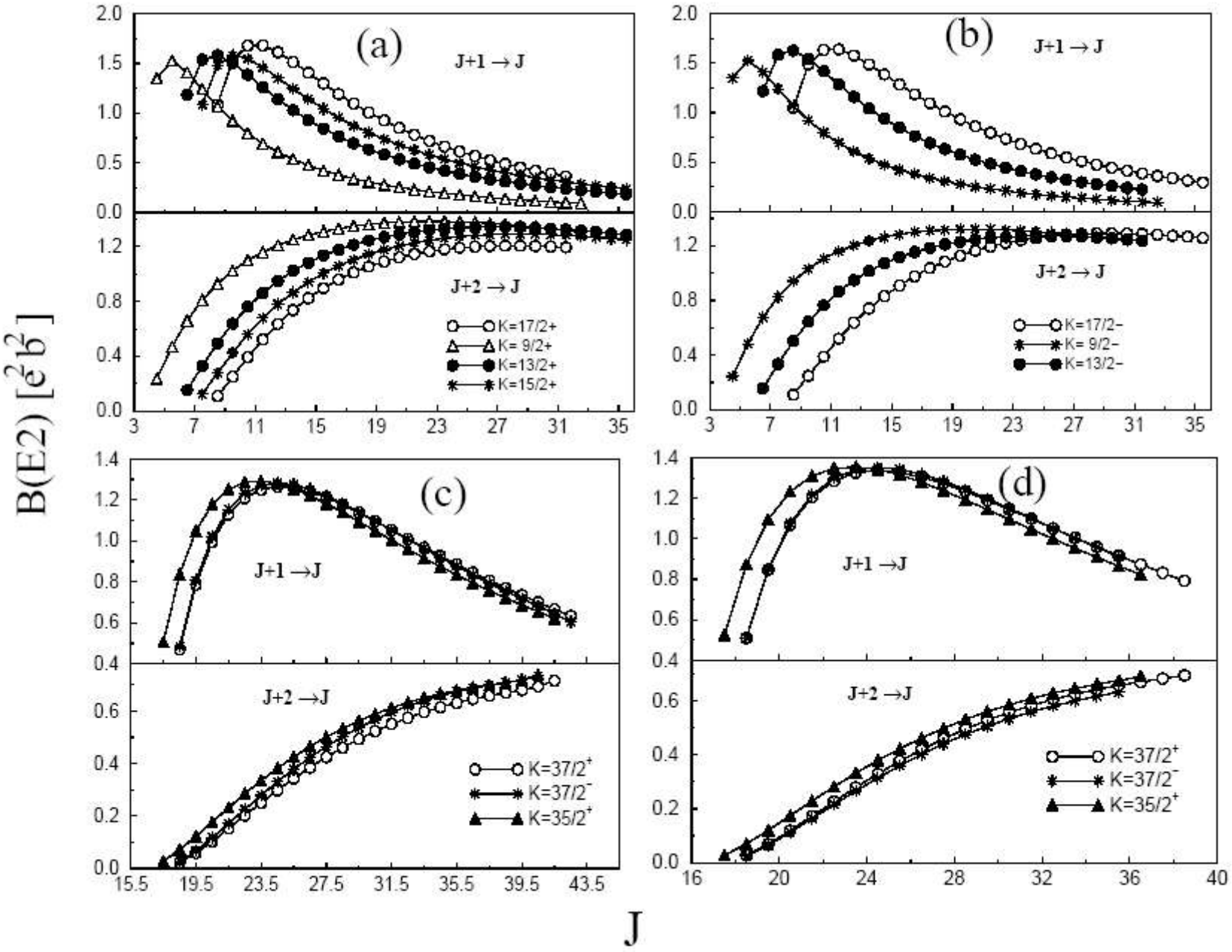
(a)
J+1 → J
J+2 → J
K=17/2+
K= 9/2+
K=13/2+
K=15/2+
(b)
J+1 → J
J+2 → J
K=17/2−
K= 9/2−
K=13/2−
(c)
J+1 →J
J+2 →J
K=37/2+
K=37/2−
K=35/2+
(d)
J+1 →J
J+2 →J
K=37/2+
K=37/2−
K=35/2+
B(E2) [e²b²]
J

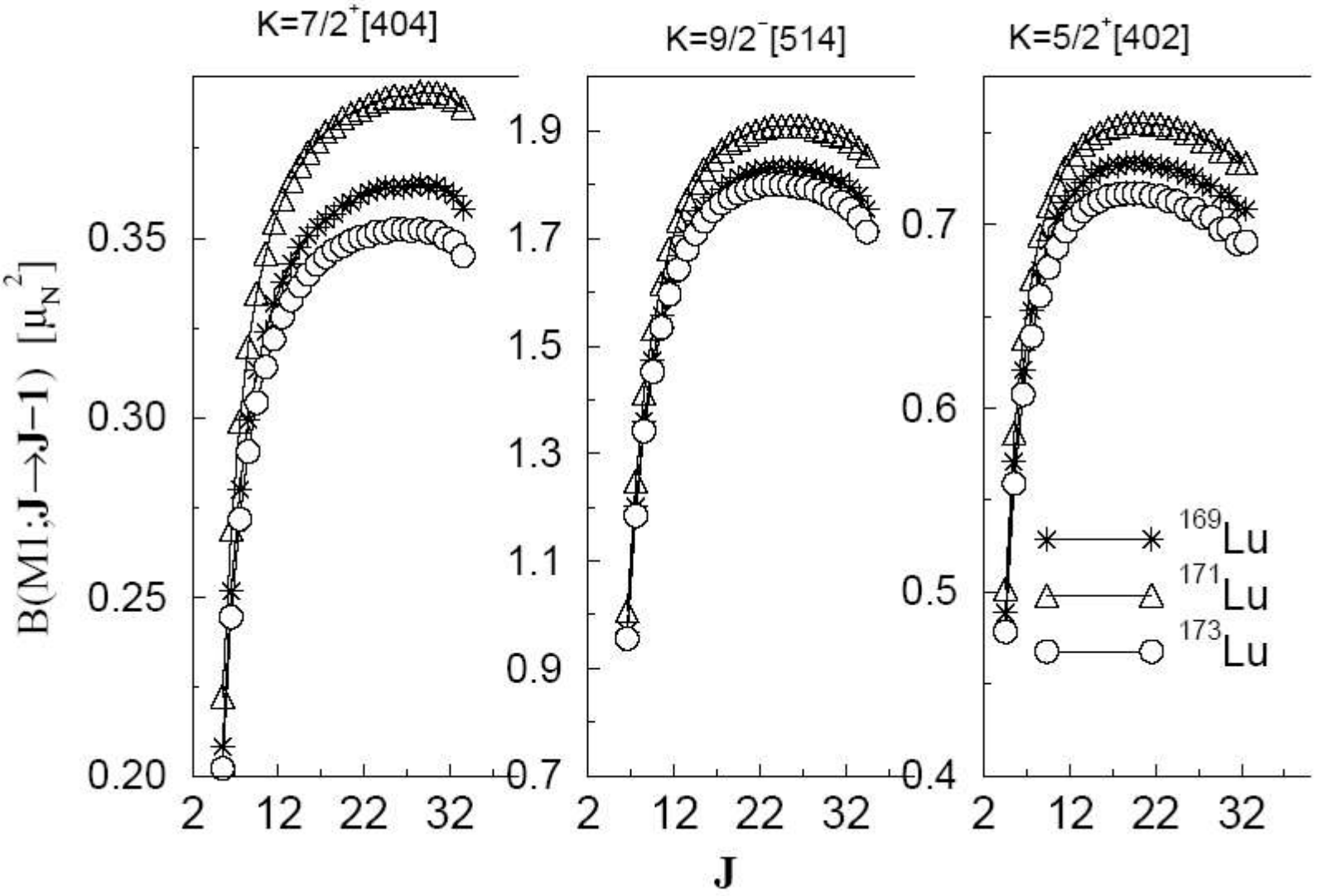
K=7/2+[404]
K=9/2-[514]
K=5/2+[402]
B(M1;J→J−1) [μN2]
0.35
0.30
0.25
0.20
1.9
1.7
1.5
1.3
1.1
0.9
0.7
0.7
0.6
0.5
0.4
2
12
22
32
J
169Lu
171Lu
173Lu

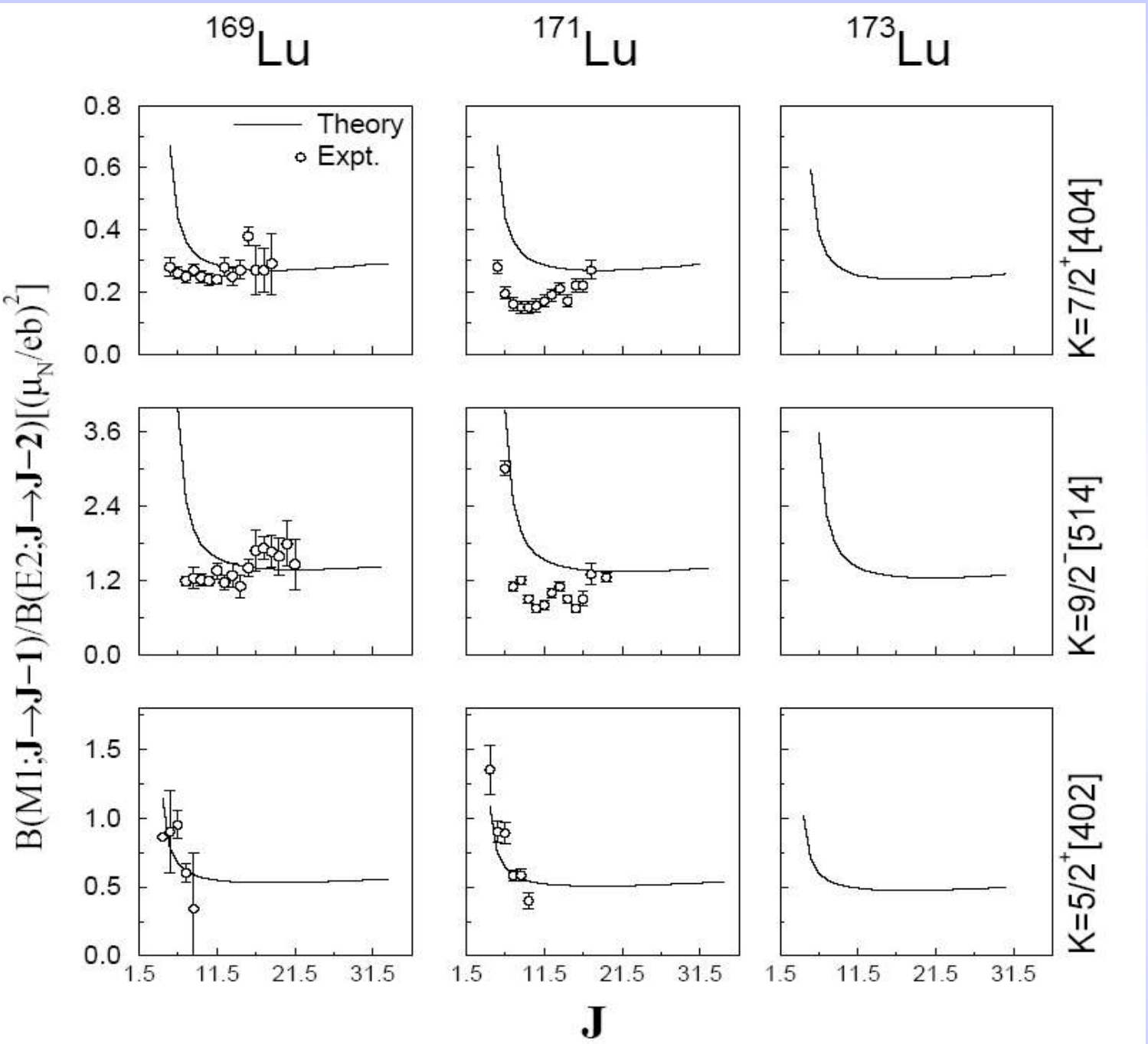
169Lu
171Lu
173Lu
Theory
Expt.
B(M1:J→J−1)/B(E2:J→J−2)[(μN/eb)2]
J
K=7/2+[404]
K=9/2−[514]
K=5/2+[402]
0.0
0.2
0.4
0.6
0.8
1.2
2.4
3.6
0.5
1.0
1.5
1.5
11.5
21.5
31.5

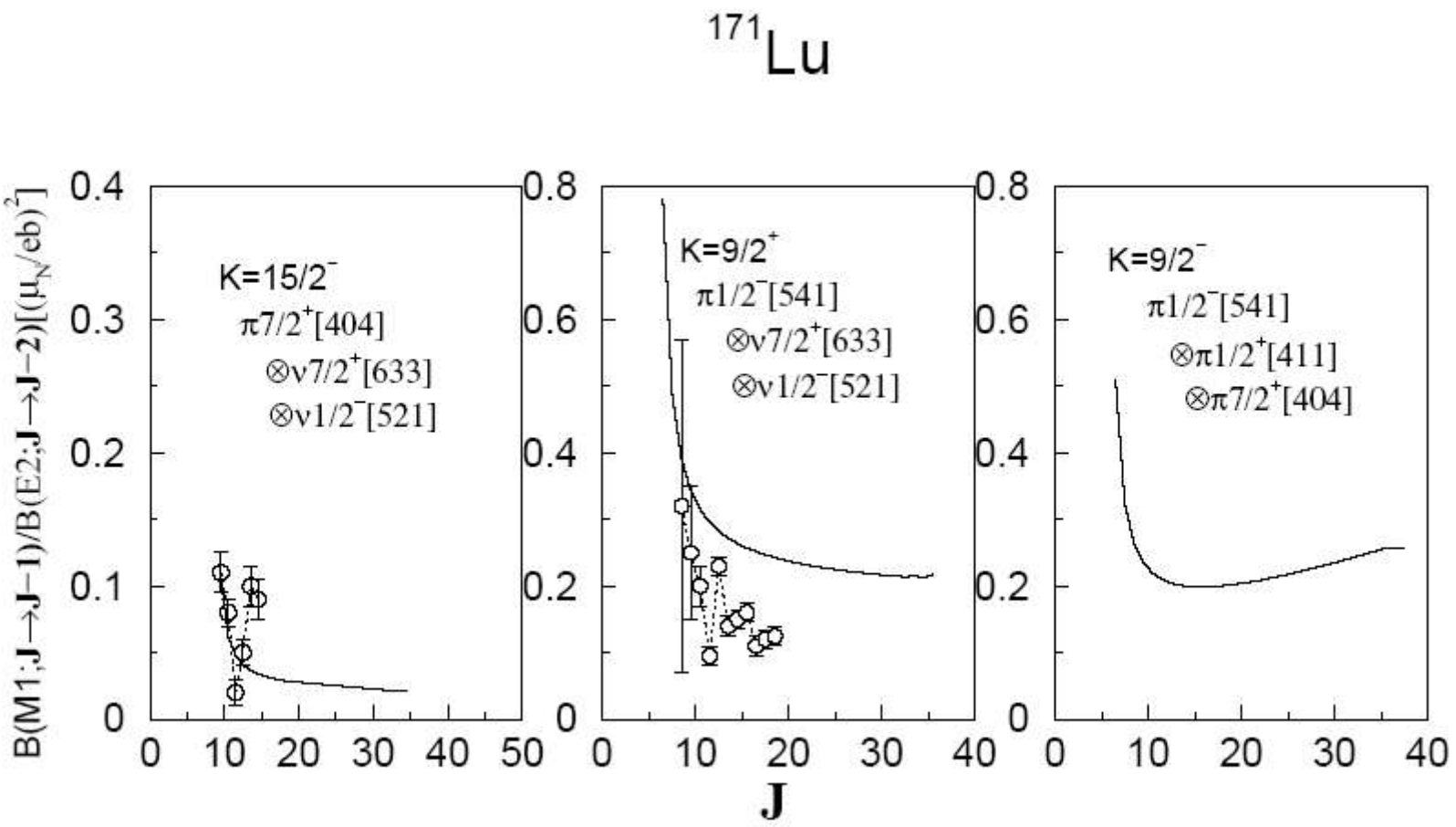
^{171}Lu
B(M1;J→J−1)/B(E2;J→J−2)[(μN/eb)²]
K=15/2⁻
π7/2⁺[404]
⊗ν7/2⁺[633]
⊗ν1/2⁻[521]
K=9/2⁺
π1/2⁻[541]
⊗ν7/2⁺[633]
⊗ν1/2⁻[521]
K=9/2⁻
π1/2⁻[541]
⊗π1/2⁺[411]
⊗π7/2⁺[404]
J

Conclusions

- Deformed HF and J projection – a general manybody method
- No phenomenological assumptions. Reliable. Good predictive power
- Superdeformed bands. K isomers. Chiral bands. Bandcrossing. Signature effects.
- Need for effective interactions in large model spaces.

- Band crossing due to intruder orbits are predicted
- B(E2) and B(M1) values are predicted
- Trends of the B(M1)/B(E2) ratios are predicted.
- "Chiral" band structure are explained
- Superdeformed bands are studied
- Other spectroscopic properties (spectra, quadrupole moments, magnetic moments, etc.,) are also quite well reproduced as compared to experimental results.

References For HF

G. Ripka, in *Advances in Nuclear Physics*, edited by M. Baranger and E. Vogt (Plenum Press, New York, 1966), Vol. 1.

D.J. Thouless, *Quantum Mechanics of Many-Body System* (Academic Press, New York, 1972).

C.R. Praharaj, J. Phys. G **14**, 843 (1988).

C.R. Praharaj and S.B. Khadkikar, Phys. Rev. Lett. **50**, 1254 (1983).

C.R. Praharaj, in *Structure of Atomic Nuclei*, edited by L. Satpathy (Narosa, New Delhi, 1999), p. 108.

References For J Projection

G. Ripka, in *Advances in Nuclear Physics*, edited by M. Baranger and E. Vogt (Plenum Press, New York, 1966), Vol. 1.

D.M. Brink, in *The Alpha-Particle Model of Light Nuclei*, Proceedings of the International School of Physics "Enrico Fermi," Course 36, edited by C. Bloch (Academic Press, New York, 1966).

C.R. Praharaj, in *Structure of Atomic Nuclei*, edited by L. Satpathy (Narosa, New Delhi, 1999), p. 108.

References For Expt.

T.L. Khoo *et al.*, Phys. Rev. Lett. **76**, 1583 (1996); R.V.F. Janssens *et al.*, Nucl. Phys. **A645**, 191 (1999).
R.A Bark *et al.*, Nucl. Phys. **A644**, 29 (1999).

S. Ogaza *et al.*, Nucl. Phys. **A559**, 100 (1993).
P. Kemnitz *et al.*, Nucl. Phys. **A209**, 271 (1973).
C. Foin *et al.*, Nucl. Phys. **A199**, 129 (1973).

Q_s and B(E2)

The Spectroscopic Quadrupole of a state with angular momentum J is given by

$$Q_S = \left(\frac{16\pi}{5}\right)^{1/2} \langle JJ \mid \sum_{i=p,n} Q^i_{20} \mid JJ \rangle$$

$$= \frac{1}{(2J+1)^{1/2}} C^{J2J}_{J0J} \left(\frac{16\pi}{5}\right)^{1/2} \langle \Psi^J_K \mid\mid \sum_{i=p,n} Q^i_2 \mid\mid \Psi^J_K \rangle$$

C^{J2J}_{J0J} is the Clebsch-Gordan Coefficient.

The B(E2) value for gamma decay from initial state αJ_1 to final state βJ_2 is

$$B(E2; \alpha J_1 \rightarrow \beta J_2) = \frac{1}{(2J_1+1)} \mid \sum_{i=p,n} \langle \Psi^{\beta J_2}_{K_2} \mid\mid Q^i_2 \mid\mid \Psi^{\alpha J_1}_{K_1} \rangle \mid^2$$

Core polarization are account by considering Effective charges.

Effective charges
proton :1.7e
neutron: 0.7e

μ and B(M1)

Magnetic moment μ is given by

$$\mu = \frac{1}{(2J+1)^{1/2}} C^{J1J}_{J0J} \left(\sum_{i=p,n} \langle \Psi^J_K \,||\, g_{l_i} l_i + g_{s_i} s_i \,||\, \Psi^J_K \rangle \right)$$

B(M1) value for γ-transition from initial state αJ_1 to final state βJ_2 is

$$B(M1; \alpha J_1 \rightarrow \beta J_2) = \frac{3}{(2J_1+1)} \frac{1}{4\pi} \left| \sum_{i=p,n} \langle \Psi^{\beta J_2}_{K_2} \,||\, g_{l_i} l_i + g_{s_i} s_i \,||\, \Psi^{\alpha J_1}_{K_1} \rangle \right|^2$$

where g_l is orbital g-factor and g_s is spin g-factor.

- g-factors (in μ_N)

	g_l	g_s
proton	1	½ × 5.586
Neutron	0	½ × (-3.826)

Superdeformed and Chiral Bands in Z = 50 region

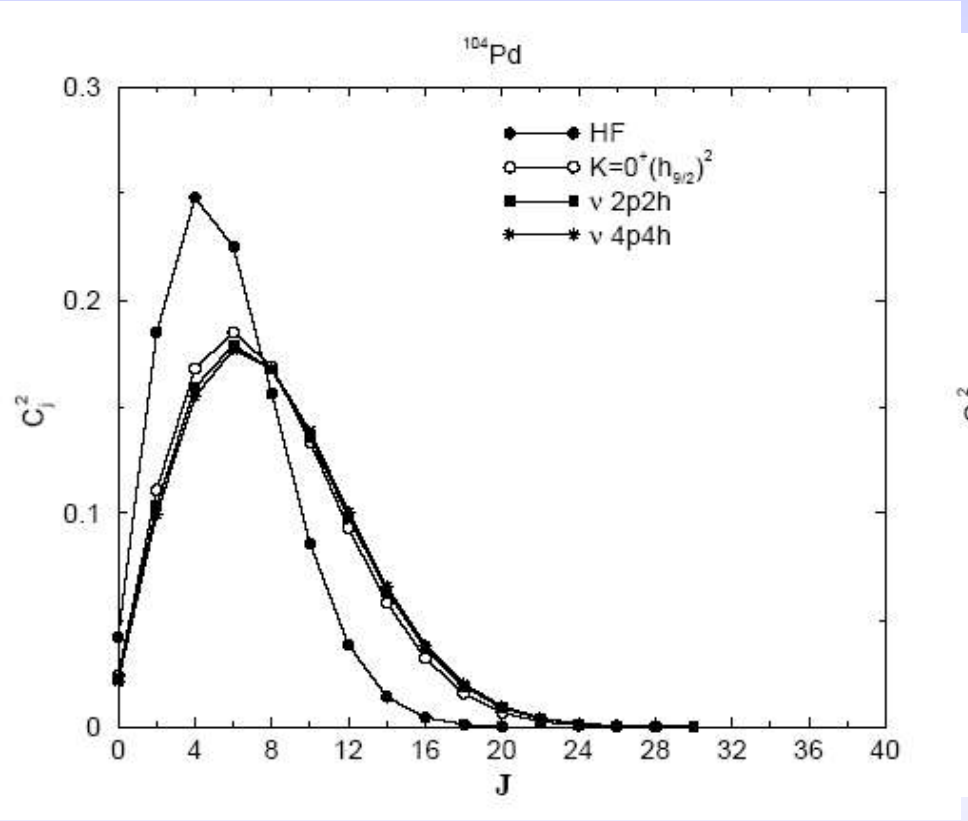

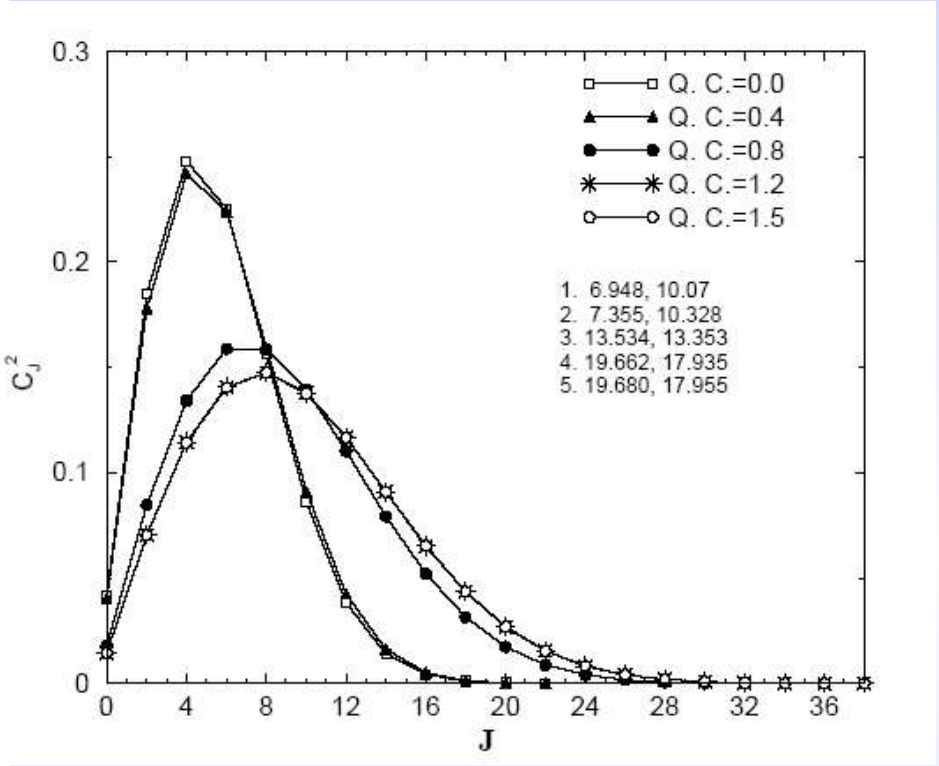

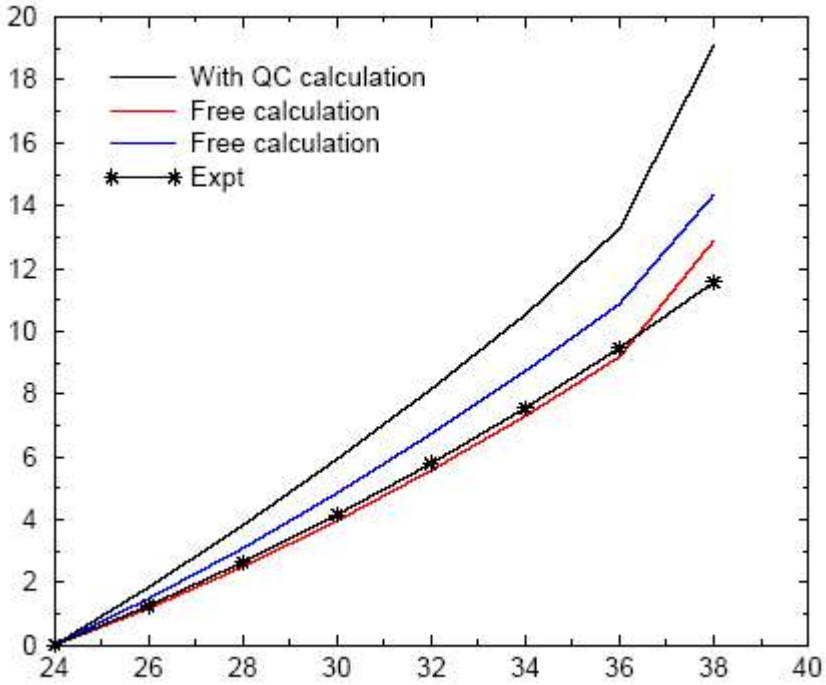
With QC calculation
Free calculation
Free calculation
Expt
20
18
16
14
12
10
8
6
4
2
0
24
26
28
30
32
34
36
38
40

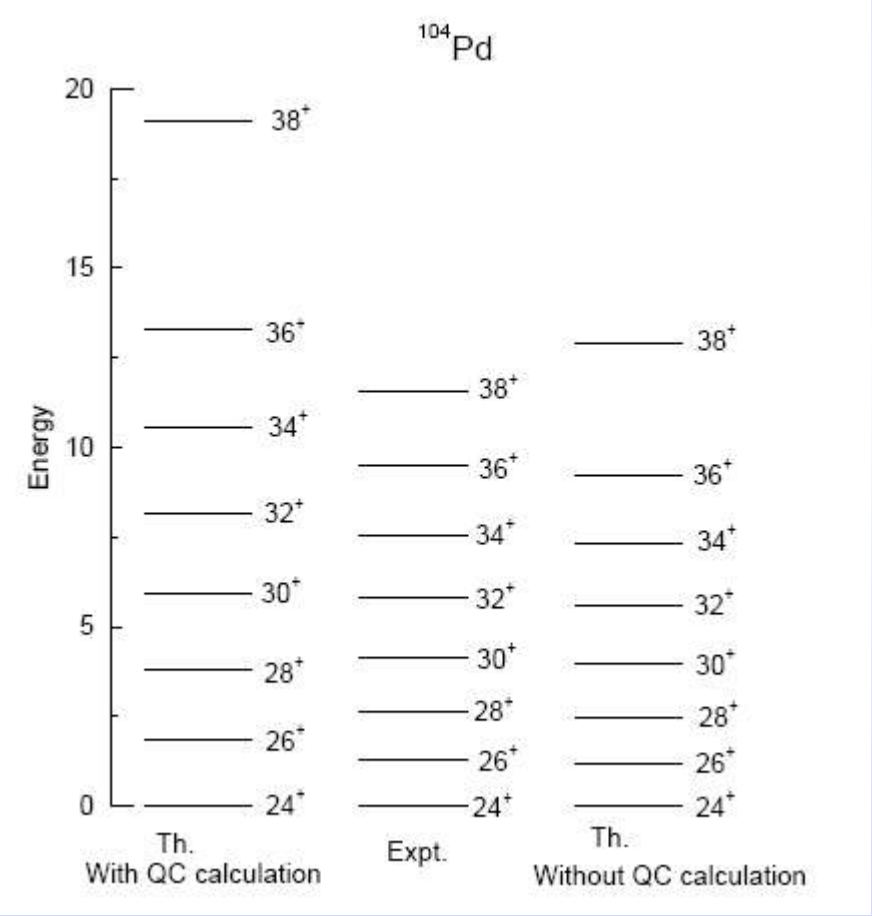
^{104}Pd
Energy
20
15
10
5
0
38+
36+
34+
32+
30+
28+
26+
24+
Th.
With QC calculation
Expt.
Th.
Without QC calculation

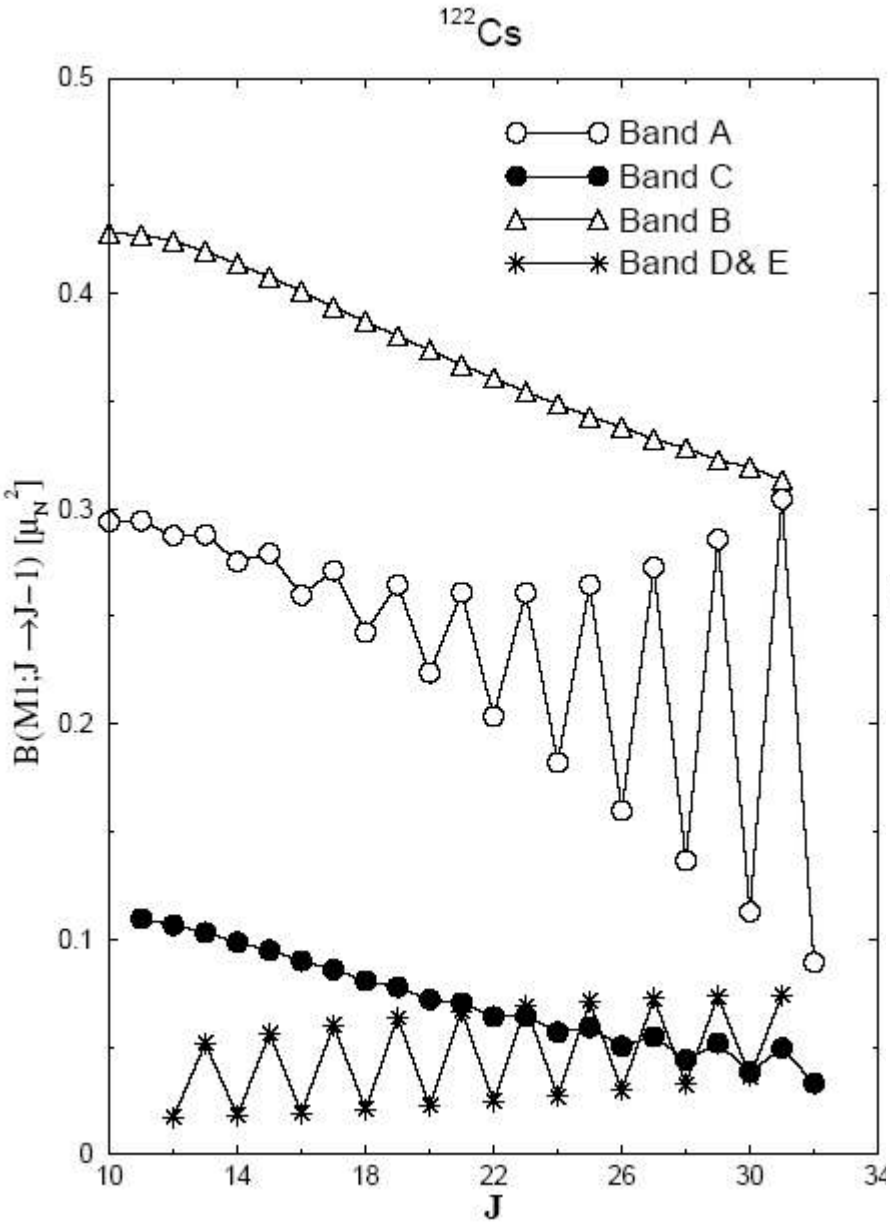

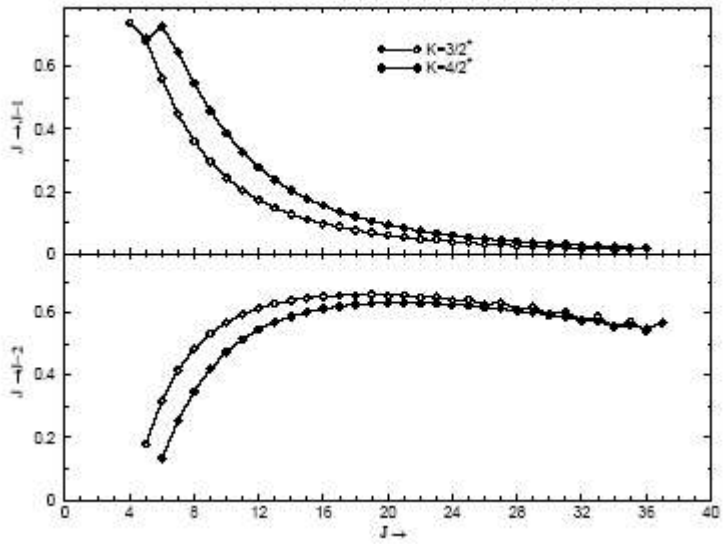

E2 Transition Matrix Elements (e^2b^2) between bands A and C

	B(E2;$K_1J \rightarrow K_2J-1$)	
J	$C \rightarrow A$	$A \rightarrow C$
19	0.14962	0.05986
18	0.17899	0.07395
17	0.18868	0.08139
16	0.20273	0.08671
15	0.20619	0.08901
14	0.21009	0.08845
13	0.20805	0.08635
12	0.20510	0.08203
11	0.19833	0.07671

Shape Coexistence in ^{52}Cr

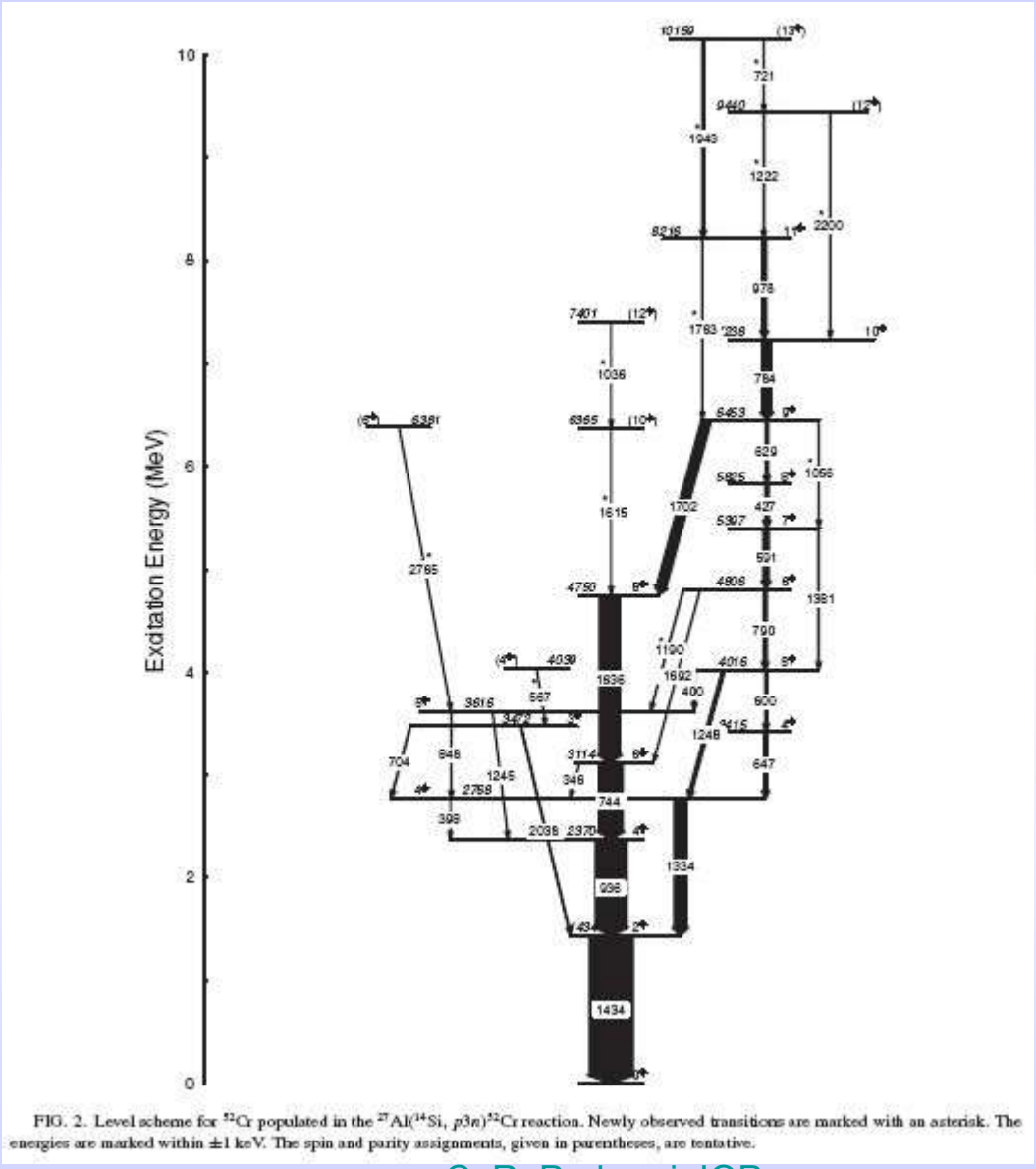

FIG. 2. Level scheme for ^{52}Cr populated in the ^{27}Al(^{14}Si, $p3n$)^{52}Cr reaction. Newly observed transitions are marked with an asterisk. The energies are marked within ±1 keV. The spin and parity assignments, given in parentheses, are tentative.

A. Comparison with Hartree-Fock microscopic model

The band structure of the ^{52}Cr nucleus has been studied with the deformed Hartree-Fock (HF) model and angular momentum (J) projection [25,26]. This is a useful microscopic model to study the spectra and the electromagnetic transition probabilities in well-deformed as well as moderately deformed nuclei [25–31]. The deformed HF equation is derived from the nuclear Hamiltonian, which consists of single-particle and residual two-body interaction terms:

$$H = \epsilon + V, \tag{5}$$

where, schematically, ϵ stands for single-particle energies of spherical shell model orbits and V stands for pp, pn, and nn two-body residual interactions. The surface delta interaction is considered as a residual interaction among the active nucleons with interaction strength $V_{pp} = V_{np} = V_{nn} =$ 0.5 MeV. We have taken $p_{1/2}$, $p_{3/2}$, $f_{5/2}$, $f_{7/2}$, and $g_{9/2}$ orbits above a $Z = N = 20$ spherical closed shell with spherical single-particle energies of 1.8, 0., 0.57, 4.6, and 5.8 MeV, respectively (with the same single-particle energies taken for protons and neutrons) for HF and J projection calculations. Axial symmetry of the HF field is assumed in this theoretical analysis.

Deformed HF orbits are obtained from the self-consistent solution of the HF equation [25,27]. The intrinsic states $|\phi_K\rangle$ are constructed by making appropriate particle-hole arrangement on the proton and neutron HF orbits near the Fermi surfaces. Because of axial symmetry of the HF field, an intrinsic state is a state of good K but not of good J. To study the spectra and electromagnetic matrix elements of the bands, we need good J states. The good angular momentum states of a given $|\phi_K\rangle$ are obtained by J projection. The J projection operator is [25]

$$P^{JM}_K = \frac{2J+1}{8\pi^2}\int d\Omega D^{J\,*}_{MK}(\Omega) R(\Omega), \tag{6}$$

where $R(\Omega)$ is the rotation operator and Ω stands for the Euler angles.

The matrix element of the Hamiltonian between the projected states of J obtained from intrinsic states ϕ_{K_1} and ϕ_{K_2} is

$$H^J_{K_1K_2} = \frac{2J+1}{2}\frac{1}{\left(N^J_{K_1K_1}N^J_{K_2K_2}\right)^{1/2}} \times \int_0^\pi d\beta \sin\beta d^J_{K_1K_2}(\beta)\langle\phi_{K_1}|He^{-i\beta J_y}|\phi_{K_2}\rangle, \tag{7}$$

where

$$N^J_{K_1K_2} = \frac{2J+1}{2}\int_0^\pi d\beta \sin\beta d^J_{K_1K_2}(\beta)\langle\phi_{K_1}|e^{-i\beta J_y}|\phi_{K_2}\rangle \tag{8}$$

is the amplitude overlap for angular momentum J.

In general, two states $|\Psi^{JM}_{K1}\rangle$ and $|\Psi^{JM}_{K2}\rangle$ projected from two intrinsic configurations $|\phi_{K_1}\rangle$ and $|\phi_{K_2}\rangle$ are not orthogonal to each other, even if the intrinsic states $|\phi_{K_1}\rangle$ and $|\phi_{K_2}\rangle$ are orthogonal. When necessary we orthonormalize for each J and then diagonalize using the equation (see Ref. [27])

$$\sum_{K'}\left(H^J_{KK'} - E_J N^J_{KK'}\right)C^J_{K'} = 0, \tag{9}$$

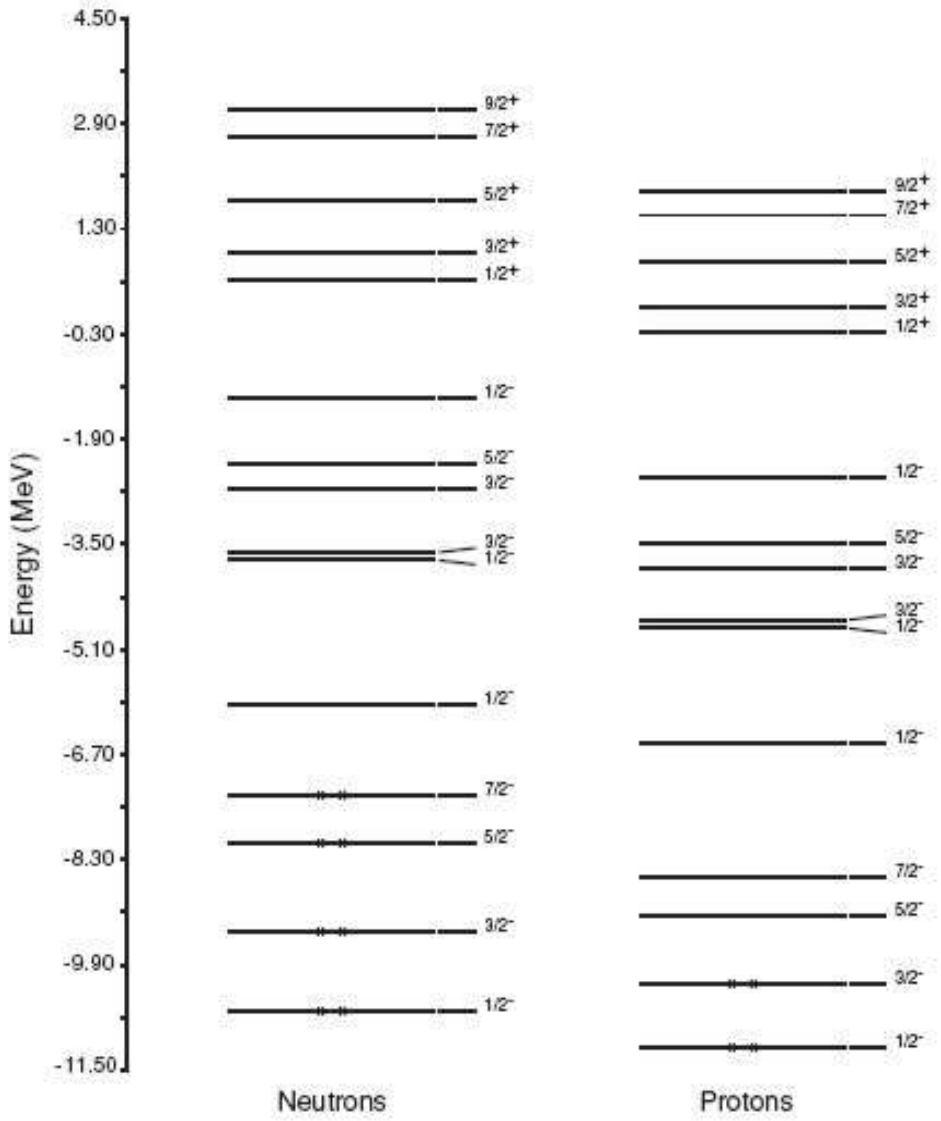

FIG. 5. The prolate deformed Hartree-Fock orbits for protons and neutrons.

where C^J_K are the orthonormalised amplitudes, which can be identified as the band-mixing amplitudes.

For ^{52}Cr, four active protons and eight active neutrons are considered above the $N = Z = 20$ core and the HF calculation is performed. The prolate HF orbits for protons and neutrons are shown in Fig. 5. Both the oblate and the prolate HF solutions are considered for J projection and band-mixing calculations. Since the two-body interaction is used in obtaining the self-consistent HF orbits, mixing of a small number of intrinsic configurations can, after J projection, describe the low-energy spectra and bands [30,32].

The following intrinsic configurations are considered for angular momentum projection and band mixing calculation:

(i) oblate configurations:
(A) $K = 0^+$ (HF) and (B) $K = 2^+\nu(1/2^- \otimes 3/2^-)$ and
(ii) prolate configurations:
(C) $K = 0^+$ (HF),
(D) $K = 1^+\pi(5/2^- \otimes -3/2^-)$,
(E) $K = 4^+\nu(7/2^- \otimes 1/2^-)$,
(F) $K = 3^+\nu(5/2^- \otimes 1/2^-)$, and
(G) $K = 5^+\nu(7/2^- \otimes 1/2^-) \otimes \pi(5/2^- \otimes -3/2^-)$.

We have considered two different sets of band mixing for the ground band. In the first case we have mixed the configurations A, B, C, and D, that is, prolate-oblate band mixing [denoted as Th(1) in Fig. 6]. In the second case [Th(2)], we consider only the oblate band mixing (configurations A and B). The lowest band after these two band mixings are compared with the experimental ground band in Fig. 6. In the Th(1) case, high spin states up to $J^\pi = 4^+$ are dominated by configuration C (prolate $K = 0^+$ band). The state $J^\pi = 6^+$ is well mixed between prolate and oblate $K = 0^+$ bands. The state $J^\pi = 8^+$ is mainly dominated by configuration A and states $J^\pi = 10^+$ and 12^+ are dominated by configuration B. In the case of Th (2), high spin states up to $J^\pi = 8^+$ are mainly of oblate configuration A and states above this are of configuration B. Both Th(1) and Th(2) give reasonable explanation of the ground-band spectrum. The calculated $B(E2)$ values for Th(1) and Th(2) are 0.0135 and 0.0066 $(e\ \mathrm{b})^2$, respectively.

The lowest band after the mixing of configurations E, F, and G is compared with the excited $K = 4^+$ experimental band in Fig. 6. In this band, high spin states up to $J^\pi = 9^+$ are dominated by configuration E and states higher than $J^\pi = 9^+$ are dominated by configuration G. For this $K = 4^+$ band we have

considered the prolate configurations because the collectivity shown by this band is only understood by J projection from the prolate ones. Among the oblate configurations only $K = 0^+$ (configuration A) shows some regular rotational feature; none of the other possible oblate configurations show the collective excitation (i.e., regular pattern in the spectrum) observed in the experimental $K = 4^+$ band. The quadrupole moment (Q_0) of the $K = 4^+$ bandhead obtained in our calculation for this band is 0.903 e b whereas for the ground band it is 0.785 e b. So the band structures seen in ^{52}Cr involve moderately deformed bands. The excited $K = 4^+$, where one neutron is excited from the $\Omega^\pi = 7/2^-$ to the $1/2^-$ prolate neutron orbit across the neutron Fermi surface, drives the nucleus toward more prolate deformation.

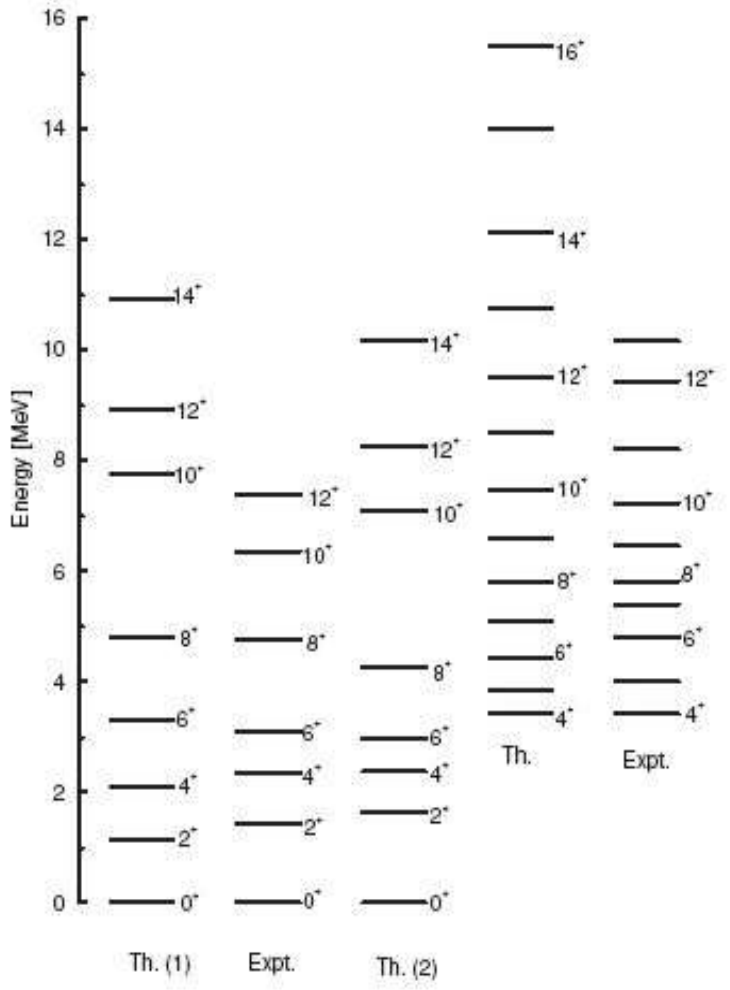

FIG. 6. Comparison of experimental levels with the results of the microscopic deformed Hartree-Fock model.

Conclusions

- We are able to explain both regular and irregular rotational bands.
- The doublet structure and departure from regular rotational behavior of the low-K bands are explained.
- We could relate staggering in spectrum with angular momentum carried by large-*j* nucleon.
- Structure of one, three, five quasi-particles bands for odd A and zero, two, four quasi-particle bands for even A are explained.

Def HF and J Projection formalism (J Phys G 14, 843 (1988)):

$$E^{\alpha}C^{\alpha}_{jm} = \varepsilon_j\, C^{\alpha}_{jm} + \Sigma V^{\mathrm{A}}(j_3 m_3 j_4 m_4; jmj_2 m_2)\, \rho_{j_2 m_2 j_4 m_4}\, C^{\alpha}_{j_3 m_3}. \tag{A.5}$$

Here V^{A} stands for two-body matrix elements antisymmetrised for identical nucleons and

$$\rho_{j_2 m_2 j_4 m_4} \equiv \langle \varphi_{\mathrm{HF}} | a^{\dagger}_{j_4 m_4} a_{j_2 m_2} | \varphi_{\mathrm{HF}} \rangle = \sum_{\substack{\alpha \\ (\text{occupied})}} C^{\alpha}_{j_2 m_2} C^{\alpha *}_{j_4 m_4} \tag{A.6}$$

is an element of the density matrix. If we restrict ourselves to axial symmetry, then we have

$$E^{\alpha}C^{\alpha}_{jm} = \varepsilon_j\, C^{\alpha}_{jm} + \Sigma V^{\mathrm{A}}(j_3 m j_4 m_2; jmj_2 m_2)\, \rho_{j_2 m_2 j_4 m_2} C^{\alpha}_{j_3 m} \tag{A.7}$$

Matrix elements of angular momentum projected states

We deal with intrinsic states specified by K, the projection of angular momentum along the intrinsic 3-axis. Such a deformed intrinsic state $|\varphi_k\rangle$ (a Slater determinant) is a superposition of states of sharp angular momenta:

$$|\varphi_K\rangle = \sum_I a^I_K |\psi_{IK}\rangle \tag{A.8}$$

The angular momentum projection operator is

$$P^{IM}_K = \frac{2I+1}{8\pi^2} \int \mathrm{d}\Omega\, D^{I*}_{MK}(\Omega) R(\Omega) \tag{A.9}$$

and operating on $|\varphi_K\rangle$ of (A.8) gives $a^I_K |\psi_{IM}\rangle$. Here Ω stands for the three Euler angles α, θ, γ and $R(\Omega)$ is the rotation operator. We also have

$$P^{IM*}_K P^{IM}_K = P^{IK}_M P^{IM}_K = P^{IK}_K. \tag{A.10}$$

The normalised state with angular momentum IM is

$$|\psi_{IM}\rangle = \frac{1}{\sqrt{N^I_{KK}}} P^{IM}_K |\varphi_K\rangle \tag{A.11}$$

where

$$N^I_{K'K} = \langle \varphi_{K'} | P^{IK'}_K | \varphi_K \rangle = \frac{2I+1}{2} \int_0^{\pi} \mathrm{d}\theta \sin\theta \mathrm{d}^I_{K'K}(\theta) \langle \varphi_{K'} | \exp(-\mathrm{i}\theta J_y) | \varphi_K \rangle \tag{A.12}$$

$$N^I_{KK} = \langle \varphi_K | P^{IK}_K | \varphi_K \rangle = (a^I_K)^2 \tag{A.13}$$

gives the intensity of angular momentum I contained in the intrinsic state $|\varphi_K\rangle$.

$$\langle \psi^I_{MK_2} | H | \psi^I_{MK_1} \rangle = \frac{2I+1}{2} \frac{1}{(N^I_{K_1K_1} N^I_{K_2K_2})^{1/2}}$$

$$\times \int_0^{\pi} \mathrm{d}\theta \sin\theta\, d^I_{K_2K_1}(\theta) \langle \varphi_{K_2} | H \exp(-\mathrm{i}\theta J_y) | \varphi_{K_1} \rangle. \tag{A.14}$$

The important quantities to be evaluated are the kernels such as $\langle \varphi_{K_2} | H \exp(-\mathrm{i}\theta J_y) | \varphi_{K_1} \rangle$ above. Let $u^{\alpha}_{K_2} \ldots$ and $u^{\beta}_{K_1} \ldots$ denote the deformed single-particle states which constitute the Slater determinants $|\varphi_{K_2}\rangle$ and $|\varphi_{K_1}\rangle$ respectively. Then for the kernel of an one-body operator O_1 we have (Brink 1966)

$$\langle \varphi_{K_2} | O_1 \exp(-\mathrm{i}\theta J_y) | \varphi_{K_1} \rangle = \langle \varphi_{K_2} | \exp(-\mathrm{i}\theta J_y) | \varphi_{K_1} \rangle \sum_{\alpha\beta} \langle u^{\alpha}_{K_2} | O_1 | u^{\beta}_{K_1} \rangle (B(\theta)^{-1})_{\beta\alpha} \tag{A.15}$$

where for an N-particle Slater determinant we have the $N \times N$ matrix $B(\theta)$ with matrix elements

$$(B(\theta))_{\alpha\beta} = \langle u^{\alpha}_{K_2} | \exp(-\mathrm{i}\theta J_y) | u^{\beta}_{K_1} \rangle. \tag{A.16}$$

For the two-body interaction V (Brink 1966)

$$\langle \varphi_{K_2} | V \exp(-\mathrm{i}\theta J_y) | \varphi_{K_1} \rangle = \tfrac{1}{2} \langle \varphi_{K_2} | \exp(-\mathrm{i}\theta J_y) | \varphi_{K_1} \rangle \sum_{\alpha\beta\gamma\delta} \langle u_\gamma u_\delta | V \exp(-\mathrm{i}\theta J_y) | u_\alpha u_\beta \rangle$$

$$\times [(B^{-1}_{(\theta)})_{\gamma\alpha} (B^{-1}_{(\theta)})_{\delta\beta} - (B^{-1}_{(\theta)})_{\gamma\beta} (B^{-1}_{(\theta)})_{\delta\alpha}]. \tag{A.17}$$

We define the 'rotated density operator'

$$\rho_{j'm_{j'}jm'_j}(\theta) = \sum_{\beta\alpha} [B^{-1}_{(\theta)}]_{\beta\alpha} C^{*K_2(\beta)}_{j'm_{j'}} \sum_{m_\alpha} C^{K_1(\alpha)}_{jm_\alpha} d^j_{m'_\alpha m_\alpha}(\theta). \tag{A.18}$$

$$\langle\varphi_{K_2}|T^k_\nu \exp(-\mathrm{i}\theta J_y)|\varphi_{K_1}\rangle$$

$$= \frac{1}{(2K+1)^{1/2}} \sum_{jj'} \langle j\|T^k\|j'\rangle \sum_{m_\alpha m'_\beta} \langle jm_\alpha j' - m'_\beta|k\nu\rangle (-1)^{j'-m'_\beta} \rho^{(\theta)}_{j'm'_\beta jm_\alpha} \tag{A.19}$$

using the identity (de Shalit and Talmi 1963, equation (15.14))

$$\sum_{m_3} \begin{pmatrix} j_1 & j_2 & j_3 \\ m_1 & m_2 & m_3 \end{pmatrix} \begin{pmatrix} l_1 & l_2 & j_3 \\ m'_1 & m'_2 & -m_3 \end{pmatrix} = \sum_{l_3 m'_3} (2l_3+1)(-1)^{l_3+j_3+m_1+m'_1} \begin{pmatrix} j_1 & l_2 & l_3 \\ m_1 & m'_2 & m'_3 \end{pmatrix}$$

$$\times \begin{pmatrix} l_1 & j_2 & l_3 \\ m'_1 & m_2 & -m'_3 \end{pmatrix} \begin{Bmatrix} j_1 & j_2 & j_3 \\ l_1 & l_2 & l_3 \end{Bmatrix} \tag{A.20}$$

we get for the two-body interaction matrix element

$$\sum_{JM} \langle j_1 m_\alpha j_2 m_\beta|JM\rangle \langle j_3 m_\gamma j_4 m_\delta|JM\rangle V_J(j_1 j_2, j_3 j_4)$$

$$= \sum_{LM_L} (-1)^{j_1+j_3+L}(2L+1)(-1)^{m_\alpha - m'_\delta} \begin{pmatrix} j_1 & j_3 & L \\ m_\alpha & -m'_\gamma & M_L \end{pmatrix}$$

$$\times \begin{pmatrix} j_2 & j_4 & L \\ m_\beta & -m'_\delta & -M_L \end{pmatrix} F_L(j_1 j_3, j_2 j_4) \tag{A.21}$$

where we have the particle–hole matrix elements

$$F_L(j_1 j_3, j_2 j_4) = \sum_J (2J+1)\, V_J(j_1 j_2, j_3 j_4) \begin{Bmatrix} j_1 & j_2 & J \\ j_4 & j_3 & L \end{Bmatrix} (-1)^{J+L+j_2+j_4}. \tag{A.22}$$

Using these, the kernel (equation (A.17)) for the two-particle interaction can be written as a product of one-body densities:

$$\langle\varphi_{K_2}|V \exp(-\mathrm{i}\theta J_y)|\varphi_{K_1}\rangle = \tfrac{1}{2}\langle\varphi_{K_2}| \exp(-\mathrm{i}\theta J_y)|\varphi_{K_1}\rangle$$

$$\times \sum_{\substack{j_1 j_2 j_3 j_4 \\ LM_L}} \sum_{\substack{m_\alpha m_\beta \\ m_\gamma m_\delta}} (-1)^{j_2+j_3+L+M_L+m_\gamma+m_\delta} F_L(j_1 j_3, j_2 j_4) \langle j_1 m_\alpha j_3 - m_\gamma|L - M_L\rangle$$

$$\times \langle j_2 m_\beta j_4 - m_\delta|LM_L\rangle \rho_{j_4 m_\delta j_2 m_\beta}(\theta)\, \rho_{j_3 m_\gamma j_1 m_\alpha}(\theta). \tag{A.23}$$

COLLABORATORS

- Zashmir Naik (TIFR)
- A.K. Rath (Sambalpur Univ)
- S.B. Khadkikar (PRL)
- S.P. Pandya (PRL)
- Experimentalists and Colleagues

from Universities and Institutions.